Cosmological Constraints on MeV-scale Dark Sectors

Abstract
In this work we present new and refined cosmological constraints on MeV-scale dark sectors and various well-motivated particle physics models. New light states thermally coupled to the Standard Model plasma can alter the expansion history of the Universe and impact the synthesis of the primordial elements. We present precise and robust constraints from Big Bang Nucleosynthesis (BBN) and the Cosmic Microwave Background (CMB). We find that BBN observations alone set a lower bound on the thermal dark matter mass to be $m_\chi > 0.4\,\mathrm{MeV}$ at 2σ. The reach of future CMB experiments is also considered.

On a more terrestrial note, we reinterpret the results of direct detection experiments which rely on nuclear recoils. Such experiments lose sensitivity for sub-GeV dark matter although this is recovered if there is an additional, sub-dominant source of particles with higher momenta. We investigate the possibility that decays of mesons from inelastic cosmic ray collisions in the atmosphere could act as such a source. The resulting constraints are then presented and mapped onto a concrete particle physics model.

Finally, we look at a well-motivated model that links neutrino masses and scalar dark matter. Bounds on parameters within the model are placed using measurements from the IceCube neutrino telescope and future sensitivity is forecast.

King's College London
PhD Upgrade – October 2019

J.B.G. Alvey
Theoretical Particle Physics and Cosmology
james.alvey@kcl.ac.uk

Panel: Diego Blas, Chris McCabe, Jean Alexandre

Publications

Many of the results in this report can be found in the following works which were performed both by myself and my collaborators. In particular, Chapter II discusses the results in Ref. [1], Chapter III presents Ref. [2] relatively fully, and Chapter IV summarises Ref. [3].

[1] *Refined Bounds on MeV-scale Thermal Dark Sectors from BBN and the CMB*
Nashwan Sabti, **James Alvey**, Miguel Escudero, Malcolm Fairbairn and Diego Blas, [1910.01649].

[2] *Light Dark Matter from Inelastic Cosmic Ray Collisions*
James Alvey, Miguel Campos, Tevong You and Malcolm Fairbairn, [1905.05776].

[3] *Linking Scalar Dark Matter and Neutrino Masses with IceCube 170922A*
J.B.G. Alvey and M. Fairbairn, JCAP 1907 (2019) 041 [1902.01450].

Contents

I Introduction

1.1 Models and Motivation

There is strong indirect evidence for the existence of some form of dark matter in the Universe including anomalies in galactic rotation curves, weak lensing of distant galaxies, observations of the bullet cluster, and Cosmic Microwave Background parameter measurements [4–7]. Nonetheless, the nature of dark matter is still unknown and thermal relics associated with the electroweak scale are under increasing pressure from the LHC as well as from direct and indirect detection experiments [8–20]. Motivated by the fact that direct detection experiments are considerably less sensitive to sub-GeV dark matter particles, attention has naturally turned to lower mass alternatives [21–24].

From a theoretical perspective, MeV-scale thermal dark matter candidates were shown to be viable some years ago [25–27] and, since then, a large number of MeV-scale dark matter models have appeared in the literature, see e.g. [28–45]. Experimentally, with the aim of testing as many scenarios as possible [46], a complementary program has been developed to test the possible existence of MeV-scale dark matter particles and potential companions Beyond the Standard Model (BSM) [21–24]. Light dark matter particles and their potential mediators with the dark sector have been searched for at particle colliders [47–54], beam dump experiments [55–57], neutrino experiments [58–63], neutrino telescopes [3, 64, 65], as well as in direct [66–73] and indirect [74–76] dark matter detection experiments. Searches for light BSM species are not only carried out in terrestrial experiments, but a variety of astrophysical [77–82] and cosmological [83–90] constraints have been also derived on states with masses at the MeV scale. Up to now, however, all these searches have been unsuccessful. Future, ongoing and planned experiments are expected to cut into relevant regions of parameter space and perhaps yield a signal [21–24, 91–95].

1.2 Cosmology and Nucleosynthesis

Big Bang Nucleosynthesis (BBN) has been widely used as a probe of new physics [96–98]. BBN occurred when the Universe was about three minutes old, in the temperature range $10\,\text{keV} \lesssim T \lesssim 1\,\text{MeV}$, and therefore represents a key stage of the Universe that new states at the MeV scale can affect. Given the excellent agreement between observations and the Standard Model (SM) prediction of the primordial light nuclei abundances [99], strong constraints can be set on the masses and properties of new light particles. Similarly, the agreement of Cosmic Microwave Background (CMB) observations with a

vanilla ΛCDM Universe [14] can be used to set strong constraints on light new physics.

In Chap. II, we perform an exhaustive and robust analysis of the cosmological implications of MeV-scale particles that are thermally coupled to electrons, neutrinos or both in the early Universe. This has been studied in the past by a number of groups [100–109], but here we update and upgrade the constraints by:

- Using up-to-date measurements of the primordial element abundances [99] and Planck 2018 CMB observations [14].
- Accurately accounting for the early Universe evolution in the presence of MeV-scale states following [109, 110].
- Using the state-of-the-art Big Bang Nucleosynthesis code `PRIMAT` [111], which outputs the most accurate theoretical predictions for the helium and deuterium abundances to date. `PRIMAT` accounts for a variety of effects, such as up-to-date nuclear reaction rates, finite temperature corrections, incomplete neutrino decoupling and several other effects relevant to the proton-to-neutron conversion rates.
- Performing a pure BBN analysis on light MeV-scale states. Namely, we set a bound on the masses of different species by using only the primordial helium and deuterium abundances and by marginalizing over any possible value of the baryon energy density.

1.3 Direct Detection of sub-GeV Dark Matter

As mentioned above, the experimental search for a direct detection signature [112] is still ongoing. Light sub-GeV dark matter, in particular, has become a prime target of such activities and encompasses a wider variety of possibilities for new physics beyond the Standard Model [23].

Acquiring sensitivity to sub-GeV dark matter typically requires detectors able to pick up lower recoil energies; a reduced momentum is expected for lighter masses given that the galactic velocity of dark matter is $\mathcal{O}(10^{-3})c$. However, Refs. [113, 114] recently showed that light dark matter interacting with nucleons or electrons necessarily leads to an energetic flux due to cosmic rays colliding elastically with dark matter in the interstellar medium. This up-scattered dark matter flux may then have enough energy to be detectable in direct detection experiments such as XENON1T (previously thought to be sensitive only to $\mathcal{O}(10-100)$ GeV dark matter) [10], as well as other dark matter or neutrino detectors [113, 114] [1].

In Chap. III, we point out another generic (albeit not irreducible) source of light dark matter flux. If mesons decay partially into dark matter, as could happen through the same coupling to nucleons that enables direct detection, then the mesons generated in inelastic cosmic ray collisions will also produce an energetic flux of dark matter. This may be viewed as a continuous cosmic beam dump experiment. It naturally provides a preexisting light dark matter source for experiments that would otherwise be insensitive to them. The different detector targets, exposure, and source geometry involved then enable distinctive opportunities relative to dedicated beam dump experiments. Indeed, we shall see

[1] See also Refs. [115–117] for ways of extending the direct detection sensitivity to lighter dark matter masses, and Refs. [118–120] for solar sources of energetic dark matter flux.

that XENON1T [10] and the future LZ experiment [121] set competitive limits for light mediators in comparison to MiniBooNE [122]. Moreover, unlike the upscattering mechanism that relies on a relic dark matter density, inelastic cosmic ray collisions can also produce other long-lived hidden sector particles, thus extending the possibilities for direct detection coverage of light sectors beyond dark matter.

In particular, we provide a first estimate of the dark matter flux from the aforementioned cosmic ray mechanism, taking into account their attenuation through the Earth. As an example of its application, we then place current and projected limits from XENON1T and LZ. We do this generally for a model-independent parametrisation of spin-independent cross-section vs dark matter mass and vs the meson branching ratio into dark matter. Finally, we consider a specific model in which the dark sector mediator is a hadrophilic scalar particle [123].

1.4 Neutrinos at IceCube

There are a number of issues with the vanilla Standard Model of particle physics [124–130]. One particularly prominent qustion is the origin of neutrino masses. In the pure $\mathrm{SU}(3) \times \mathrm{SU}(2) \times \mathrm{U}(1)$ SM, neutrinos are massless. This is in contradiction to evidence for neutrino oscillations [131]. Such a hint of new physics beyond the SM is of interest to model builders looking for extensions to the current known particle content [129, 132, 133].

In Chap. IV, we consider an effective model of particle Dark Matter that consistently generates neutrino masses [125, 132–146]. In particular, we look to place complementary bounds to those discussed in Section 1.1 using the IceCube neutrino experiment. IceCube is a relatively new facility located at the South Pole, which detects high energy astrophysical neutrinos [147–154]. On the 22^{nd} September 2017, IceCube detected a 290 TeV muon neutrino. After analysis of the trajectory of the event, it is generally believed that this neutrino came from the blazar TXS 0506+056. This active galactic nuclei is located approximately 1.3 Gpc away in comoving distance co-ordinates. The fact that the blazar neutrino propagates over gigaparsecs of cosmological distance means that we may be able to compute the mean free path of the neutrino within the new framework and find something comparable with this distance. Note that this is non-trivial in the sense that the SM prediction for the neutrino mean free path after the neutrino sector decouples from the photon bath is $\mathcal{O}(10^{11})$ Gpc.

The result of this study are competitive exclusion limits on the complex scalar Dark Matter candidate in this model. The constraint is complimentary (and slightly weaker) to current constraints from Big Bang Nucleosynthesis and the Cosmic Microwave Background such as those detailed in Chap. II. We also explore how future higher energy events could improve this bound.

1.5 Summary of the Work

To summarise, the rest of the work is organised as follows. In Chap. II, we present the bounds coming from Big Bang Nucleosynthesis and the Cosmic Microwave Background. We also consider the sensitivity of future CMB experiments such as the Simons Observatory and CMB-S4. In Chap. III, we calculate the expected flux of high-momenta dark matter that may arise in inelastic collisions of cosmic

rays with the atmosphere. In turn, limits are placed on the spin-indepdent Dark Matter-Nucleon cross section using the XENON1T and LZ experiments. Finally, in Chap. IV, the propagation of neutrinos across a few gigaparsecs of cosmological distance is considered within the framework of an effective theory that radiatively generates neutrino masses. Observations at the IceCube neutrino telescope are then used to constrain the model and forecasts are made regarding the impact of higher energy neutrino measurements.

II | Big Bang Nucleosynthesis

As discussed breifly in the Introduction, Big Bang Nucleosynthesis is a useful probe of new physics. In particular, new light states thermally coupled to the SM plasma can affect the synthesis of the primordial elements. While we are mostly interested in constraining MeV-scale dark matter particles, our analysis applies more generally to any additional BSM particles that are in thermal equilibrium with the SM during BBN and with a mass in the MeV range. This includes dark matter particles and mediators with the dark sector. In practice, this equilibrium should be maintained at temperatures below that of neutrino decoupling $T_\nu^{\rm dec} \sim 2\,{\rm MeV}$ [155]. The requirement of being in thermal contact at least prior to neutrino decoupling restricts the couplings and masses of the particles we are able to constrain. For the case of weakly-interacting, stable, thermal BSM particles (WIMPs), it is well known that annihilation interactions with the SM plasma will decouple from chemical equilibrium at $T \sim m/20$ [156]. Hence, our analysis will apply to thermal WIMPs with $m \lesssim 20\, T_\nu^{\rm dec} \sim 40\,{\rm MeV}$. In the case of unstable particles that decay into SM species, they will be in thermal equilibrium with the SM plasma during BBN, provided that their lifetime is $\tau \lesssim 0.1\,{\rm s}$. In other words, the lifetime should be shorter than the age of the Universe at the time of neutrino decoupling. Our analysis will constrain particles that efficiently annihilate or decay into neutrinos or electrons/photons prior and during neutrino decoupling. This is the case if the interaction rate is larger than the expansion rate H at neutrino decoupling:

$$\Gamma \gtrsim H|_{T=T_\nu^{\rm dec}} \simeq 10\,{\rm s}^{-1}. \tag{2.1}$$

Throughout the text we will denote a generic BSM particle as χ. For a particle that annihilates into SM species, the rate is $\Gamma \sim n\,\langle\sigma v\rangle \sim g_\chi^2 g_{\rm SM}^2 T^3/(16\pi m_\chi^2)$ and our analysis will generally be sensitive to

$$\text{Stable Particles with} \qquad \sqrt{g_\chi g_{\rm SM}} \gtrsim 2\times 10^{-5}\sqrt{\frac{m_\chi}{\rm MeV}} \qquad \text{and} \qquad m_\chi \lesssim 20\,{\rm MeV}\,, \tag{2.2}$$

where g_χ and $g_{\rm SM}$ are coupling constants. If the χ particle is unstable, then $\Gamma \sim g_{\rm SM}^2 m_\chi/(4\pi)\, K_1(m_\chi/T_\nu^{\rm dec})$ – K_1 being a modified Bessel function of the first kind – and our analysis will constrain

$$\text{Unstable Particles with} \qquad g_{\rm SM} \gtrsim 5\times 10^{-10}\sqrt{\frac{m_\chi}{\rm MeV}}\left(1+\sqrt{\frac{\rm MeV}{m_\chi}}\right) \qquad \text{and} \qquad m_\chi \lesssim 20\,{\rm MeV}. \tag{2.3}$$

In summary, the bounds we derive in this paper will generically constrain MeV-scale particles coupled to the SM bath with couplings $\gtrsim 10^{-5}$ if they are stable[1] and with couplings as small as 10^{-9} if they are unstable. Note that our bounds will apply even if these unstable BSM particles decay into other BSM states, under the condition that they possess couplings $\gtrsim 10^{-9}$ to SM particles.

2.1 Cosmology with Light WIMPs

The implications of light, thermally coupled BSM particles with the SM plasma at temperatures $T \sim 1\,{\rm MeV}$ are twofold [100]: *i)* they contribute to the expansion rate of the early Universe and *ii)* they release entropy into the plasma. In addition, if the new particles interact with both neutrinos and electrons/photons, they would efficiently delay the process of neutrino decoupling [101, 109].

2.1.1 Temperature Evolution and Universe's Expansion

In order to accurately account for such effects we follow [109] and assume that all relevant species can be described by thermal distributions and characterized by a temperature T_i. We then calculate the evolution of neutrino decoupling in terms of the temperature of the neutrinos and electromagnetic components of the plasma. For the details, methodology and differential equations governing this evolution, see Appendix A.1. By solving the relevant equations, we find all the key background evolution quantities as a function of time, scale factor and temperature. In addition, we evaluate the number of effective relativistic degrees of freedom $N_{\rm eff}$ as relevant for CMB observations,

$$N_{\rm eff} \equiv \frac{8}{7}\left(\frac{11}{4}\right)^{4/3}\left(\frac{\rho_{\rm rad}-\rho_\gamma}{\rho_\gamma}\right) = 3\left(\frac{11}{4}\right)^{4/3}\left(\frac{T_\nu}{T_\gamma}\right)^4, \tag{2.4}$$

2.1.2 Nucleosynthesis in the Presence of Thermal BSM Particles

MeV-scale thermal relics affect the synthesis of the light elements, see e.g. [100–104]. In this work, we have modified the publicly available state-of-the-art BBN code `PRIMAT` [111] to accommodate for the presence of light BSM particles in thermal equilibrium with the SM plasma. This is done by computing the background cosmology externally using `NUDEC_BSM` [109, 110] and then passing on the relevant parameters[2] to the section of `PRIMAT` that takes care of the nuclear reaction rates and the time evolution of nuclei abundances. We have explicitly verified that the differences in the primordial

[1] This would cover well the case of thermal dark matter, for which $\sqrt{g_\chi g_{\rm SM}} \sim 10^{-3}\sqrt{\frac{m_\chi}{10\,{\rm MeV}}}\sqrt[4]{\frac{\langle\sigma v\rangle}{3\times 10^{-26}\,{\rm cm}^3/s}}$.

[2] This includes the evolution as a function of time and scale factor of T_γ, T_ν, H and the residual entropy transfer between neutrinos and electrons as parametrized by $\mathcal{N}$ in `PRIMAT` [111].

element abundances between the default version of `PRIMAT` and with the SM evolution as calculated in [109, 110] are below 0.1 %, and hence one order of magnitude smaller than current observational errors. Our results agree quantitatively and qualitatively with previous studies [100–104][3] modulo differences we attribute to updated nuclear reaction rates and the fact that we account for non-instantaneous neutrino decoupling, see Appendix A.3 for details.

2.1.3 Cosmological Implications

In this section we review the main cosmological implications of light BSM particles in thermal equilibrium with the Standard Model plasma during neutrino decoupling and Big Bang Nucleosynthesis. The reader is referred to [100–104] for previous and complementary discussions of the impact of such particles on BBN and the CMB and to [96–98] for reviews on the role of BBN as a probe of physics beyond the Standard Model.

Cosmic Microwave Background – Modifications to N_{eff}

Once neutrinos decouple from the SM plasma at $T_\nu^{\rm dec} \lesssim 2\,\text{MeV}$, a light, neutrinophilic BSM particle of mass $m_\chi \lesssim 20\,\text{MeV}$ will annihilate/decay into neutrinos, which results in $\rho_\nu > \rho_\nu^{\rm SM}$ or equivalently $N_{\rm eff} > N_{\rm eff}^{\rm SM}$. Analogously, an electrophilic particle will dump energy into the electromagnetic sector of the plasma at temperatures $T < T_\nu^{\rm dec}$ and yield $N_{\rm eff} < N_{\rm eff}^{\rm SM}$. In the upper panel of Figure 2.1, we display the corresponding value of $N_{\rm eff}$ for neutrinophilic and electrophilic BSM particles in thermal equilibrium with the SM plasma as a function of their mass. The grey contours correspond to the $\pm 2\sigma$ measurements by Planck (see below). With the sole exception of an electrophilic scalar particle, it is clear that regardless of what the spin and number of internal degrees of freedom of a given species are, Planck would set a lower bound on its mass.

Big Bang Nucleosynthesis

Light BSM particles in thermal equilibrium during BBN lead to three main effects on the cosmological evolution that impact the synthesis of the primordial elements. Firstly, additional species present in the early Universe will alter the expansion rate and therefore also the temperature-to-time relation. This is important because they will modify the time at which various weak and nuclear processes freeze-out, in particular the proton-to-neutron conversion and $p + n \leftrightarrow D + \gamma$. Secondly, the presence of these particles can change the evolution of the neutrino-to-photon temperature ratio. This has relevant implications because this ratio enters the proton-to-neutron conversion rates. Finally, light species thermally coupled to the electromagnetic sector of the plasma will release entropy after nucleosynthesis and therefore dilute the number density of all nuclei for a given primordial baryon-to-photon ratio. The impact of the particles considered in this work on the primordial abundances of helium and deuterium is depicted in the middle and lower panels of Figure 2.1 and can be suitably categorised into three mass regions:

[3] We agree particularly well with [103, 104], see Appendix A.3.

A. $m_\chi \lesssim 0.05\,MeV$

Very light neutrinophilic particles simply contribute to the expansion rate of the Universe during BBN, and do not alter the baryon-to-photon ratio. As such, they simply shorten the timescales on which the weak and nuclear processes freeze out, increasing both $Y_{\rm P}$ – which is approximately proportional to the neutron-to-proton ratio at $T \sim 0.07\,\text{MeV}$ [96–98] – and $\text{D/H}|_{\rm P}$ relative to the SM. Whilst very light electrophilic particles contribute to the expansion rate, which increases the value of $Y_{\rm P}$, they also release substantial amounts of entropy into the electromagnetic plasma *after* nucleosynthesis. This acts to dilute number of baryons per photon and hence leads to a smaller value of $\text{D/H}|_{\rm P}$ than in the SM (since $\text{D/H}|_{\rm P} \propto \Omega_{\rm b}h^2$).

B. $0.5\,MeV \lesssim m_\chi \lesssim 10\,MeV$

Electrophilic particles in this region lead to a smaller energy density of the Universe during nucleosynthesis and again to entropy release. This leads to lower values for both $Y_{\rm P}$ and $\text{D/H}|_{\rm P}$ as is seen in the lower two panels of Figure 2.1. For neutrinophilic particles on the other hand, there is a larger energy density than in the SM, and hence a larger expansion rate. This leads to larger values for both $Y_{\rm P}$ and $\text{D/H}|_{\rm P}$ for a given $\Omega_{\rm b}h^2$.

C. $m_\chi \gtrsim 30\,MeV$

In this region of masses the energy density of the particles at the time of nucleosynthesis is negligible since their number density is Boltzmann suppressed. As such, one recovers the SM predictions for the primordial element abundances.

Of course, the abundances of other light elements like ^{3}He or ^{7}Li are also affected by the presence of light thermal BSM particles. However, such abundances are not typically used as cosmological probes [99], and therefore we do not use them in this work. The interested reader is referred to Appendix A.5 for the effect of different types of thermal BSM particles on these abundances.

Expectations

From Figure 2.1 we notice that thermal species of mass $m_\chi \lesssim 0.4 - 3\,\text{MeV}$ will be ruled out by current $Y_{\rm P}$ measurements. Note that $Y_{\rm P}$ is only logarithmically dependent upon the baryon energy density $\Omega_{\rm b}h^2$. One might also expect current $\text{D/H}|_{\rm P}$ measurements to set stringent constraints on the mass of various BSM particles; about $m_\chi \lesssim 3 - 10\,\text{MeV}$. However, note that the $\text{D/H}|_{\rm P}$ predictions are shown for a fixed value of $\Omega_{\rm b}h^2$ and $\text{D/H}|_{\rm P} \propto \Omega_{\rm b}h^2$, thus deuterium measurements will only yield constraints provided that $\Omega_{\rm b}h^2$ is inferred from CMB observations or in conjunction with $Y_{\rm P}$ measurements.

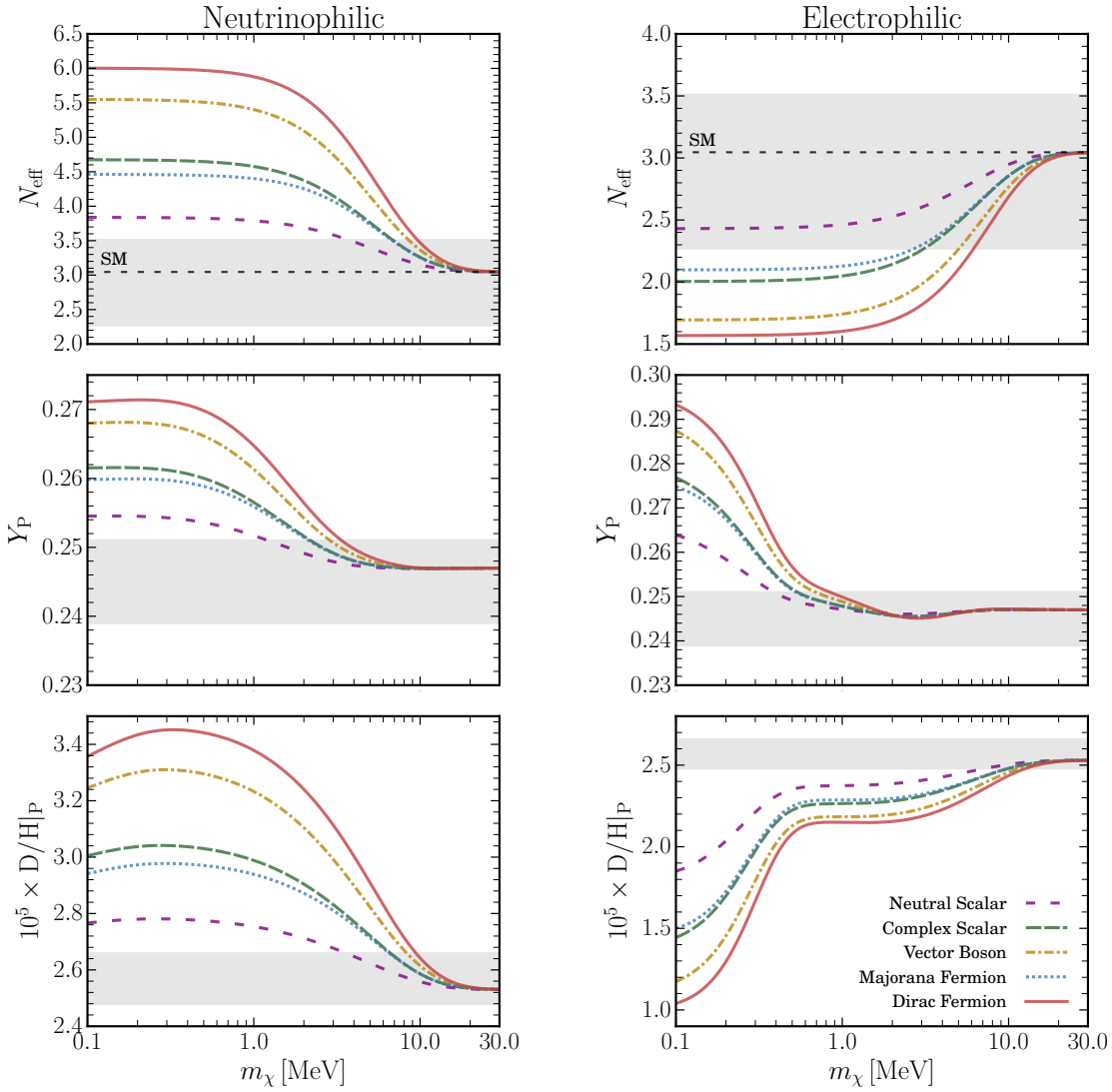

Figure 2.1 Cosmological impact of light BSM particles in thermal equilibrium with the SM plasma as a function of their mass m_χ. The *left/right panel* corresponds to neutrinophilic/electrophilic particles. *Upper panels:* The number of effective relativistic neutrino species $N_{\rm eff}$ as relevant for CMB observations. *Middle panels:* Primordial helium abundance $Y_{\rm P}$. *Lower panels:* Primordial deuterium abundance ${\rm D/H}|_{\rm P}$. The $Y_{\rm P}$ and ${\rm D/H}|_{\rm P}$ predictions are computed with $\Omega_{\rm b}h^2 = 0.021875$ and $\tau_n = 879.5\,{\rm s}$. The grey contours correspond to the mean $\pm 2\sigma$ measurements that enter our BBN and Planck data analyses, see Eqs. (2.9), (2.10) and (2.11).

Analysis	Cosmological Data	Description
BBN	($Y_{\rm P}$, D/H$\vert_{\rm P}$)	Mean values and error bars as recommended by the PDG. Theoretical uncertainties in the predictions are accounted for.
BBN+$\Omega_{\rm b}h^2$	($Y_{\rm P}$, D/H$\vert_{\rm P}$, $\Omega_{\rm b}h^2$)	Same as BBN but with $\Omega_{\rm b}h^2 = 0.02225 \pm 0.00066$ from CMB observations. This represents a conservative and model independent range for $\Omega_{\rm b}h^2$.
Planck	($\Omega_{\rm b}h^2$, $N_{\rm eff}$, $Y_{\rm P}$)	From the Planck2018-TTTEEE+lowE analysis. Assumes ΛCDM + varying $N_{\rm eff}$ and $Y_{\rm P}$.
Planck+H_0	($\Omega_{\rm b}h^2$, $N_{\rm eff}$, $Y_{\rm P}$)	From the Planck2018-TTTEEE+lowE+lensing+BAO+H_0 analysis. Assumes ΛCDM + varying $N_{\rm eff}$ and $Y_{\rm P}$.
Planck+BBN	($\Omega_{\rm b}h^2$, $N_{\rm eff}$, $Y_{\rm P}$)+ ($Y_{\rm P}$, D/H$\vert_{\rm P}$)	Joint constraint from Planck 2018 CMB observations and $Y_{\rm P}$ and D/H$\vert_{\rm P}$ determinations as recommended by the PDG.

Table II.1: Summary of the different baseline analyses carried out in this work in order to constrain light BSM particles in thermal equilibrium with the SM plasma during BBN. For each analysis, a likelihood is computed on a grid of ($\Omega_{\rm b}h^2$, m_χ).

2.2 Cosmological Data and Analysis

In order to set constraints on the masses of various BSM particles, we perform very conservative analyses using the latest determinations of the primordial element abundances and CMB observations by the Planck satellite as described below. Table II.1 provides a summary of the main data sets used in each analysis.

2.2.1 Big Bang Nucleosynthesis

We use the PDG recommended means and error bars for the observed primordial abundances of helium and deuterium, which at 1σ read [99]:

$$Y_{\rm P} = 0.245 \pm 0.003\,, \tag{2.5}$$

$$\mathrm{D/H}|_{\rm P} = (2.569 \pm 0.027) \times 10^{-5}\,. \tag{2.6}$$

These values are based on the analyses/measurements of [157–159] and [160–163] for helium and deuterium respectively. In addition to the observational uncertainties in $Y_{\rm P}$ and D/H$\vert_{\rm P}$, we account for theoretical uncertainties in the predicted abundances arising from uncertainties in the neutron lifetime[4] and various nuclear reaction rates. These are given by [111]:

$$\sigma(Y_{\rm P})^{\rm Theo} = 0.00017\,, \tag{2.7}$$

$$\sigma(\mathrm{D/H}|_{\rm P})^{\rm Theo} = 0.036 \times 10^{-5}\,. \tag{2.8}$$

[4]Since we account for the uncertainty in the neutron lifetime, in all analyses presented in this work, we shall fix the neutron lifetime to the default value in `PRIMAT`: $\tau_n = 879.5\,$s. This value is compatible with the PDG within 1σ, $\tau_n = 880.2 \pm 1\,$s [99]. Choosing $\tau_n = 880.2\,$s will not alter any of the results presented in this study.

Assuming Gaussian statistics and combining in quadrature the observational and theoretical errors, we define the following effective BBN χ^2:

$$\chi^2_{\rm BBN} = \frac{\left[Y_{\rm P} - Y_{\rm P}^{\rm Obs}\right]^2}{\sigma^2_{Y_{\rm P}}|^{\rm Theo} + \sigma^2_{Y_{\rm P}}|^{\rm Obs}} + \frac{\left[{\rm D/H}|_{\rm P} - {\rm D/H}|_{\rm P}^{\rm Obs}\right]^2}{\sigma^2_{{\rm D/H}|_{\rm P}}|^{\rm Theo} + \sigma^2_{{\rm D/H}|_{\rm P}}|^{\rm Obs}}\,, \tag{2.9}$$

which we will use to quantify deviations from the observed primordial abundances due to the presence of the new particles in the thermal bath.

2.2.2 Cosmic Microwave Background: Planck 2018

CMB observations measure very precisely three parameters that are relevant for our analysis: $\Omega_{\rm b}h^2$, $N_{\rm eff}$, $Y_{\rm P}$. The baryon abundance $\Omega_{\rm b}h^2$ is one of the 6 parameters in ΛCDM and Planck reports measurements on $\Omega_{\rm b}h^2$ with greater than 1% accuracy. $N_{\rm eff}$ represents one of the most important cosmological parameters and the current accuracy by the Planck satellite on this parameter is $\mathcal{O}(10\,\%)$. $Y_{\rm P}$ is also constrained by CMB observations, albeit with error bars that are typically a factor of 6 - 7 larger than those inferred from blue compact galaxies [99], see Equation (2.5).

In this work, we use the latest CMB observations by the Planck satellite to set constraints on the masses and interactions of various BSM particles. Since the disagreement between local [164] and CMB determinations of the Hubble constant [14] could potentially be attributed to additional contributions to $N_{\rm eff}$ [165, 166], we consider two data sets: *i)* in which we consider the 2018 Planck baseline TTTEEE+lowE analysis and *ii)* where we combine Planck CMB data with Baryon Acoustic Oscillation (BAO) measurements [167–169] and the local measurement of H_0 as reported by the SH0ES collaboration [164]. We shall call the former data set Planck and the latter Planck+H_0.

We build a Gaussian likelihood for the relevant parameters:

$$\chi^2_{\rm CMB} = (\Theta - \Theta_{\rm Obs})^T\, \Sigma^{-1}_{\rm CMB}\, (\Theta - \Theta_{\rm Obs})\,, \qquad \text{with} \qquad \Sigma_{\rm CMB} = \begin{pmatrix} \sigma_1^2 & \sigma_1\sigma_2\rho_{12} & \sigma_1\sigma_3\rho_{13} \\ \sigma_1\sigma_2\rho_{12} & \sigma_2^2 & \sigma_2\sigma_3\rho_{23} \\ \sigma_1\sigma_3\rho_{13} & \sigma_2\sigma_3\rho_{23} & \sigma_3^2 \end{pmatrix}, \tag{2.10}$$

where $\Theta = (\Omega_{\rm b}h^2,\, N_{\rm eff},\, Y_{\rm P})$ and

Planck 2018

$$\begin{aligned} (\Omega_{\rm b}h^2,\, N_{\rm eff},\, Y_{\rm P})|_{\rm Obs} &= (0.02225,\, 2.89,\, 0.246), \\ (\sigma_1,\, \sigma_2,\, \sigma_3) &= (0.00022,\, 0.31,\, 0.018), \\ (\rho_{12},\, \rho_{13},\, \rho_{23}) &= (0.40,\, 0.18,\, -0.69)\,, \end{aligned} \tag{2.11}$$

Planck 2018+BAO+H_0

$$\begin{aligned} (\Omega_{\rm b}h^2,\, N_{\rm eff},\, Y_{\rm P})|_{\rm Obs} &= (0.02345,\, 3.36,\, 0.249), \\ (\sigma_1,\, \sigma_2,\, \sigma_3) &= (0.00025,\, 0.25,\, 0.020), \\ (\rho_{12},\, \rho_{13},\, \rho_{23}) &= (0.011,\, 0.50,\, -0.64)\,, \end{aligned} \tag{2.12}$$

where the covariance matrix for the Planck 2018 analysis has been extracted from the Planck database [14, 170]. The covariance matrix for the Planck 2018+BAO+H_0 analysis was obtained by running a Markov-Chain-Monte-Carlo analysis using `CLASS` [171, 172] and `Monte Python` [173, 174] with Planck 2018 data [14, 170], various BAO measurements [167–169] and by including a Gaussian

likelihood on H_0 from the results of [164]. Clearly, the main implication of including local measurements of H_0 in the fit is the upward shift on the reconstructed value of $N_{\rm eff}$ from 2.89 to 3.36.

2.2.3 BBN+CMB Data Combinations

Combining measurements of the primordial element abundances and CMB observations proves useful in constraining light thermal species coupled to the SM plasma.

In this work, we will combine BBN+CMB data in two ways: *i)* by constructing a joint χ^2 that is obtained by summing the individual Planck and BBN χ^2's as defined in Eqs. (2.9) and (2.10) (labelled BBN+Planck across the paper) and *ii)* by adding to $\chi^2_{\rm BBN}$ a measurement of $\Omega_{\rm b}h^2 = 0.02225 \pm 0.00066$, which is to be regarded as a cosmological model-independent Planck determination of the baryon energy density[5] (we shall call this analysis BBN+$\Omega_{\rm b}h^2$). See Appendix A.4 for details.

2.2.4 Statistical Assessment

For each of the scenarios considered, the quantities $\chi^2_{\rm BBN}$ and $\chi^2_{\rm CMB}$ are computed on a grid of $(\Omega_{\rm b}h^2,\, m_\chi)$ and subsequently marginalized over $\Omega_{\rm b}h^2$. Then, by comparing the marginalized 1-D $\chi^2(m_\chi)$ with the minimum $\chi^2_{\rm min}$, we consider a scenario to be ruled out at 2σ when $\Delta\chi^2 \equiv \chi^2 - \chi^2_{\rm min} = 4$. The statistical compatibility of each $\chi^2_{\rm min}$ is estimated by computing its p-value, which is found to be acceptable in all cases presented in this work. This is as expected, given that BBN predictions and CMB observations are compatible with each other within the Standard Model.

2.3 Current Cosmological Constraints

Using different sets of cosmological observations, we set stringent constraints on the mass of various BSM species that are thermally coupled to the SM plasma. In Table II.1 we provide a summary of the data sets used in each analysis, and in Table II.2 we report the 95.4% CL lower bounds on the mass of such BSM species.

In order to illustrate the extent to which cosmological observations constrain the masses of light thermally coupled BSM species, we depict in the upper frames of Figure 2.2 the 1σ and 2σ confidence intervals in the $(\Omega_{\rm b}h^2,\, m_\chi)$ plane for our four baseline analyses for the case of a Majorana fermion. We observe degeneracies between $\Omega_{\rm b}h^2$ and m_χ in some regions of parameter space for the BBN analysis, but thanks to the precision with which the primordial element abundances are measured and the CMB is observed, a lower bound on m_χ can be set. From the lower panels of Figure 2.2 we see that neutrinophilic BSM states with $m_\chi \lesssim 1$ MeV are strongly disfavoured by BBN. In the case of electrophilic states, the same holds, albeit for relatively lighter BSM particles with $m_\chi \lesssim 0.3$ MeV. These results show that current cosmological observations set very stringent constraints on light species in thermal equilibrium during the time of BBN. In addition, the constraints derived from BBN are independent of the assumed cosmological model. In particular, BBN disfavours thermal particles with $m_\chi < 0.1$ MeV at more than 5σ – with the sole exception of a neutrinophilic neutral scalar that is disfavoured at 3.3σ. This is done only by using the observed values of $Y_{\rm P}$ and $\left.{\rm D/H}\right|_{\rm P}$.

[5] The value $\Omega_{\rm b}h^2 = 0.02225 \pm 0.00066$ has an error 4.4 times larger than the one associated with ΛCDM using Planck 2018 observations [14], and furthermore it covers well the inferred value of $\Omega_{\rm b}h^2$ in a well-motivated 12-parameter extension of ΛCDM using different data sets [175, 176].

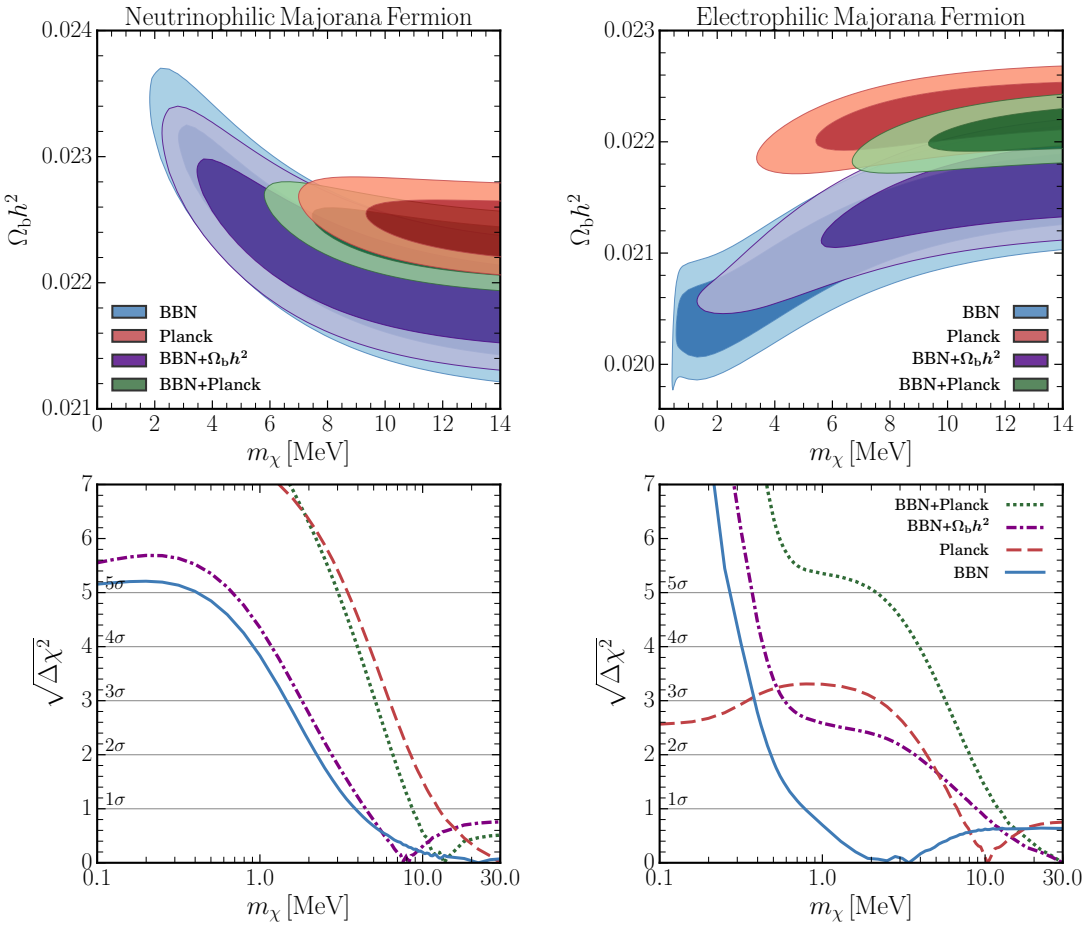

Figure 2.2 *Upper Panels:* Contour plots showing the 1σ and 2σ confidence intervals in the $(\Omega_b h^2, m_\chi)$ plane for a Majorana fermion with mass m_χ in thermal equilibrium with the SM plasma. *Lower Panels:* Marginalized $\Delta\chi^2$ as a function of m_χ. Solid lines correspond to BBN constraints, dashed to Planck CMB 2018 observations, dash-dotted to the combination BBN+$\Omega_b h^2$ and dotted to BBN+Planck. The *left/right panel* corresponds to neutrinophilic/electrophilic particles.

BBN and BBN+$\Omega_b h^2$

From Table II.2 we observe that from the current determinations of the primordial helium and deuterium abundances (BBN) alone we are able to place a lower bound on the mass of $m_\chi > 0.4$ MeV at 95.4% CL. This bound is independent of the spin, number of internal degrees of freedom of the species at hand and also of whether the particle interacts only with neutrinos or electrons/photons. We notice that the bounds for neutrinophilic species, $m_\chi > (1.2 - 3.7)$ MeV, are stronger as compared with the bounds for electrophilic species, $m_\chi > (0.4 - 0.7)$ MeV. When very conservative information about the value of $\Omega_b h^2$ from CMB observations is included (BBN+$\Omega_b h^2$), the bounds get slightly stronger to the level of $m_\chi > (1.3 - 4.4)$ MeV for neutrinophilic species and $m_\chi > (0.6 - 7.0)$ MeV for electrophilic ones. For more information on the range for $\Omega_b h^2$, see Appendix A.4.

Type	BSM Particle		Current Constraints					Forecasted Constraints	
	Particle	g-Spin	BBN	BBN+$\Omega_b h^2$	Planck	Planck+H_0	BBN+Planck	Simons Obs.	CMB-S4
Neutrinophilic	Majorana	2-F	2.2	2.8	8.4	4.9	6.6	12.5	13.5
	Dirac	4-F	3.7	5.4	11.3	8.0	9.4	15.3	16.2
	Scalar	1-B	1.2	1.3	5.6	1.6	3.7	9.8	10.7
	Complex Scalar	2-B	2.3	2.9	8.5	5.1	6.7	12.5	13.5
	Vector	3-B	3.1	4.4	10.1	6.8	8.3	14.1	15.1
Electrophilic	Majorana	2-F	0.5	3.7	4.4	9.2	8.0	12.2	13.2
	Dirac	4-F	0.7	7.0	7.4	12.0	10.9	14.9	15.9
	Scalar	1-B	0.4	0.6	2.4*	6.4	5.2	9.4	10.5
	Complex Scalar	2-B	0.5	4.0	4.6	9.2	8.1	12.2	13.2
	Vector	3-B	0.6	5.8	6.3	10.9	9.8	13.8	14.8

Table II.2: Lower bounds at 95.4% CL on the masses of various thermal BSM particles in MeV. The columns correspond to constraints using data from various sources as detailed in Sections 2.2 and 2.4 for current and forecasted constraints respectively. The rows correspond to BSM particles with a different number of internal degrees of freedom g and spin (F: fermion, B: boson). The upper/lower parts of the table correspond to purely neutrinophilic/electrophilic particles. *This bound is only at 86% CL.

Planck

From the Planck column in Table II.2 one can clearly see that Planck typically sets more restrictive constraints than BBN. For neutrinophilic relics $m_\chi > (5.6 - 11.3)\,\text{MeV}$, while for electrophilic relics $m_\chi > (4.4 - 7.4)\,\text{MeV}$. The sole exception to this is an electrophilic scalar boson that cannot be constrained at 2σ from Planck CMB observations (as can be seen from Figure 2.1). Nonetheless, we find that a lower bound of $m_\chi > 2.4$ MeV at 86% CL can still be set.

Planck+H_0

Planck constraints are based solely on CMB observations. However, the actual value of $N_{\rm eff}$ may be different if local determinations of the Hubble constant are taken into account as discussed in Section 2.2. We find that when local measurements of H_0, BAO data and Planck CMB observations are considered, the bounds for neutrinophilic relics are relaxed as compared to Planck data alone, while the bounds for electrophilic relics become stronger. This is because the inclusion of the local determination of H_0 results in a higher mean value of $N_{\rm eff}$, which leads to a preference for neutrinophilic relics that generally contribute to $N_{\rm eff} > N_{\rm eff}^{\rm SM}$. Still, this data combination rules out thermal BSM particles of $m_\chi > 1.6\,\text{MeV}$ at 95.4% CL.

BBN+Planck

Finally, when $Y_{\rm P}$ and $\text{D/H}|_{\rm P}$ data are combined with Planck CMB observations we find that the constraints for neutrinophilic species are slightly relaxed as compared to Planck alone, yielding $m_\chi > (3.7 - 9.4)\,\text{MeV}$, while the bounds get stronger for electrophilic relics, yielding $m_\chi > (5.2 - 10.9)\,\text{MeV}$. This is a mere result of a slight $\sim 0.9\sigma$ tension between the $\Omega_b h^2$ that is inferred from BBN and CMB observations [111]. Note that from the lower panels of Figure 2.2, Plank+BBN data strongly disfavours very light BSM thermal species.

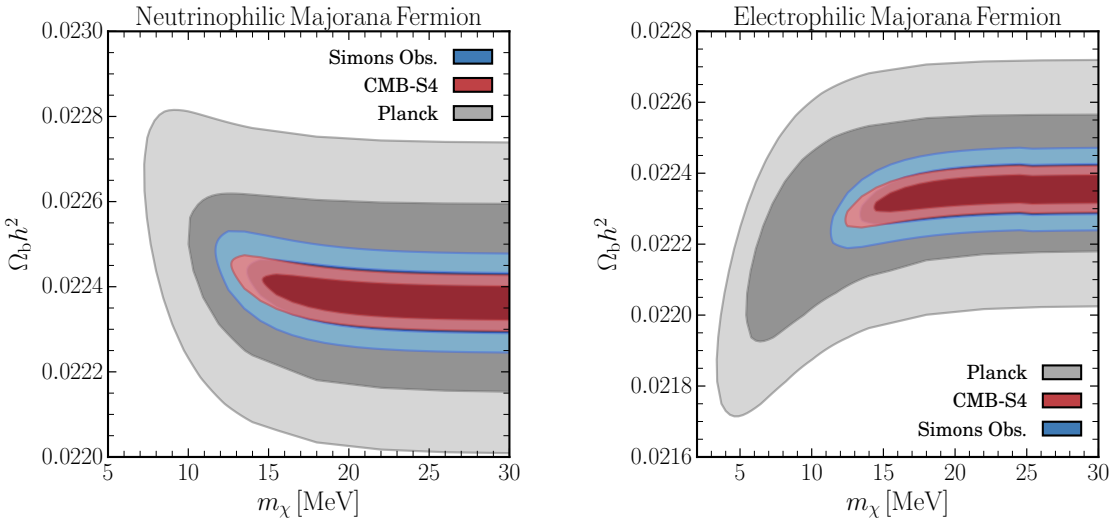

Figure 2.3 Contour plots showing the current and forecasted 1σ and 2σ confidence intervals in the $(\Omega_b h^2, m_\chi)$ plane for a BSM Majorana fermion in thermal equilibrium with the SM plasma during BBN. The grey contours correspond to current constraints by Planck 2018, while the blue and red contours correspond to the expected reach of the Simons Observatory and CMB-S4 experiments respectively. *Left*: Neutrinophilic. *Right*: Electrophilic.

Summary

We have set strong constraints from a combination of cosmological measurements, including the primordial helium and deuterium abundances and CMB observations by the Planck satellite. For the combination of BBN+Planck data, we find that the mass of purely electrophilic and neutrinophilic BSM species in thermal equilibrium with the SM plasma – independently of their spin and number of degrees of freedom – should satisfy $m_\chi > 3.7\,\text{MeV}$ at 95.4% CL.

2.4 Future Cosmological Constraints

2.4.1 Cosmic Microwave Background

There are a number of proposed future CMB experiments that would provide an accurate determination of the relevant cosmological parameters for this study: $\Omega_b h^2$, N_{eff}, Y_P. Proposed experiments include satellite missions like PICO [177] or CORE [178] and ground-based experiments like the Simons Observatory [179], CMB-S4 [180, 181] and CMB-HD [182]. In this section we consider the reach of the Simons Observatory[6], because it is fully funded and expected to deliver measurements within the next few years, and that of CMB-S4[7], because it aims to reach a sub-percent determination of N_{eff}.

We use the Fisher Matrix method to forecast the reach of CMB-S4 (see Appendix A.6 for details) and use the baseline covariance matrix from the Simons Observatory collaboration. In analogy with (2.10), the relevant parameters read:

[6] https://simonsobservatory.org/.
[7] https://cmb-s4.org/.

Simons Observatory	*CMB-S4*
$(\Omega_{\rm b}h^2,\, N_{\rm eff},\, Y_{\rm P})\vert_{\rm Fiducial} = (0.022360,\, 3.046,\, 0.2472)\,,$	$(\Omega_{\rm b}h^2,\, N_{\rm eff},\, Y_{\rm P})\vert_{\rm Fiducial} = (0.022360,\, 3.046,\, 0.2472)\,,$
$(\sigma_1,\, \sigma_2,\, \sigma_3) = (0.000073,\ \ 0.11,\, 0.0066)\,,$	$(\sigma_1,\, \sigma_2,\, \sigma_3) = (0.000047,\, 0.081,\, 0.0043)\,,$
$(\rho_{12},\, \rho_{13},\, \rho_{23}) = (0.072,\, 0.33,\, -0.86)\,,$	$(\rho_{12},\, \rho_{13},\, \rho_{23}) = (0.25,\, 0.22,\, -0.84)\,,$

Note that the forecasted errors on $N_{\rm eff}$ look substantially larger than what is typically quoted in the literature and this is simply a result of the fact we also allow $Y_{\rm P}$ to vary.

Figure 2.3 shows the reach of future CMB observations to m_χ and $\Omega_{\rm b}h^2$ for a Majorana fermion. From Table II.1, we notice that future CMB experiments will be able to probe substantially heavier BSM states than current CMB observations. In particular, the Simons Observatory is expected to set a lower bound on the mass of light BSM species of $m_\chi > 9.4$ MeV, while CMB-S4 is expected to extend this bound to $m_\chi > 10.5$ MeV, both at 95.4% CL.

2.4.2 Big Bang Nucleosynthesis

Forecasting the reach of future determinations of the light primordial element abundances is not straightforward. However, from an observational perspective, the precision with which the primordial deuterium abundance is measured, is expected to improve by an order of magnitude with upcoming 30 m telescope facilities [160, 183]. From a theoretical perspective, the nuclear reaction rates that significantly contribute to the error budget in the theoretical prediction of $\mathrm{D/H}|_{\rm P}$ are expected to be measured with higher accuracy by the LUNA collaboration [184]. It is therefore feasible that, in the near future, a per mille determination of $\mathrm{D/H}|_{\rm P}$ could be achieved. Regarding $Y_{\rm P}$, while the situation is much less clear, it is still conceivable that $Y_{\rm P}$ could be narrowed down with greater than 1 % accuracy in the future [183].

In order to account for many possible future scenarios, and in a similar spirit to [185], we estimate the reach of future measurements of $Y_{\rm P}$ and $\mathrm{D/H}|_{\rm P}$ to the mass of thermal BSM state by assuming that the measured values of $Y_{\rm P}$ and $\mathrm{D/H}|_{\rm P}$ correspond to the values as predicted by `PRIMAT` using $\Omega_{\rm b}h^2 = 0.02236$ and $\tau_n = 879.5$ s – namely, $Y_{\rm P} = 0.2472$ and $\mathrm{D/H}|_{\rm P} = 2.439 \times 10^{-5}$ – and by varying the joint theoretical + observational accuracy with which they are determined.

In Figure 2.4, we show the forecasted 2σ lower bounds on the mass of a Majorana fermion in thermal equilibrium with the SM plasma as a function of the fractional error in $Y_{\rm P}$ and $\mathrm{D/H}|_{\rm P}$. It is clear that the bounds are largely driven by helium measurements, while $\mathrm{D/H}|_{\rm P}$ measurements are instead expected to provide accurate determinations of $\Omega_{\rm b}h^2$. As such, if a prior for $\Omega_{\rm b}h^2$ is provided from CMB observations, then $\mathrm{D/H}|_{\rm P}$ measurements do play an important role in constraining light BSM species in thermal equilibrium with the SM plasma.

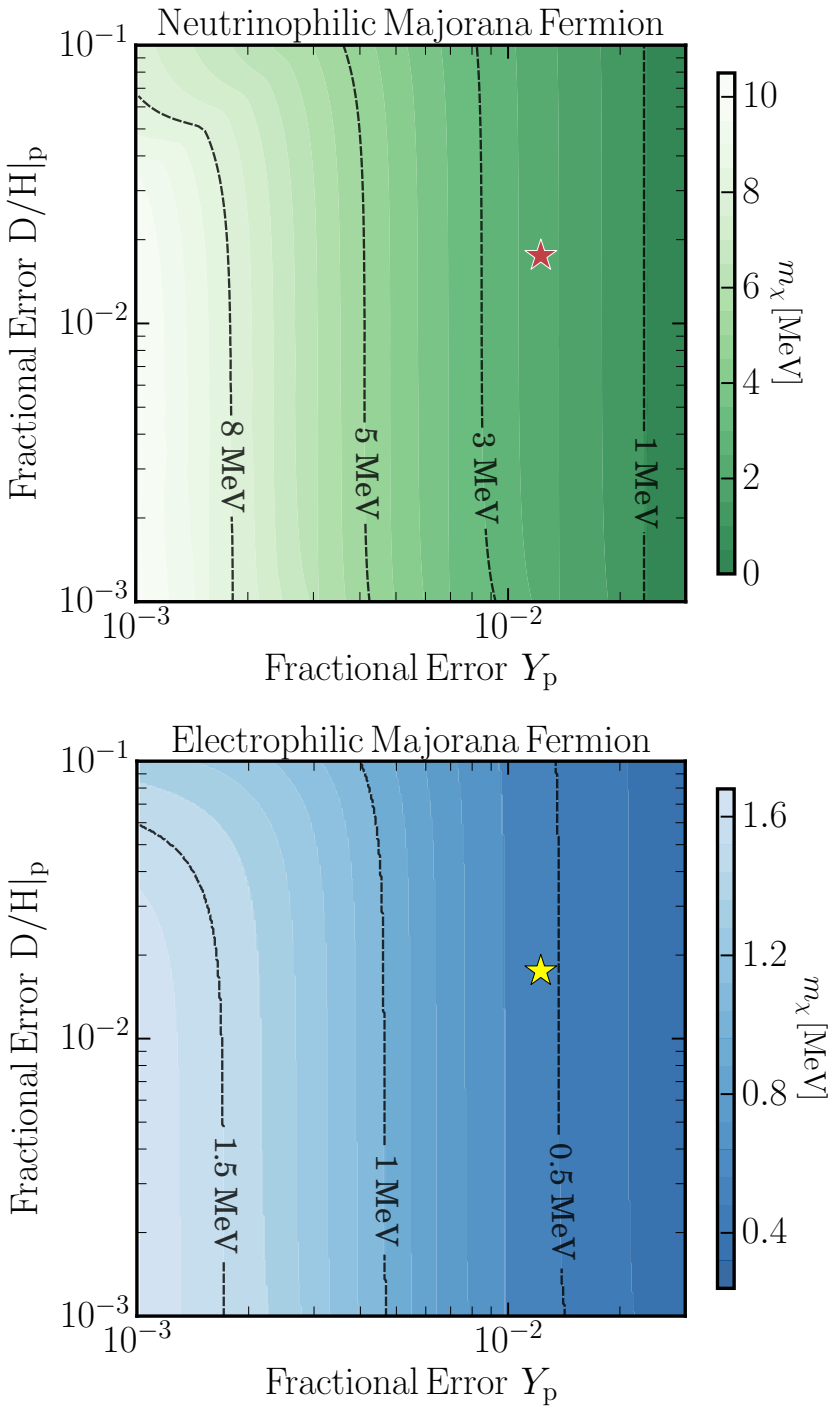

Figure 2.4 Projected 2σ exclusion limits for the mass of a Majorana BSM particle in thermal equilibrium during BBN. Bounds are shown as a function of the fractional errors (joint theoretical and observational) in the primordial helium and deuterium abundances. The red and yellow stars correspond to the current precision. *Top*: Neutrinophilic. *Bottom*: Electrophilic.

2.5 Discussion

In this section we comment on some of the implications of the constraints on thermal BSM species derived in this work. In particular, we discuss examples of theoretical scenarios in which these bounds are relevant, how the bounds are altered when additional BSM states are present and the robustness of our constraints with respect to non-standard expansion histories of the Universe. Finally, we provide a brief comparison with recent literature.

2.5.1 Particle Physics Scenarios

Our constraints on thermally coupled BSM species apply to various particle physics models, typically within the context of thermal dark matter. The bounds outlined in Table II.2 apply to both s-wave and p-wave annihilating thermal relics. Such bounds are particularly relevant for s-wave and p-wave dark matter particles annihilating to neutrinos [28–32], since they are difficult to test at neutrino experiments [3, 62–65]. In addition, these bounds will be relevant for p-wave annihilating relics to electrons and positrons, as in the case of Majorana/Dirac dark matter annihilating via dark photon/Higgs exchange [22–24, 35]. Furthermore, the bounds apply to species that need not to be the entirety of the dark matter, see e.g. [85], and have also been applied to scenarios in which dark matter particles interact with quarks [186].

The bounds derived in [1] for BSM species that annihilate into electrons and neutrinos with different ratios are, for instance, relevant for scenarios involving a gauging of SM global symmetries such as $U(1)_{L_\mu - L_\tau}$ [39, 187, 188] or $U(1)_{B-L}$ [189, 190]. Finally, these bounds also apply to asymmetric dark matter sectors interacting with SM species [191, 192]. Asymmetric dark matter set-ups require annihilation cross sections that are larger than for WIMPs, and as such thermal equilibrium in the early Universe is realised. Note, however, that these bounds do not apply to scenarios in which the given BSM species is never brought into thermal equilibrium, as in the case of freeze-in [41, 44], or simply for significantly smaller couplings than those outlined in Equations (2.2) and (2.3) [193]. For slightly smaller couplings than those in Equations (2.2) and (2.3), BBN can still serve as a useful probe [194].

The bounds presented in this study do not only apply to dark matter particles, but also to unstable mediators. For example, the bounds constrain relevant parameter spaces for various neutrinophilic scalars and vector bosons, regardless of whether they are related to dark matter [34, 63] or not [195]. Similarly, light dark Higgses or dark photons are also constrained. The constraints are particularly relevant for dark photons that decay into hidden sector species. Specifically, the bounds rule out MeV-scale dark photons that decay invisibly for kinetic mixing parameters in the range $10^{-7} \lesssim \epsilon \lesssim 10^{-5}$. This region of parameter space is mildly constrained from colliders, beam dump experiments and supernova cooling [79, 196, 197].

2.5.2 Modified Cosmological Histories

The bounds derived above were obtained assuming that only one particle alters the usual SM picture of a radiation dominated Universe between neutrino decoupling and recombination. Here we comment on

how we expect the constraints to be altered when additional BSM species are present or non-standard thermal histories are considered.

Typically, dark matter particles are accompanied with mediators of similar mass. The presence of two (or more) neutrinophilic/electrophilic particles in thermal equilibrium in the early Universe would result in stronger bounds on the individual masses of the particles as compared to those outlined in Table II.2. Another very plausible contribution to the energy density in the Universe during BBN and recombination is massless dark radiation adding to $\Delta N_{\rm eff}$. Massless dark radiation will contribute to the expansion rate of the Universe and hence lead to an enhancement of $Y_{\rm P}$ with respect to the SM prediction [96–98]. This is precisely the same effect as the light BSM particles we consider (see middle panels of Figure 2.1) and hence the BBN bounds should simply strengthen in such a scenario. The CMB constraints on the other hand, will be relaxed in the case of electrophilic particles [198] but strengthen for neutrinophilic species. Similarly, perhaps a more exotic non-negligible primordial leptonic asymmetry could be present and modify nucleosynthesis and $N_{\rm eff}$ as relevant for CMB observations [155]. In such a scenario, we expect the bounds presented here to be modified [199] but not substantially given the accuracy with which $N_{\rm eff}$ and the helium and deuterium abundances have now been measured.

One of the key assumptions to derive the bounds in this study was that the particles we consider must have been in thermal equilibrium. Since we know from both BBN and CMB observations that the Universe should have at least reached a temperature of $T > 1.8\,\text{MeV}$ [200, 201], the particles we consider will indeed have reached thermal equilibrium.

Another assumption in order to derive these bounds is that the baryon-to-photon ratio remains constant between the end of BBN and recombination. This is well justified on the basis that late time electromagnetic energy injections are strongly constrained by BBN [202–204] and CMB spectral distortions [205, 206].

2.5.3 Comparison with Previous Literature

The cosmological implications of MeV-scale thermal dark matter particles were highlighted a while ago in [100]. Since then, a number of groups [100–109] have used BBN and/or CMB observations to set constraints on the masses and properties of various thermally coupled species in the early Universe.

One of the main differences between previous studies and the one presented here is the accuracy with which the primordial element abundances have been calculated. In particular, we account for non-instantaneous neutrino decoupling in the presence of light BSM particles [109, 110] and we use the state-of-the-art BBN code `PRIMAT` [111]. With respect to previous CMB analyses, we find very similar results to those presented in [109] that accounted for the same effects and used Planck 2018 data. Regarding BBN constraints, we can differentiate between two types of studies: some that fixed the baryon-to-photon ratio to be the best-fit from CMB observations at the time [101, 102, 105, 108], while others allowed $\Omega_{\rm b}h^2$ to vary and then fitted it to measurements of $Y_{\rm P}$ and $\text{D/H}|_{\rm P}$ simultaneously with m_χ [103, 104, 107]. In this work, we marginalize over all possible values of $\Omega_{\rm b}h^2$. The comparison with each reference goes as follows: firstly, when comparing with [103], we find that the constraints presented in this work on purely electrophilic BSM states are a factor $1.5-2.5$ more stringent. Secondly, a direct comparison with [104] is not possible since there are no bounds reported from a BBN only

analysis. Thirdly, [107] did not found a BBN bound for a real neutrinophilic scalar boson at 95.4% CL while we find $m_\chi > 1.2\,\mathrm{MeV}$ at such CL. We believe that these differences with previous studies are largely driven by the use of more recent and precise determinations of Y_P and $\mathrm{D/H}|_\mathrm{P}$.

2.6 Conclusions

MeV-scale BSM species in thermal equilibrium with the Standard Model plasma during Big Bang Nucleosynthesis have important cosmological consequences, as can be seen from Figure 2.1. In this work, we have analyzed in detail and with precision the impact of such states on the synthesis of the primordial element abundances and CMB observations. To this end, we have modelled the early Universe evolution using the methods of [109, 110] and by modifying the state-of-the-art BBN code `PRIMAT` [111]. We have used a suite of cosmological observations, as summarized in Table II.1, to set constraints on the masses of various types of BSM states in thermal equilibrium with the SM plasma during BBN. We summarize the derived constraints in Table II.2 for purely electrophilic and neutrinophilic BSM states. The main conclusions that can be drawn from this study are:

- BBN observations set a lower bound on electrophilic/neutrinophilic thermal species of $m_\chi > 0.4/1.2\,\mathrm{MeV}$ at 95.4% CL. This bound is independent of the spin and the number of internal degrees of freedom of the species at hand. In particular, any WIMP, irrespective of its annihilation being s-wave or p-wave and the annihilation final state, is bounded to have $m_\chi > 0.4\,\mathrm{MeV}$ at 95.4% CL.

- Very light ($m_\chi < 0.1\,\mathrm{MeV}$) thermal relics are highly disfavoured by current measurements of the primordial light elements (at more than 5σ). The sole exception to this rule is a purely neutrinophilic neutral scalar state, which is nonetheless ruled out at 3.3σ.

- BBN and CMB observations jointly constrain neutrinophilic and electrophilic thermal BSM states to have a mass $m_\chi > 3.7\,\mathrm{MeV}$ at 95.4% CL. This bound is independent of the spin or internal degrees of freedom of the given species and applies to both s-wave and p-wave annihilating dark matter relics, as well as to unstable dark sector mediators. Table II.2 summarizes the constraints for various BSM states.

- We argue that the bounds presented in this study are expected to be strengthened in the presence of additional species beyond those considered here. In addition, bounds based on BBN are largely insensitive to modifications of the assumed cosmological model.

- In [1], there are also constraints set on BSM particles with masses $m_\chi \lesssim 20\,\mathrm{MeV}$ that interact with both electrons and neutrinos. Such states efficiently delay the process of neutrino decoupling, which allows BBN to constrain the temperature of neutrino decoupling to be $T_\nu^\mathrm{dec} > 0.34\,\mathrm{MeV}$ at 95.4% CL. Moreover, we find that decoupling temperatures $T_\nu^\mathrm{dec} < 0.2\,\mathrm{MeV}$ are highly disfavoured ($> 5\sigma$) by BBN and/or CMB observations.

- Future CMB experiments such as the Simons Observatory [179] and CMB-S4 [180, 181], will constrain generic thermal BSM particles of $m_\chi \lesssim (10-15)\,\mathrm{MeV}$. Similarly, we highlighted the

impact of future primordial helium and deuterium determinations to light BSM states in thermal equilibrium with the SM plasma during nucleosynthesis.

To summarize, cosmology strongly constrains new physics at the MeV scale. Cosmological constraints are competitive with and complementary to those from colliders, beam dump and neutrino experiments, (in)direct dark matter searches, as well as from astrophysical probes.

III | Inelastic Cosmic Ray Collisions

Dark Matter direct detection experiments lose sensitivity to sub-GeV particles due to prohibitively small nuclear recoil energies. On the other hand, previous work such as [113, 114] suggests that light dark matter may naturally lead to a sub-dominant flux of higher momenta particles. This would lead to a reinterpretation of the current direct detection limits. Here we present a calculation of such a flux arising from inelastic cosmic ray collisions in the atmosphere. We also derive limits from the XENON1T experiment and forecast the reach of the LZ detector.

3.1 Cosmic Ray Dark Matter Flux

We distinguish two possible sources for a dark matter flux arising from the mechanism described in the Introduction: inelastic cosmic ray collisions with protons in the interstellar medium and with the atmosphere on Earth. According to our calculations, the former yields a flux several orders of magnitude lower than the latter; therefore, we may safely neglect it and focus on our modelling of interactions at the atmosphere.

The incoming cosmic ray flux is taken to be the local interstellar proton spectrum parametrised as in Ref. [207]; alternatively we have also checked that using the AMS02 spectrum [208] leads to identical results. The differential intensity dI/dR as a function of particle rigidity R is converted to a flux $d\Phi_p/dT_p = 2\pi(dR/dT_p)(dI/dR)$ per unit area, time, and kinetic energy T_p, over a hemispherical solid angle. We performed a Monte-Carlo simulation of this incoming flux using EPOS-LHC [209], as implemented in the CRMC package [210], to simulate the collisions assuming the atmospheric nuclei target to be nitrogen at rest. The resulting π^0 and η mesons undergo two subsequent two-body decays via a vector or scalar mediator [1] to a pair of dark matter particles, with a branching ratio that we keep as a free parameter. The rate of interactions is then integrated as follows over the volume of the atmosphere to obtain the total dark matter flux at the detector.

The differential cosmic ray flux gets attenuated through the atmosphere as a function of height h from ground level:

$$\frac{d}{dh}\left(\frac{d\Phi_p}{dT_p}\right) = \sigma_{pN}(T_p) n_N(h) \frac{d\Phi_p}{dT_p}\,, \tag{3.1}$$

where σ_{pN} is the inelastic proton-nitrogen cross-section and n_N is the number density of air, taken from Ref. [211], which is assumed to be entirely nitrogen for simplicity. (3.1) neglects higher order effects

[1] Here we consider only on-shell mediators though the sensitivity could in principle be extended to heavier off-shell mediators.

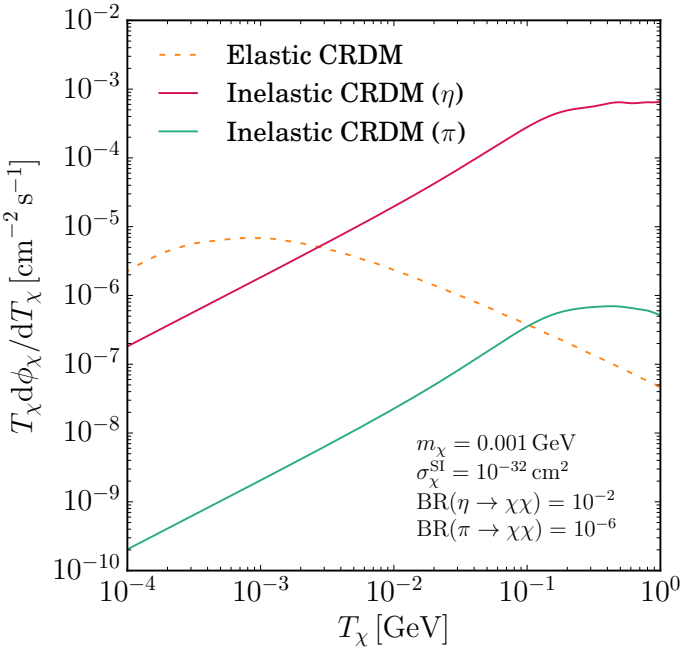

Figure 3.1 Dark matter flux from cosmic rays for elastic collisions in dotted orange with $m_\chi = 1$ MeV, and for inelastic collisions with $BR(\pi^0 \to \chi\chi + ...) = 10^{-6}$ in solid green and $BR(\eta \to \chi\chi + ...) = 10^{-2}$ in solid red.

such as regenerations and secondary scatterings involved in a detailed cosmic ray shower model, but it is sufficient to provide a conservative estimate of our hidden sector flux. Since $\sigma_{pN} \simeq 255$ mb is constant to a good approximation over the relevant energy range, we may write $\frac{d\Phi_p}{dT_p}(T_p, h) \equiv y(h) \cdot \frac{d\Phi_p}{dT_p}(T_p)$ and solve for the attenuation factor $y(h)$. The dark matter flux at a detector located at a depth z_d below ground is then given by

$$\frac{d\Phi_\chi}{dT_\chi} = \int_{R_E}^{R_E+h} R^2 dR \int_0^{2\pi} d\phi \int_{\cos\theta_{\max}}^{1} \frac{d(\cos\theta)}{2\pi l\,(R,\theta,z_d)^2}$$
$$y\,(R-R_E)\,\frac{d\Phi_p}{dT_p} n_N\,(R-R_E)\,\sigma_{pN\to M} BR_{M\to\chi\chi} \equiv \frac{d\Phi_p}{dT_p} n_N^0 H_{\mathrm{eff}} \sigma_{pN\to M} BR_{M\to\chi\chi} \tag{3.2}$$

where R_E is the radius of the Earth and $\theta_{\max}$ is a maximum angle dependent on the path length attenuation through the Earth, as described in the next Section. The line of sight distance $l(R, \theta, z_d)$ is given by

$$l^2 = (R_E - z_d)^2 + R^2 - 2(R_E - z_d) R \cos\theta\,. \tag{3.3}$$

It determines the rate dilution factor in the emission from source to detector that we have conservatively assumed to be isotropically distributed over a hemisphere. In the last line of (3.2) we defined an equivalent effective height at a constant number density taken to be the ground-level value, $n_N^0 \simeq 5 \times 10^{19}\mathrm{cm}^{-3}$ [211]. For example, with $\cos\theta_{\max} = -1$, i.e. the Earth completely transparent to dark matter, we obtain $H_{\mathrm{eff}} \simeq 5$ km.

The resulting dark matter flux in the transparent Earth case is plotted in Fig. 3.1 in solid red for $BR(\eta \to \chi\chi + ...) = 10^{-2}$ and green for $BR(\pi^0 \to \chi\chi + ...) = 10^{-6}$, close to their experimental upper limits. The fluxes are rather insensitive to the mediator and dark matter masses when these are produced on-shell. For comparison, we show in dotted orange the up-scattered flux for $m_\chi = 1$ MeV coming from elastic collisions of cosmic rays with interstellar dark matter, calculated as in Ref. [113]. Finally we have also checked that, when restricting to an opaque Earth, the muon flux obtained in our approach is in good agreement with data [212, 213].

3.2 Attenuation through the Earth

As dark matter travels from the point of production through the Earth a large enough nucleus interaction cross-section can prevent it from reaching the detector. The mean free path length together with the line of sight distance through the Earth to the detector then determines the maximum polar angle at which we cut off the atmospheric volume integral in (3.2). This line of sight distance through the Earth is given by

$$\begin{aligned} l_E &= \frac{1}{2}\left(b + \sqrt{b^2 + 4(R_E^2 - (R_E - z_d)^2)}\right) , \\ b &\equiv \text{Sign}\left[R_E - z_d - (R_E + h)\cos\theta\right] \\ &\quad \times 2(R_E - z_d)\sqrt{1 - \frac{(R_E + h)^2 \sin^2\theta}{l^2}} . \end{aligned} \tag{3.4}$$

The mean free path length is determined by solving for the kinetic energy loss assuming a uniform distribution of nuclear recoil energy in elastic scattering, $d\sigma_{\chi N}/dT_r = \sigma_{\chi N}/T_r^{\max}$, following Ref. [113]. Summing over the nuclei N, we then have

$$\frac{dT_\chi}{dz} = -\sum_N n_N \int_0^{T_r^{\max}} \frac{d\sigma_{\chi N}}{dT_r} T_r dT_r \underset{(T_\chi \ll m_N)}{\simeq} -\frac{1}{2m_\chi L}\left(T_\chi^2 + 2m_\chi T_\chi\right) ,$$

where we used

$$T_r^{\max} = \frac{T_\chi^2 + 2m_\chi T_\chi}{T_\chi + (m_\chi + m_N)^2/(2m_N)} , \tag{3.5}$$

and defined the mean free path length

$$L \equiv \left(\sum_N n_N \sigma_{\chi N} \frac{2m_N m_\chi}{(m_\chi + m_N)^2}\right)^{-1} . \tag{3.6}$$

Integrating this equation gives the incoming energy T_χ^0 that is required to arrive at the detector with energy T_χ^z a distance l_E through the Earth:

$$T_\chi^0 = \frac{2m_\chi T_\chi^z e^{l_E/L}}{2m_\chi + T_\chi^z(1 - e^{l_E/L})} . \tag{3.7}$$

From this we obtain $\theta_{\rm max}$ when $T_\chi^0 \to \infty$. The mean free path length is calculated by summing over the average number density of the elements given in Table 2 of Ref. [214]. We relate the nuclear interaction cross-section to the per nucleon spin-independent cross-section $\sigma_\chi^{\rm SI}$ as

$$\sigma_{\chi N} = \sigma_\chi^{\rm SI} A^2 \left(\frac{m_N}{m_p} \frac{(m_\chi + m_p)}{(m_\chi + m_N)} \right)^2 . \tag{3.8}$$

In practise we find that at the depth of the XENON1T detector the attenuation starts cutting off the atmospheric volume integral for cross-sections above $\sigma_\chi^{\rm SI} \gtrsim 10^{-32}\,{\rm cm}^2$, with transmission falling exponentially above $\sim 10^{-28}\,{\rm cm}^2$.

3.3 Limits

Finally, we obtain the expected rate at a detector coming from our inelastic cosmic ray dark matter flux by integrating within the detector nuclear recoil thresholds T_1 and T_2:

$$\Gamma_N = N_T \int_{T_1}^{T_2} dT_N \int_{T_\chi^{\rm min}(T_N)}^{\infty} dT_\chi \epsilon(T_N) \frac{d\Phi_\chi}{dT_\chi} \frac{d\sigma_{\chi N}}{dT_N} , \tag{3.9}$$

where N_T is the number of target atoms, ϵ is the detector nuclear recoil energy efficiency, and

$$T_\chi^{\rm min} = \left(\frac{T_N}{2} - m_\chi \right) \left(1 \pm \sqrt{1 + \frac{2T_N}{m_N} \frac{(m_\chi + m_N)^2}{(2m_\chi - T_N)^2}} \right) , \tag{3.10}$$

with a plus sign if $T_\chi > 2m_N$ and minus sign otherwise. As an illustrative example we will focus on the limits from XENON1T. Its nuclear recoil energy threshold window is from $T_1 = 4.9$ keV to $T_2 = 40.9$ keV and the detector is located at a water-equivalent depth of 3.6 km, corresponding to 1.4 km of rock [10]. For the 90% CL limits we require a total number of events $N_{90\%\ \rm CL} = 3.56$ for the full exposure of 278.8 days of data collection with 1.3t fiducial mass. This event count, in Table 1 of Ref. [10], is the best fit given by a likelihood analysis for a 200 GeV WIMP whose recoil spectrum is comparable to that of the energetic light dark matter flux.

For comparison with Ref. [113], we first assume a uniform recoil energy distribution, $d\sigma_{\chi N}/dT_N = \sigma_{\chi N}/T_{r,N}^{\rm max}$, and similarly obtain the resulting XENON1T limits on $\sigma_\chi^{\rm SI}$. This is plotted in Fig. 3.2 as a function of the dark matter mass for a fixed mediator mass and branching ratio values (*top*), and as a function of the meson branching ratio into dark matter for a fixed mediator and dark matter mass (*bottom*). The 90% CL limits on inelastic cosmic ray dark matter from π^0 and η decays are shown in green and red, respectively. As mentioned previously, the dark matter flux is relatively insensitive to their masses when these are light enough to be produced on-shell. We note that despite the rate of neutral pion production being an order of magnitude larger than for η mesons, the branching ratio of pions is experimentally bounded to be at most $\sim 10^{-6}$ [213]. The projected limits for the future LZ experiment [121] are shown as dashed lines; we see that they improve on the cross-section sensitivity by almost two orders of magnitude. The corresponding limits from the irreducible flux of up-scattered dark matter for $m_\chi = 1$ MeV is given by the orange band and is independent of branching ratio.

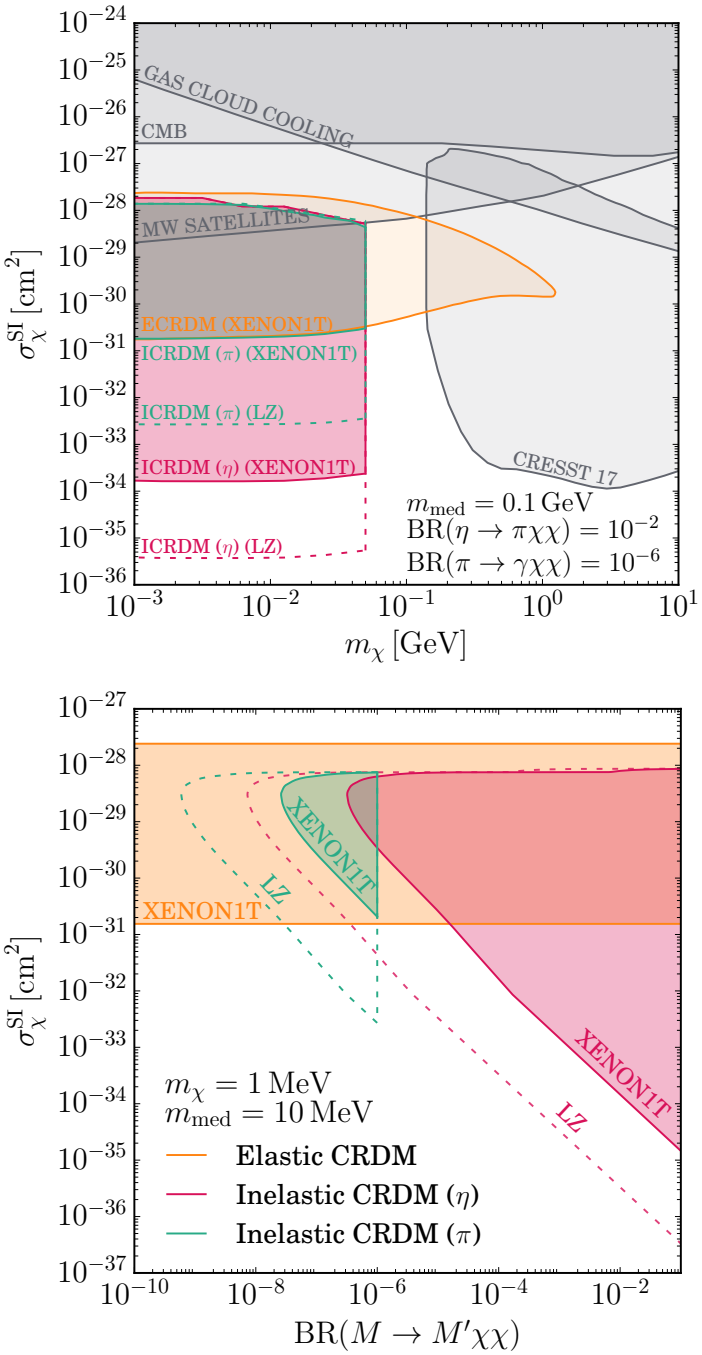

Figure 3.2 90% CL limits on the spin-independent dark matter-nucleon cross-section as a function of dark matter mass for a fixed branching ratio (*top*) and as a function of branching ratio for a fixed dark matter mass (*bottom*), as labelled. The inelastic cosmic ray dark matter limits from XENON1T [10] are indicated in red and green for the flux originating from meson $M = \eta$ and π^0 decays, respectively, and in orange for elastic cosmic ray dark matter. The dashed lines are projections for the future LZ experiment [121]. Other limits in grey are taken from Ref. [113] (based on CRESST [215], CMB [83], and gas cloud cooling [216]), and from Milky-way satellites [217].

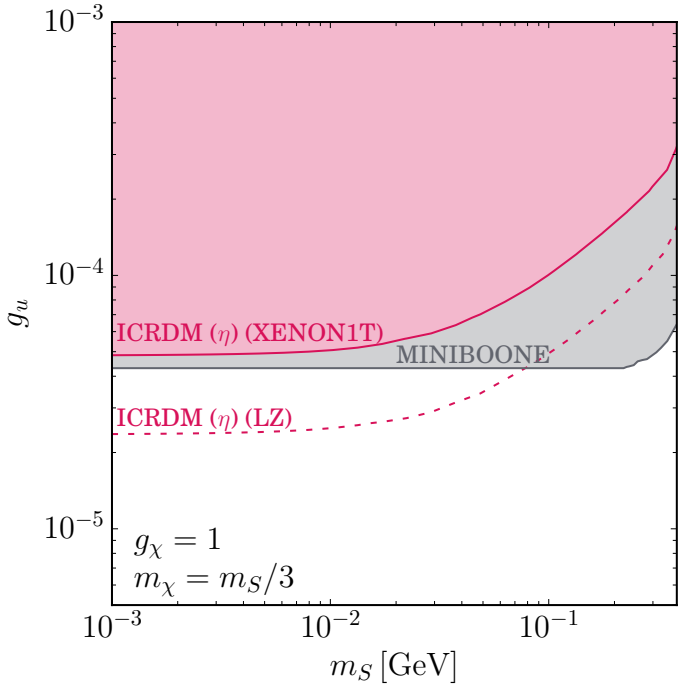

Figure 3.3 90% CL limits from inelastic cosmic ray dark matter flux from η decays in red, for a hadrophilic scalar mediator of mass m_S with up-quark coupling g_u, setting $g_\chi = 1, m_\chi = m_S/3$. The solid line denotes current limits from XENON1T [10]; the dashed line are future projections for the LZ experiment [121]. Current MiniBooNE limits from Ref. [122] are shown in grey.

However, there is a (model-dependent) relation between the two—a dark matter coupling to nucleons will generically induce meson decay into dark matter, if kinematically allowed.

Next, we consider the hadrophilic scalar mediator model of Ref. [123]. The singlet scalar S couples to a Dirac fermion dark matter χ and to the up quark through the Lagrangian terms

$$\mathcal{L} \supset -g_\chi S \bar{\chi}_L \chi_R - g_u S \bar{u}_L u_R + \text{h.c.}\,. \tag{3.11}$$

The couplings to other flavours are assumed to be sub-dominant, so that we are left with four free parameters characterising the simplified model: m_S, m_χ, g_u, and g_χ. The branching ratio of η mesons decaying into dark matter is given by

$$BR(\eta \to \pi^0 S) = \frac{C^2 g_u^2 B^2}{16\pi m_\eta \Gamma_\eta} \lambda^{1/2}\left(1, \frac{m_S^2}{m_\eta^2}, \frac{m_\pi^2}{m_\eta^2}\right), \tag{3.12}$$

where $B \simeq m_\pi^2/(m_u + m_d)$, $C \equiv \sqrt{1/3}\cos\theta' - \sqrt{2/3}\sin\theta'$ with $\theta' \simeq -20^\circ$ and $\lambda(a,b,c) = a^2 + b^2 + c^2 - 2ab - 2bc - 2ac$. We assume here that $BR(S \to \chi\chi) = 1$. For the differential χ-nucleus cross-section

involving a scalar mediator we have

$$\frac{d\sigma_{\chi N}}{dT_N} = \frac{\left(Z y_{Spp} + (A-Z) y_{Snn}\right)^2 g_\chi^2}{8\pi} \times \frac{(2m_N + T_N)(2m_\chi^2 + m_N T_N)}{(T_\chi^2 + 2m_\chi T_\chi)(2m_N T_N + m_S^2)^2} F_H^2(\sqrt{2m_N T_N}) \,, \tag{3.13}$$

where Z ($A-Z$) are the number of protons (neutrons), $y_{Spp} = 0.014 \cdot g_u m_p/m_u$, $y_{Snn} = 0.012 \cdot g_u m_n/m_u$, and F_H is the Helm form factor [218]. Computing the rate as described above, we obtain the 90% CL limits shown in Fig. 3.3 in red on the g_u vs m_S plane, for $g_\chi = 1, m_\chi = m_S/3$. The Earth suppresses the flux significantly only for values of g_u greater than displayed. The MiniBooNE limits from Ref. [123] are shown in grey. Note that for $g_\chi = 1$ the constraints from the E787/E949 experiment are stronger than the MiniBooNE and XENON1T limits [123]; however, they are set by invisible Kaon decays and are independent of g_χ, whereas direct detection constraints from η decay sources will grow quadratically with the dark matter coupling.

3.4 Summary and Conclusions

As the search for dark matter broadens, it is becoming increasingly important to maximise every resource that we have, both technological and astrophysical. In this respect cosmic rays provide a valuable tool. It has long been appreciated that cosmic rays are a natural accelerator for probing high energies, or as a background to indirect signals of dark matter decay; here we studied the potential of cosmic rays as a *source* of dark matter for direct detection. This opens up the potential of extending the sensitivity of various experiments to explore complementary parameter space, as we have illustrated for the case of XENON1T. It is remarkable that in this example the resulting limits are comparable to dedicated beam dump experiments such as MiniBooNE. These limits will improve in the future with the LZ experiment, by about two orders of magnitude. In forthcoming work we also plan to study the sensitivity of neutrino detectors, as well as cosmic ray production of long-lived hidden sectors that can decay back to Standard Model particles.

IV | Dark Matter at IceCube

The existence of a mass for the SM neutrino is a puzzle within the vanilla $\mathrm{SU}(3) \times \mathrm{SU}(2) \times \mathrm{U}(1)$ picture of particle physics. As such, it provides an interesting technical challenge to build extensions to the SM that solve this problem. Of interest in this Chapter is an effective theory which contains a stable Dark Matter candidate as well as radiatively generating neutrino masses. We consider the effect of such a model on the propagation of neutrinos across the Universe. In particular we look at how the mean free path is modified, and compare this to sources identified at the IceCube neutrino observatory. We use this to place limits on parameters in the model which are competitive and complementary to those from cosmology, astrophysics, and collider searches.

4.1 How to Generate a Neutrino Mass

In the neutrino sector, there are two possible types of mass term in the Lagrangian [130, 132, 143, 219];

- *Dirac Neutrino Masses* arise after the introduction of a right-handed neutrino field ν_R^i with $i = e, \mu, \tau$. The mass then arises under the Higgs mechanism due to a coupling;

$$\mathcal{L}_{\mathrm{lept},\phi} \propto \lambda^{ij} \bar{\psi}^i \Phi \ell^j + \lambda_\nu^{ij} \bar{\psi}^i \Phi^c \nu_R^i \tag{4.1}$$

  where ψ^i is the left handed SU(2) lepton doublet, Φ is the SU(2) Higgs doublet, and ℓ^j is the right-handed lepton singlet. After electroweak symmetry breaking (EWSB), the neutrinos get a mass term;

$$-\sum_i m_\nu^i \left(\bar{\nu}_R^i \nu_L^i + \bar{\nu}_L^i \nu_R^i\right) \tag{4.2}$$

- *Majorana Masses* are a qualitatively different scenario that is possible if the fermion is neutral, as in the case of the neutrino. In this case, the right-handed neutrino field is not independent of the left-handed one.[1] The mass term becomes;

$$-\frac{1}{2}\sum_i m_\nu^i \left(\bar{\nu}_L^{i,c} \nu_L^i + \bar{\nu}_L^i \nu_L^{i,c}\right) \tag{4.3}$$

[1] To be precise, $\nu_R(x) = \nu_L^c(x)$ where c represents the charge conjugated field.

We will focus on the second scenario. This can't arise at tree level in the Standard Model. The lowest dimension for which such a term is generated is at dimension 5 via an operator of the form [124];

$$\Lambda^{-1}\phi^0\phi^0\nu_L^i\nu_L^j \tag{4.4}$$

Being dimension 5, the operator is not renormalisable, and as such this can only be an effective coupling, valid up to some large mass scale Λ.

4.2 The Low Energy Effective Field Theory

The discussion of UV complete theories [135, 138, 140] presents a concrete scenario to implement the ideas of radiatively generating neutrino mass, as well as providing a dark matter candidate. On the other hand, at a given low energy scale, our experiments will not be able to probe the UV structure of the theory, only the effective degrees of freedom remaining at the scale in question (e.g. the energy scale at the LHC, or in cosmological scenarios).

In this section, we will present a low energy effective theory that contains a scalar Dark Matter candidate coupled to neutrinos. This was originally proposed in [125, 135, 138, 142, 143]. A key distinction will be between real and complex scalar Dark Matter, since the two have qualitatively different constraints. We will focus on the phenomenological consequences of the model and be as clear as possible as to exactly what constraints these place on the couplings and masses within the theory. These include astrophsyical, particle physics, and cosmological bounds [125, 135, 138, 142, 143]. To see how the model radiatively generates neutrino masses, see Appendix B.1.

It is not within the scope of this work to present a full UV completion of this effective theory. Nonetheless, [135, 138] present such a completion in the real case. In [140] the same is done for complex dark matter. The fact that the particle content of the effective model can arise from a fully gauge invariant theory is important since it provides a clear understanding of where the relevant degrees of freedom come from, as well as the scale of new physics.

4.2.1 Lagrangian and Particle Content

Our focus is on a low energy particle spectrum that consists of the Standard Model along with [125, 142];

- A scalar field, δ, which may be real or complex;
- Two or more massive right-handed fermions N_R^i, in what follows, we will assume these to be of *Majorana* type.

In addition to this, we assume that there is a residual $\mathbb{Z}_2$ symmetry [129, 132, 136] under which the new particles are odd, and the Standard Model is even. This has a number of effects;

1. It ensures that the lightest particle in the spectrum is stable, providing a Dark Matter candidate.
2. It prohibits a term of the form $\phi^0 \bar{N}_R^i \nu_L^\alpha$, so that after EWSB, there is no Dirac mass term linking N_R^i and ν_L^α. This means that the neutrino mass is not generated at tree level.
3. The new scalar, δ, cannot acquire a VEV, due to the structure of the Higgs sector.

The key feature we are interested in however is the interaction part of the Lagrangian which couples this new dark sector to the neutrino sector in the Standard Model. In our effective theory, we take the couplings to be of the form;

$$g_{i\alpha} \delta \bar{N}_R^i \nu_L^\alpha + \text{h.c.} \tag{4.5}$$

Where there is an implicit sum over the right-handed fermion species, i, and the Standard Model neutrino species, α. Later we will be interested in constraining the values of the coupling constants. To see the explicit contributions to the neutrino mass see Appendix B.1.

4.2.2 Astrophysical, Cosmological, and Particle Physics Constraints

So far we have illustrated (i) how neutrino mass is generated within the effective framework, and, (ii) discussed which are the relevant degrees of freedom when it comes to suitable dark matter candidates. We now discuss the vital question as to what constraints have already been placed on the model across a range of scenarios. We will investigate the constraints that arise from the two key scenarios [125, 135, 137, 138, 142, 143];

1. The cosmological bound on the Dark Matter annihilation cross section;
2. The bounds that arise due to light meson and tau decay.
3. Bounds that arise from observations of the CMB and Big Bang Nucleosynthesis (BBN)

For completeness, we will also discuss some of the other astrophysical bounds in slightly more general terms.

Dark Matter Annihilation Cross Section

Within this effective model, there are three annihilation channels in the case that N_R^i is a Majorana fermion, given by $\delta\delta \to \{\nu\nu, \nu\bar{\nu}, \bar{\nu}\bar{\nu}\}$. As in [143], we take $\Lambda \sim 200\,\text{GeV}$, $0.01\,\text{eV} < m_\nu < 1\,\text{eV}$. Furthermore, we also use the fact that sub-GeV Dark Matter requires $\langle \sigma v \rangle \simeq 5 \times 10^{-26}\,\text{cm}^3\text{s}^{-1}$ in order for the correct relic abundance to be obtained [220].

Real Scalar Dark Matter

In the real case, this gives the constraints;

$$\mathcal{O}(1\,\text{MeV}) \lesssim m_\delta < m_N \lesssim 10\,\text{MeV}, \quad 3 \times 10^{-4} \lesssim g \lesssim 10^{-3} \tag{4.6}$$

This is a strong bound on the coupling, and in fact we can *only* obtain new constraints in the complex case. The real case is too weakly coupled. From now on therefore, whilst we will of course mention the real case, our focus will be on the complex scenario.

Complex Scalar Dark Matter

In the complex case [143], we get less stringent constraints on the masses;

$$(1\,\mathrm{MeV})^2 \lesssim \left|m_{\delta_2}^2 - m_{\delta_1}^2\right| \lesssim (20\,\mathrm{MeV})^2 \tag{4.7}$$

We note that now m_N is a free parameter, so is far less constrained than in the real case. In turn, this implies that g is less constrained, although we shall see that there are different bounds due to light meson decay.

Light Meson and Tau Decay

Consider the decay $K^+ \to e^+/\mu^+ + \nu$ [125, 138, 142]. Then generically if the coupling in (4.5) is present, new decay modes $K^+ \to e^+/\mu^+ + N_R^i + \delta$ should exist. This means we should see $K^+ \to e^+/\mu^+ +$ missing energy compared to the Standard Model. This can be tested by experiments such as KLOE. Importantly, in this case the bounds are valid in the real *and* complex scenarios. They are presented in [125, 138, 139, 142];

$$\sum_i |g_{ie}|^2 < 10^{-5}, \quad \sum_i |g_{i\mu}|^2 \lesssim 10^{-4}, \quad \sum_i |g_{i\tau}|^2 < 10^{-1} \tag{4.8}$$

There are a couple of important observations that need to be made with respect to these bounds;

- Provided $\max(m_\delta, m_{N^i}) \ll m_{K,\pi} \simeq \mathcal{O}(500\,\mathrm{MeV})$, the bounds are similar in both the complex and the real case;
- With the bounds as above, we note that the couplings themselves can have magnitudes;

$$|g_{ie}| \lesssim 3 \times 10^{-3}, \quad |g_{i\mu}| \lesssim 10^{-2}, \quad |g_{i\tau}| \lesssim 3 \times 10^{-1} \tag{4.9}$$

- In the heavy case [142], $m_K < m_\delta + m_{N^i} < m_D$, where m_D is the mass of the D meson, the bounds above do not apply. Instead the strongest bounds have $|g_{ie}| \lesssim 0.4$ and $g_{i\mu} \lesssim \mathcal{O}(1)$.

CMB Constraints on the Scalar Mass

There are additional constraints on light particle dark matter that arise from measurements of the CMB, the light element abundance, and the expansion rate of the Universe. They apply here because, firstly, the existence of a light species such as our dark matter candidate during BBN at $z \sim 3 \times 10^8$ could change the rate of expansion and hence the time of weak freeze-out, changing relic abundances. Secondly, additional energy might be injected into the neutrino sector as this dark matter candidate annihilates. The relevant constraints are shown in Table IV.1 and are based on [134], [221], and [222].

Kinematically, the constraints are relevant in this scenario because the centre of mass energy of the $\nu\nu \to \delta\delta$ interaction determines the maximum mass m_δ of the scalar particle that can be produced;

$$m_\delta \leq \frac{1}{2}\sqrt{s} = \frac{1}{2}\sqrt{2E_\nu m_\nu} \tag{4.10}$$

Constraint	Mass Bound [MeV]	Min. Neutrino Energy [PeV]
N_{eff} [134]	3.90	0.76
BBN + Planck + N_{eff} + Y_p [221]	6.74	2.27
BBN + Planck + N_{eff} [221]	6.98	2.43
Planck + BAO + H_0 + N_{eff} [222]	7.80	3.04

Table IV.1: Table illustrating the constraints on complex scalar dark matter coming from various cosmological sources as well as the corresponding minimum neutrino energy that would need to be observed to probe parameter space outside of these bounds.

where E_ν is the energy of the high-energy neutrino from the blazar. We see therefore that the CMB bounds on the mass of the scalar are related to a minimum neutrino energy above which the method set out in this paper will probe parameter space unconstrained by the CMB, although we note this is not quite the case for the currently observed event. Stated another way the fact we are only sensitive to MeV scale dark matter is partly due to the centre of mass energy for the $\nu\nu \to \delta\delta$ interaction being less than the threshold energy for larger scalar masses. The 290 TeV neutrino is not at the upper end of the expected blazar neutrino flux distribution, so it is not unreasonable to expect that higher energy neutrinos will be observed, immediately allowing us to probe higher mass regimes, less sensitive to CMB constraints. To investigate this quantitatively, we choose $m_\nu = 0.04\,\text{eV}$ to be the lightest neutrino species. This ensures that $\sum m_\nu < 0.17\,\text{eV}$. Then, for each bound we may compute the minimum neutrino energy that must be observed to probe new parameter space. These reference neutrino energies are also shown in Table IV.1. We consider how this maps onto the expected constraints that would be obtained with observations of higher energy neutrinos in Figure 4.1.

As a final comment, there is work being done currently that re-explores some of the assumptions in deriving these constraints based on entropic or decay arguments, see for example [223]. Figure 3 in [224] proves a useful reference to see the separate constraints from BBN and the CMB. With this in mind, we view the bounds presented in this paper as complementary to those from Cosmology, requiring different (in this case astrophysical) assumptions.

Additional Constraints

The two methods of constraining the effective theory given above provide the most stringent bounds on the couplings and the masses. Furthermore, they also provide two very distinct scenarios for comparison. The first investigates the phenomenology in the setting of thermalizing early universe cosmology, whilst the second is a pure particle physics test. Within the literature [138, 143], there are a couple of other suggestions for additional, or future methods of constraint. These include;

1. *Supernova Core Collapse:* It is suggested [137, 138] that we could search for a dip in the neutrino energy spectrum coming from neutrinos produced during supernova core collapse.

2. *Large Scale Structure:* This places constraints on the mass [145] due to the damping length of $\mathcal{O}(\text{keV}) \lesssim m$.

4.2.3 $\nu\nu \to \delta\delta$ Cross-Section

We are interested in the processes of the form;

$$\nu\ \nu \longrightarrow \delta\ \delta$$
$$\nu\ \overline{\nu} \longrightarrow \delta\ \delta$$

If the neutrinos are Majorana, both of these processes can occur and the cross-section is given by;

$$\sigma(s) = \frac{g^4 m_N^2}{32\pi}\left[\sqrt{\frac{\frac{1}{4}s - m_\delta^2}{s}}\frac{2}{\left(m_\delta^2 - m_N^2 - \frac{1}{2}s\right)^2 - s\left(\frac{1}{4}s - m_\delta^2\right)}\right.$$
$$\left. + \frac{1}{s\left(m_\delta^2 - m_N^2 - \frac{1}{2}s\right)}\log\left(\frac{m_\delta^2 - m_N^2 - \frac{1}{2}s + \sqrt{s\left(\frac{1}{4}s - m_\delta^2\right)}}{m_\delta^2 - m_N^2 - \frac{1}{2}s - \sqrt{s\left(\frac{1}{4}s - m_\delta^2\right)}}\right)\right] \tag{4.11}$$

4.3 IceCube, IceCube 170922A and TXS 0506+056

The IceCube neutrino observatory [149] is located at the South Pole, consisting of one cubic kilometre of Antarctic ice. The goal of the project is to detect very high energy neutrinos from astrophysical sources. In this regard it is sensitive to energies in the range 300 GeV to 1 EeV. The important specifics of the design are that it is a Cherenkov detector. When a muon neutrino interacts with the ice via charged current interactions, a muon is produced which emits Cherenkov radiation as it propagates through the medium. The energy of this muon, $\hat{E}_\mu$ is measured along with the propagation path. This can then be used to reconstruct;

- The neutrino energy E_ν, from the muon energy prior, $\hat{E}_\mu$ via for example Figure S5 in [150]. As a reference, in [147], an estimated fit is given which can be used in simple practical cases;

$$\left(\frac{E_\nu}{\text{TeV}}\right) = 1.92\left(\frac{\hat{E}_\mu}{\text{TeV}}\right)^{1.14} \tag{4.12}$$

- The declination and right ascension of the original neutrino path.[2] This is vital in matching up events with possible sources, and has lead to the deduction that the neutrino events we will be interested were most likely sourced from a blazar, TXS 0506+056, at a redshift of $z \simeq 0.3365$.

The IceCube experiment is searching for high energy astrophysical neutrinos. Only very particular types of astrophysical object can produce such energetic particles. Of particular interest to us are objects known as *blazars*. These are *Active Galactic Nuclei (AGN)*, which consist of a supermassive black hole that converts the gravitational and rotational energy of accreting matter into highly relativistic jets [151] pointing in our direction. In particular, IceCube believes to have detected high energy neutrinos from a known γ-ray source TXS 0506+056. The key fact regarding this blazar is that it is at a redshift [147];

$$z_{\text{TXS}} \simeq 0.3365 \Rightarrow d_{\text{TXS}} \simeq 1.3\,\text{Gpc} \tag{4.13}$$

[2] One can access this data *here*.

where $d_{\rm TXS}$ is the comoving distance to the blazar.[3] This therefore presents a very interesting regime in which to test fundamental physics: we have TeV - PeV energy neutrinos propagating across gigaparsecs of distance. Along the way, we can therefore consider interactions with dark matter, the cosmic neutrino background etc. As we shall discuss further below, it also presents a prime example of the utility of *multimessenger astronomy* [147, 151] where neutrino events are calibrated with other γ and X-ray experiments such as Fermi-LAT, H.E.S.S., and the Swift XRT.

To understand the relationship between the flaring γ-ray source TXS 0506+056 and IceCube, one should note that on 22 Septemeber 2017, a neutrino with an energy of $\sim 290\,\text{TeV}$ was observed at IceCube (IceCube-170922A). This prompted a couple of responses;

- *Multimessenger Approach:* Immediately after the event, multiple collaborations began to establish the coincidence of the neutrino alert with the flaring state of TXS 0506+056. Broadly this relies on correlating γ-ray and X-ray measurements of known catalogs of astrophysical objects with the angular position of the reconstructed neutrino path. For a more detailed account of this, see [151], however the salient point is that the chance coincidence is currently ruled out at $3 - 3.5\sigma$.

- *Historical Approach:* It also provoked a search into data taken in $2014 - 15$ where it was found that 13 ± 5 excess events [147] appear to *also* be coincident with TXS 0506+056 in its flaring state. It thus appears that this blazar is a source of high energy astrophsyical neutrinos.

We will be interested in the high energy event to place our own constraints on the model under consideration. The careful analysis in [151] provides a most probable energy of 290 TeV with a 90% confidence level lower bound of 183 TeV. More information on the analysis of the coincidence of IceCube-170922A with the flaring of TXS 0506+056 as well as the historical data can be found in [147, 148, 150, 151]. Furthermore, the viability of blazars as neutrino sources is discussed in [150, 153].

4.3.1 The Neutrino Luminosity from TXS 0506+056

We intend to use the mean free path, which we can define via;

$$\ell^{-1} = \sum_i n_{X_i} \sigma(\nu X_i \to Y_i) \tag{4.14}$$

to place bounds on the model. In order to use the observation of the 290 TeV neutrino as a constraint on fundamental interactions within the dark and neutrino sectors, we first must discuss the validity of comparing the mean free path to the comoving distance from the blazar. If the neutrino luminosity associated to the blazar is of a magnitude that saturates the maximum bound, we may deduce that the mean free path of the neutrinos is likely to be *larger* than the comoving distance. To do so, we extract the 7.5 year upper bound on the neutrino luminosity as given in Figure 4 of [151]. Referring to 1.7 in [225], the *luminosity* radiated by a source between energies ϵ_1 and ϵ_2 is then simply;

$$L[\epsilon_1, \epsilon_2] = 4\pi d_L^2 \int_{\log \epsilon_1}^{\log \epsilon_2} \mathrm{d} \log \epsilon \, \nu F_\nu \tag{4.15}$$

[3] $1\,\text{Gpc} \simeq 3.08567 \times 10^{27}\,\text{cm}$

Source	**Energy Range**	**Luminosity** $\mathrm{erg\,s^{-1}}$	**Reference**
Neutrino Source	186 TeV - 7.9 PeV	$\lesssim 10^{46}$	[151]
γ *Source (HAWC)*	0.8 TeV - 74.0 TeV	$\lesssim 4.1 \times 10^{45}$	[151, 230]

Table IV.2: Numerical Results for the luminosity in the given energy range for the γ-ray and neutrino components of the blazar flux. Note that in the neutrino case, we are considering the 7.5 year exposure presented in [151]

where d_L is the photometric distance to the source. This upper bound is shown in Table IV.2 along with the upper bound provided by the HAWC experiment on the photon flux. It should be emphasised that the main comparison point here is the neutrino luminosity, not the photon luminosity which is given to provide support for a given production mechanism. The value for the photons does not affect the conclusions regarding the bounds on the neutrino couplings. The inclusion of the photon flux will be discussed further in the next section. To proceed, we compare the neutrino luminosity with upper bounds derived in blazar modelling scenarios, in particular those given in [226]. Other references which make a detailed record of the relevant production mechanisms inside the jet environements of the blazar include [148, 227–229]. We make the following observations. It might appear that there is a conflict between the upper bound of $\sim 10^{45}\,\mathrm{erg\,s^{-1}}$ in [226] and that presented in Table IV.2. There are two reasons this is not the case;

1. The value quoted in Table IV.2 is an upper bound on the measurement due to the fact that an ensemble of distant sources may lead to a neutrino observation even if the expectation value for one source is very small [226].

2. The value quoted in [226] assumes that there is only one emmiting region within the blazar jet. Other studies such as [231] find luminosities that saturate this upper bound due to multiple emitting regions.

With this in mind, the data is consistent with the different theoretical predictions for the expected neutrino luminosity. Up to the uncertainty in this modelling, it appears that the measured luminosity is indeed close to saturating this bound. We then make a key deduction of this work, that therefore the mean free path of the 290 TeV neutrino is likely to be greater than the distance to the blazar. This will be the definition of our bound. For a discussion regarding the consistency of the neutrino and photon flux, see Appendix B.9.

4.4 Results

There are a number of motivated assumptions that go into deriving the following constraints regarding the neutrino mass hierarchy, neutrino mass eigenstates, the redshift of the neutrino energy as it propagates across the Universe, and the contribution of other channels. This is detailed in Appendix B. Before presenting the results, we discuss the methodology applied, in particular what parameter space we explore, and which effects are included in the analysis. For a given set of parameters $(g_{ie}, \cdots, m_\delta, m_N)$, the approach taken is as follows;

1. Consider the scattering of a 290 TeV muon-neutrino off the mass eigenstates in the cosmic neutrino background.

2. Compute the cross-section at the centre of mass energy *for each* mass eigenstate. This allows us to include the different neutrino hierarchies.[4]

3. Compute the mean free path, including the redshifting effect and compare to the distance to the blazar.

4. Reject parameters sets for which the mean free path is less than this distance.

4.4.1 Parameter Choices

In terms of the parameters we choose, we are informed by the current leading observational bounds on (i) the total neutrino mass, and, (ii) the coupling constants in the effective theory. Before proceeding, we make it clear that we could not improve on the constraints $g_\ell \lesssim 10^{-3}$ in the case of real dark matter. The mean free path was always significantly larger than the distance to the blazar. All the results that follow are in the complex case, where for example, the coupling to the tau neutrino is far less constrained. Taking the constraints from (4.9), we choose the following for our computations;

- The mean free path is most sensitive to the coupling, $g_{i\mu}$, as such we choose to vary this parameter in the range $g_{i\mu} \in [10^{-5}, 10^{-1}]$.
- We also vary the mass of the mediator $m_N \in [m_\delta, 10\,\text{MeV}]$.
- We fix the mass of the scalar m_δ for values $m_\delta = 0.1, 0.5, 1.0, 1.5\,\text{MeV}$.
- The electron neutrino coupling is the most constrained, and indeed we find that the conclusions are insensitive to this parameter. As such, we set $g_{ie} = 0$, removing the dependence.
- In all the plots below we have take $g_\tau = 3 \times 10^{-1}$, at the upper bound of the current constraints. We acknowledge that this may be slightly optimistic.
- Finally we consider values of the lightest neutrino (in both hierarchies) of $m_\nu = 0.01, 0.03, 0.04\,\text{eV}$. All of these values are within the Planck bound of $\sum_\nu m_\nu < 0.17\,\text{eV}$. Although, since this bound appears to be getting tighter, the lower neutrino masses e.g. $m_\nu = 0.01 \Rightarrow \sum_\nu m_\nu \simeq 0.06\,\text{eV}$ perhaps lead to stronger conclusions.

4.4.2 Analysis

A selection of results are shown in Figure 4.2 across a range of neutrino and scalar masses. For a complete set of plots, the reader should consult [3]. Note that the shaded regions in each figure are those that are ruled out by the mean free path, relic abundance, and kaon decay constraints. For example, masses of the mediator above 10 MeV are ruled out by the thermal cross-section calculations. As we will discuss shortly, the constraints we obtain in this way are stronger than those from Kaon decays, but slightly weaker than the constraints from BBN and CMB, we shall discuss this in more

[4] In the complex case, we include an additional factor of 3 as discussed in Section B.4

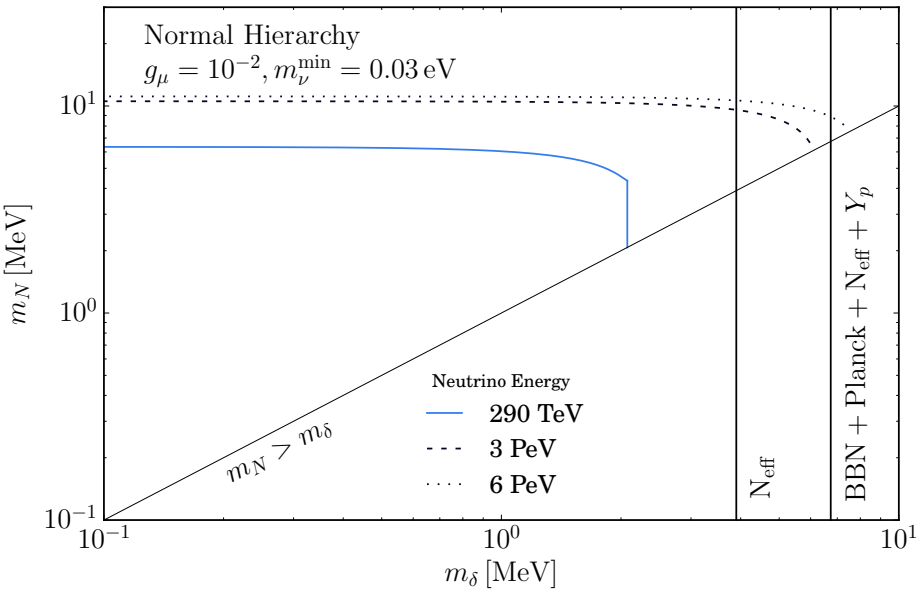

Figure 4.1 Expected constraints if higher energy neutrinos were detected from a source located at the same distance as TXS 0506+056. In this figure, we have taken $g_\mu = 10^{-2}$, $g_e = 0$, $g_\tau = 3 \times 10^{-1}$, and $m_\nu^{\min} = 0.03$ in the normal hierarchy. Shown vertically are CMB constraints [134] and CMB+BBN constraints [221].

detail very shortly. We see from the plots that at low mediator masses $m_N \lesssim 5\,\text{MeV}$, we see a big improvement over the kaon decay constraints. Indeed in the $m_\delta = 0.1\,\text{MeV}$ scenario, we see an order of magnitude improvement across a decent range of mediator masses. There is also not a strong dependence on the neutrino masses. This suggest that even if the cosmological bounds on the total sum of neutrino masses tightens, these constraints will not weaken significantly. Furthermore, whilst there is a slight difference between the neutrino hierarchies due to the different couplings to the mass eigenstates, this is again not significant. Hence, we are not sensitive to future revelations from the neutrino sector.

In addition, we have also neglected additional processes that would decrease the mean free path. These include $\nu\delta \to \nu\delta$. As discussed in Section B.2, we do believe that this will be a negligble contribution. Nonetheless, again the conclusions are insensitive to this. This is because any decrease in the mean free path would only *strengthen* the constraints.

We now turn to comparing our constraints with those from cosmology, in particular it turns out that the contribution to the neutrino temperature in the early Universe due to the interaction of the thermal bath with these light dark matter candidates is significant. Modification of the neutrino temperature affects the CMB, for example by changing the epoch of matter radiation equality.

In [134] the authors looked at the effect of a change in neutrino temperature on the CMB, while in [221], the effect of a different temperature of neutrinos on both the CMB and BBN were also taken into account (see also [222]. These two studies lead to a stronger constraint on the mass of scalar dark matter coupled to the neutrino sector than the limits we are currently able to obtain from IceCube. As an aside, it is interesting that two constraint from such radically different astrophysical environments

lead to similar numbers. In Figure 4.1 we plot these constraints neglecting any dependence on the mediator mass and we estimate what energy neutrino we would have to observe from TXS 0506+056 in order to get a stronger constraint. The CMB and BBN constraints on the model change the acceptable region where mass generation in this way is acceptable but leave enough parameter space open to not rule out the mechanism all together.

Taking a slightly bigger picture view, this shows that the exciting new data from IceCube can lead to new constraints on physics beyond the standard model, as shown also in [147]. Ultimately detecting neutrinos is difficult, and this analysis will only improve with more observations. As the IceCube experiment runs longer and longer, more regions of parameter space can be tested, as discussed in Section 4.2.2 and illustrated in Figure 4.1. It would also allow for a statistical treatment of the phenomenon which is simply not appropriate here with a single event.

To extend the analysis, we should consider the splitting of the mass eigenstates. In the case that there was a very large mass splitting, the constraints would weaken slightly as the centre of mass energy may not be sufficient to excite all the interaction modes. This will ultimately only lead to a maximum of a factor of 3 difference in the mean free path, which is subdominant compared to changes in e.g. the coupling constants.

4.5 Discussion

To summarise, we have considered new constraints on an effective theory that links Dark Matter and neutrino masses. Within this framework, we used the IceCube event 170922A to obtain bounds on the interaction of neutrinos with MeV scalar dark matter. Our constraints are an order of magnitude improvement on the constraints which can be obtained by Kaon decay and are competitive with those coming from CMB and BBN, although not yet quite as strong. We have calculated the energy of neutrinos that would need to be detected in order to beat the CMB and BBN constraint. Independent of the performance, it indicates the utility of IceCubce as a probe of fundamental physics. We also extended the analysis in [147] regarding the blazar dynamics to address some of the subtleties that arise in the higher energy neutrino regime. We argued that the various astrophysical papers [148, 226, 229] support the conclusion that the mean free path was a suitable comparison parameter in a fairly model independent fashion.

In terms of the assumptions contained in our analysis, we would like to ultimately relax the mass splitting assumption, although as noted above, we do not believe this would make a significant difference. For a very precise calculation, we should also include the effects of neutrino clustering for example.

Looking forward, the biggest improvement will be found once IceCube observes more ultra high energy astrophysical neutrinos from sources gigaparsecs away. The coincidence of the centre of mass energy and the scalar mass makes this sort of event the perfect setting to consider the effective model. Further work could then implement a fuller statistical analysis and provide confidence intervals on the bounds. One could also place similar constraints on the remaining portion of the models detailed in [232]. Moreover, one could look to investigate the amount of data required for clear discrimination between models. This would be a valuable step towards making this method of constraint a precise tool.

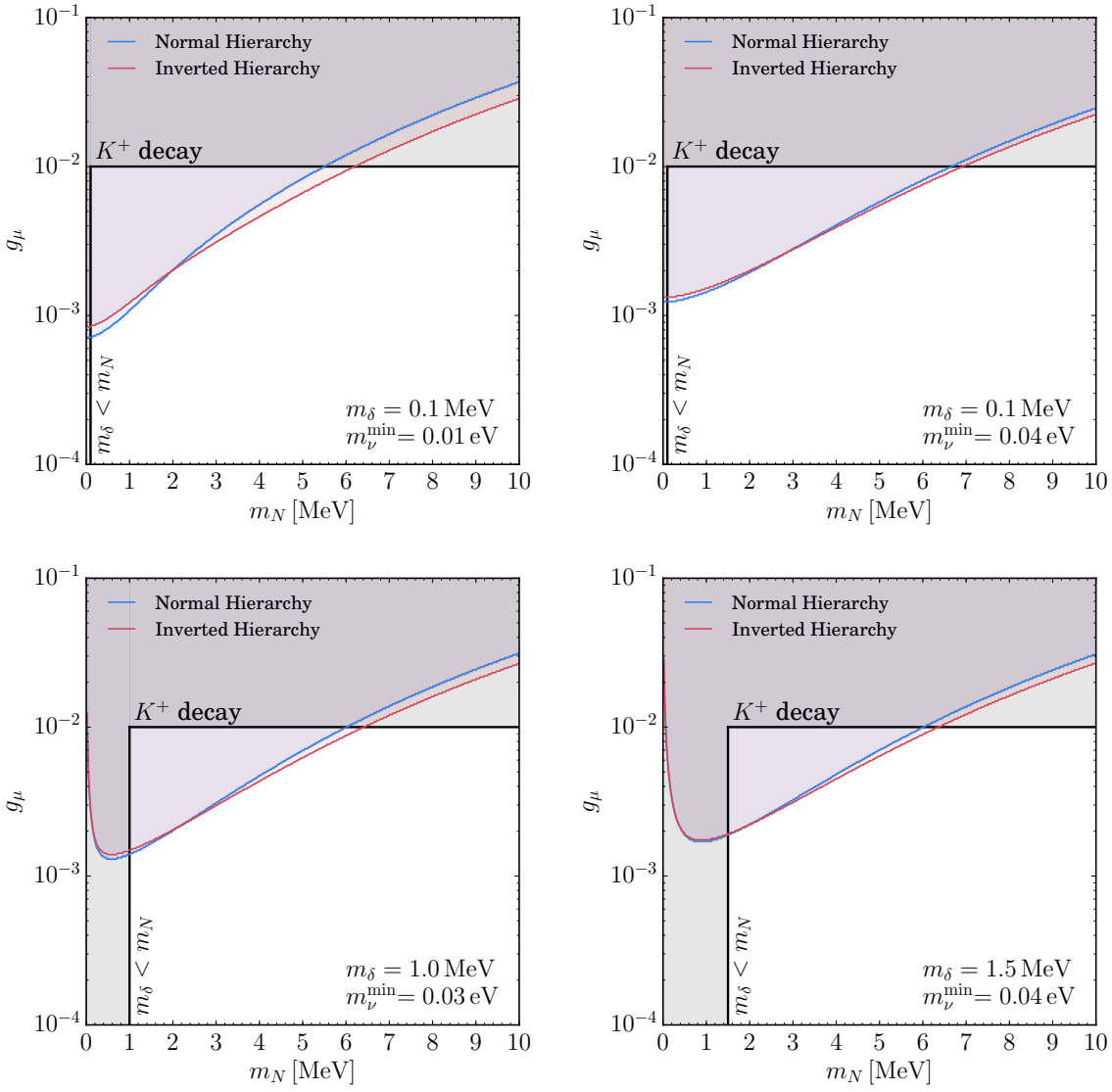

Figure 4.2 Selection of constraint plots for the case of complex scalar dark matter. In each plot, $g_e = 0$, $g_\tau = 3 \times 10^{-1}$, and the shaded regions are those that are ruled out by the mean free path constraints.

References

[1] N. Sabti, J. Alvey, M. Escudero, M. Fairbairn and D. Blas, *Refined Bounds on MeV-scale Thermal Dark Sectors from BBN and the CMB*, 1910.01649.

[2] J. Alvey, M. Campos, M. Fairbairn and T. You, *Light Dark Matter from Inelastic Cosmic Ray Collisions*, 1905.05776.

[3] J. B. G. Alvey and M. Fairbairn, *Linking Scalar Dark Matter and Neutrino Masses with IceCube 170922A*, *JCAP* **1907** (2019) 041 [1902.01450].

[4] G. Bertone, D. Hooper and J. Silk, *Particle dark matter: Evidence, candidates and constraints*, *Phys. Rept.* **405** (2005) 279 [hep-ph/0404175].

[5] M. Cirelli, *Indirect Searches for Dark Matter: a status review*, *Pramana* **79** (2012) 1021 [1202.1454].

[6] J. M. Gaskins, *A review of indirect searches for particle dark matter*, *Contemp. Phys.* **57** (2016) 496 [1604.00014].

[7] T. R. Slatyer, *Indirect Detection of Dark Matter*, in *Proceedings, Theoretical Advanced Study Institute in Elementary Particle Physics : Anticipating the Next Discoveries in Particle Physics (TASI 2016): Boulder, CO, USA, June 6-July 1, 2016*, pp. 297–353, 2018, 1710.05137, DOI.

[8] ATLAS collaboration, M. Aaboud et al., *Search for dark matter and other new phenomena in events with an energetic jet and large missing transverse momentum using the ATLAS detector*, *JHEP* **01** (2018) 126 [1711.03301].

[9] CMS collaboration, A. M. Sirunyan et al., *Search for narrow and broad dijet resonances in proton-proton collisions at $\sqrt{s} = 13$ TeV and constraints on dark matter mediators and other new particles*, *JHEP* **08** (2018) 130 [1806.00843].

[10] XENON collaboration, E. Aprile et al., *Dark Matter Search Results from a One Ton-Year Exposure of XENON1T*, *Phys. Rev. Lett.* **121** (2018) 111302 [1805.12562].

[11] LUX collaboration, D. S. Akerib et al., *Results from a search for dark matter in the complete LUX exposure*, *Phys. Rev. Lett.* **118** (2017) 021303 [1608.07648].

[12] PandaX-II collaboration, X. Cui et al., *Dark Matter Results From 54-Ton-Day Exposure of PandaX-II Experiment*, *Phys. Rev. Lett.* **119** (2017) 181302 [1708.06917].

[13] Fermi-LAT collaboration, M. Ackermann et al., *The Fermi Galactic Center GeV Excess and Implications for Dark Matter*, *Astrophys. J.* **840** (2017) 43 [1704.03910].

[14] Planck collaboration, N. Aghanim et al., *Planck 2018 results. VI. Cosmological parameters*, 1807.06209.

[15] M. Escudero, A. Berlin, D. Hooper and M.-X. Lin, *Toward (Finally!) Ruling Out Z and Higgs Mediated Dark Matter Models*, *JCAP* **1612** (2016) 029 [1609.09079].

[16] G. Arcadi, M. Dutra, P. Ghosh, M. Lindner, Y. Mambrini, M. Pierre et al., *The waning of the WIMP? A review of models, searches, and constraints*, *Eur. Phys. J.* **C78** (2018) 203 [1703.07364].

[17] L. Roszkowski, E. M. Sessolo and S. Trojanowski, *WIMP dark matter candidates and searches?current status and future prospects*, *Rept. Prog. Phys.* **81** (2018) 066201 [1707.06277].

[18] GAMBIT collaboration, P. Athron et al., *Status of the scalar singlet dark matter model*, *Eur.*

Phys. J. **C77** (2017) 568 [1705.07931].
[19] G. Arcadi, A. Djouadi and M. Raidal, *Dark Matter through the Higgs portal*, 1903.03616.
[20] C. Blanco, M. Escudero, D. Hooper and S. J. Witte, *Z' Mediated WIMPs: Dead, Dying, or Soon to be Detected?*, 1907.05893.
[21] R. Essig et al., *Working Group Report: New Light Weakly Coupled Particles*, 2013, 1311.0029.
[22] J. Alexander et al., *Dark Sectors 2016 Workshop*, 2016, 1608.08632.
[23] M. Battaglieri et al., *US Cosmic Visions: New Ideas in Dark Matter 2017: Community Report*, 2017, 1707.04591.
[24] J. Beacham et al., *Physics Beyond Colliders at CERN: Beyond the Standard Model Working Group Report*, 1901.09966.
[25] C. Boehm and P. Fayet, *Scalar dark matter candidates*, *Nucl. Phys.* **B683** (2004) 219 [hep-ph/0305261].
[26] C. Boehm, D. Hooper, J. Silk, M. Casse and J. Paul, *MeV dark matter: Has it been detected?*, *Phys. Rev. Lett.* **92** (2004) 101301 [astro-ph/0309686].
[27] J. L. Feng and J. Kumar, *The WIMPless Miracle: Dark-Matter Particles without Weak-Scale Masses or Weak Interactions*, *Phys. Rev. Lett.* **101** (2008) 231301 [0803.4196].
[28] C. Boehm, Y. Farzan, T. Hambye, S. Palomares-Ruiz and S. Pascoli, *Is it possible to explain neutrino masses with scalar dark matter?*, *Phys. Rev.* **D77** (2008) 043516 [hep-ph/0612228].
[29] Y. Farzan, *A Minimal model linking two great mysteries: neutrino mass and dark matter*, *Phys. Rev.* **D80** (2009) 073009 [0908.3729].
[30] Y. Farzan, *Flavoring Monochromatic Neutrino Flux from Dark Matter Annihilation*, *JHEP* **02** (2012) 091 [1111.1063].
[31] B. Batell, T. Han, D. McKeen and B. Shams Es Haghi, *Thermal Dark Matter Through the Dirac Neutrino Portal*, *Phys. Rev.* **D97** (2018) 075016 [1709.07001].
[32] P. Ballett, M. Hostert and S. Pascoli, *Neutrino Masses from a Dark Neutrino Sector below the Electroweak Scale*, *Phys. Rev.* **D99** (2019) 091701 [1903.07590].
[33] J. M. Lamprea, E. Peinado, S. Smolenski and J. Wudka, *Strongly Interacting Neutrino Portal Dark Matter*, 1906.02340.
[34] M. Blennow, E. Fernandez-Martinez, A. Olivares-Del Campo, S. Pascoli, S. Rosauro-Alcaraz and A. V. Titov, *Neutrino Portals to Dark Matter*, *Eur. Phys. J.* **C79** (2019) 555 [1903.00006].
[35] G. Krnjaic, *Probing Light Thermal Dark-Matter With a Higgs Portal Mediator*, *Phys. Rev.* **D94** (2016) 073009 [1512.04119].
[36] K. Bondarenko, A. Boyarsky, T. Bringmann, M. Hufnagel, K. Schmidt-Hoberg and A. Sokolenko, *Direct detection and complementary constraints for sub-GeV dark matter*, 1909.08632.
[37] Y. Hochberg, E. Kuflik, T. Volansky and J. G. Wacker, *Mechanism for Thermal Relic Dark Matter of Strongly Interacting Massive Particles*, *Phys. Rev. Lett.* **113** (2014) 171301 [1402.5143].
[38] P. Agrawal, Z. Chacko and C. B. Verhaaren, *Leptophilic Dark Matter and the Anomalous Magnetic Moment of the Muon*, *JHEP* **08** (2014) 147 [1402.7369].
[39] A. Kamada, K. Kaneta, K. Yanagi and H.-B. Yu, *Self-interacting dark matter and muon $g-2$ in a gauged $U(1)_{L_\mu - L_\tau}$ model*, *JHEP* **06** (2018) 117 [1805.00651].
[40] S. Knapen, T. Lin and K. M. Zurek, *Light Dark Matter: Models and Constraints*, *Phys. Rev.* **D96** (2017) 115021 [1709.07882].
[41] L. J. Hall, K. Jedamzik, J. March-Russell and S. M. West, *Freeze-In Production of FIMP Dark Matter*, *JHEP* **03** (2010) 080 [0911.1120].
[42] X. Chu, T. Hambye and M. H. G. Tytgat, *The Four Basic Ways of Creating Dark Matter Through a Portal*, *JCAP* **1205** (2012) 034 [1112.0493].
[43] T. Hambye, M. H. G. Tytgat, J. Vandecasteele and L. Vanderheyden, *Dark matter from dark photons: a taxonomy of dark matter production*, 1908.09864.

[44] C. Dvorkin, T. Lin and K. Schutz, *Making dark matter out of light: freeze-in from plasma effects*, *Phys. Rev.* **D99** (2019) 115009 [1902.08623].

[45] J. A. Evans, C. Gaidau and J. Shelton, *Leak-in Dark Matter*, 1909.04671.

[46] G. Bertone and M. P. Tait, Tim, *A new era in the search for dark matter*, *Nature* **562** (2018) 51 [1810.01668].

[47] N. Borodatchenkova, D. Choudhury and M. Drees, *Probing MeV dark matter at low-energy e+e- colliders*, *Phys. Rev. Lett.* **96** (2006) 141802 [hep-ph/0510147].

[48] B. Batell, M. Pospelov and A. Ritz, *Probing a Secluded U(1) at B-factories*, *Phys. Rev.* **D79** (2009) 115008 [0903.0363].

[49] P. J. Fox, R. Harnik, J. Kopp and Y. Tsai, *LEP Shines Light on Dark Matter*, *Phys. Rev.* **D84** (2011) 014028 [1103.0240].

[50] R. Essig, J. Mardon, M. Papucci, T. Volansky and Y.-M. Zhong, *Constraining Light Dark Matter with Low-Energy e^+e^- Colliders*, *JHEP* **11** (2013) 167 [1309.5084].

[51] BaBar collaboration, J. P. Lees et al., *Search for a Dark Photon in e^+e^- Collisions at BaBar*, *Phys. Rev. Lett.* **113** (2014) 201801 [1406.2980].

[52] KLOE-2 collaboration, A. Anastasi et al., *Search for dark Higgsstrahlung in $e^+e \to \mu^+\mu$ and missing energy events with the KLOE experiment*, *Phys. Lett.* **B747** (2015) 365 [1501.06795].

[53] BaBar collaboration, J. P. Lees et al., *Search for Invisible Decays of a Dark Photon Produced in e^+e^- Collisions at BaBar*, *Phys. Rev. Lett.* **119** (2017) 131804 [1702.03327].

[54] LHCb collaboration, R. Aaij et al., *Search for Dark Photons Produced in 13 TeV pp Collisions*, *Phys. Rev. Lett.* **120** (2018) 061801 [1710.02867].

[55] J. D. Bjorken, R. Essig, P. Schuster and N. Toro, *New Fixed-Target Experiments to Search for Dark Gauge Forces*, *Phys. Rev.* **D80** (2009) 075018 [0906.0580].

[56] B. Batell, M. Pospelov and A. Ritz, *Exploring Portals to a Hidden Sector Through Fixed Targets*, *Phys. Rev.* **D80** (2009) 095024 [0906.5614].

[57] S. Andreas, C. Niebuhr and A. Ringwald, *New Limits on Hidden Photons from Past Electron Beam Dumps*, *Phys. Rev.* **D86** (2012) 095019 [1209.6083].

[58] S. Palomares-Ruiz and S. Pascoli, *Testing MeV dark matter with neutrino detectors*, *Phys. Rev.* **D77** (2008) 025025 [0710.5420].

[59] R. Harnik, J. Kopp and P. A. N. Machado, *Exploring nu Signals in Dark Matter Detectors*, *JCAP* **1207** (2012) 026 [1202.6073].

[60] P. deNiverville, D. McKeen and A. Ritz, *Signatures of sub-GeV dark matter beams at neutrino experiments*, *Phys. Rev.* **D86** (2012) 035022 [1205.3499].

[61] B. Batell, P. deNiverville, D. McKeen, M. Pospelov and A. Ritz, *Leptophobic Dark Matter at Neutrino Factories*, *Phys. Rev.* **D90** (2014) 115014 [1405.7049].

[62] N. Klop and S. Ando, *Constraints on MeV dark matter using neutrino detectors and their implication for the 21-cm results*, *Phys. Rev.* **D98** (2018) 103004 [1809.00671].

[63] K. J. Kelly and Y. Zhang, *Mononeutrino at DUNE: New Signals from Neutrinophilic Thermal Dark Matter*, *Phys. Rev.* **D99** (2019) 055034 [1901.01259].

[64] A. Kamada and H.-B. Yu, *Coherent Propagation of PeV Neutrinos and the Dip in the Neutrino Spectrum at IceCube*, *Phys. Rev.* **D92** (2015) 113004 [1504.00711].

[65] C. A. ArgÃijelles, A. Kheirandish and A. C. Vincent, *Imaging Galactic Dark Matter with High-Energy Cosmic Neutrinos*, *Phys. Rev. Lett.* **119** (2017) 201801 [1703.00451].

[66] R. Essig, M. Fernandez-Serra, J. Mardon, A. Soto, T. Volansky and T.-T. Yu, *Direct Detection of sub-GeV Dark Matter with Semiconductor Targets*, *JHEP* **05** (2016) 046 [1509.01598].

[67] S. K. Lee, M. Lisanti, S. Mishra-Sharma and B. R. Safdi, *Modulation Effects in Dark Matter-Electron Scattering Experiments*, *Phys. Rev.* **D92** (2015) 083517 [1508.07361].

[68] S. Derenzo, R. Essig, A. Massari, A. Soto and T.-T. Yu, *Direct Detection of sub-GeV Dark Matter with Scintillating Targets*, *Phys. Rev.* **D96** (2017) 016026 [1607.01009].

[69] R. Essig, T. Volansky and T.-T. Yu, *New Constraints and Prospects for sub-GeV Dark Matter Scattering off Electrons in Xenon*, *Phys. Rev.* **D96** (2017) 043017 [1703.00910].
[70] SuperCDMS collaboration, R. Agnese et al., *First Dark Matter Constraints from a SuperCDMS Single-Charge Sensitive Detector*, *Phys. Rev. Lett.* **121** (2018) 051301 [1804.10697].
[71] DarkSide collaboration, P. Agnes et al., *Constraints on Sub-GeV Dark-MatterâĂŞElectron Scattering from the DarkSide-50 Experiment*, *Phys. Rev. Lett.* **121** (2018) 111303 [1802.06998].
[72] SENSEI collaboration, O. Abramoff et al., *SENSEI: Direct-Detection Constraints on Sub-GeV Dark Matter from a Shallow Underground Run Using a Prototype Skipper-CCD*, *Phys. Rev. Lett.* **122** (2019) 161801 [1901.10478].
[73] XENON collaboration, E. Aprile et al., *Light Dark Matter Search with Ionization Signals in XENON1T*, 1907.11485.
[74] T. R. Slatyer, *Indirect dark matter signatures in the cosmic dark ages. I. Generalizing the bound on s-wave dark matter annihilation from Planck results*, *Phys. Rev.* **D93** (2016) 023527 [1506.03811].
[75] R. Essig, E. Kuflik, S. D. McDermott, T. Volansky and K. M. Zurek, *Constraining Light Dark Matter with Diffuse X-Ray and Gamma-Ray Observations*, *JHEP* **11** (2013) 193 [1309.4091].
[76] R. Bartels, D. Gaggero and C. Weniger, *Prospects for indirect dark matter searches with MeV photons*, *JCAP* **1705** (2017) 001 [1703.02546].
[77] G. G. Raffelt, *Stars as laboratories for fundamental physics*. 1996.
[78] H. K. Dreiner, J.-F. Fortin, C. Hanhart and L. Ubaldi, *Supernova constraints on MeV dark sectors from e^+e^- annihilations*, *Phys. Rev.* **D89** (2014) 105015 [1310.3826].
[79] J. H. Chang, R. Essig and S. D. McDermott, *Supernova 1987A Constraints on Sub-GeV Dark Sectors, Millicharged Particles, the QCD Axion, and an Axion-like Particle*, *JHEP* **09** (2018) 051 [1803.00993].
[80] W. DeRocco, P. W. Graham, D. Kasen, G. Marques-Tavares and S. Rajendran, *Supernova signals of light dark matter*, 1905.09284.
[81] Y. Farzan, *Bounds on the coupling of the Majoron to light neutrinos from supernova cooling*, *Phys. Rev.* **D67** (2003) 073015 [hep-ph/0211375].
[82] L. Heurtier and Y. Zhang, *Supernova Constraints on Massive (Pseudo)Scalar Coupling to Neutrinos*, *JCAP* **1702** (2017) 042 [1609.05882].
[83] W. L. Xu, C. Dvorkin and A. Chael, *Probing sub-GeV Dark Matter-Baryon Scattering with Cosmological Observables*, *Phys. Rev.* **D97** (2018) 103530 [1802.06788].
[84] A. Olivares-Del Campo, C. BÅŞhm, S. Palomares-Ruiz and S. Pascoli, *Dark matter-neutrino interactions through the lens of their cosmological implications*, *Phys. Rev.* **D97** (2018) 075039 [1711.05283].
[85] A. Berlin, D. Hooper, G. Krnjaic and S. D. McDermott, *Severely Constraining Dark Matter Interpretations of the 21-cm Anomaly*, *Phys. Rev. Lett.* **121** (2018) 011102 [1803.02804].
[86] R. J. Wilkinson, C. Boehm and J. Lesgourgues, *Constraining Dark Matter-Neutrino Interactions using the CMB and Large-Scale Structure*, *JCAP* **1405** (2014) 011 [1401.7597].
[87] B. Bertoni, S. Ipek, D. McKeen and A. E. Nelson, *Constraints and consequences of reducing small scale structure via large dark matter-neutrino interactions*, *JHEP* **04** (2015) 170 [1412.3113].
[88] H. Vogel and J. Redondo, *Dark Radiation constraints on minicharged particles in models with a hidden photon*, *JCAP* **1402** (2014) 029 [1311.2600].
[89] M. Escudero, D. Hooper, G. Krnjaic and M. Pierre, *Cosmology with A Very Light L_μ - L_τ Gauge Boson*, *JHEP* **03** (2019) 071 [1901.02010].
[90] A. D. Dolgov, S. L. Dubovsky, G. I. Rubtsov and I. I. Tkachev, *Constraints on millicharged particles from Planck data*, *Phys. Rev.* **D88** (2013) 117701 [1310.2376].
[91] Belle-II collaboration, W. Altmannshofer et al., *The Belle II Physics Book*, 1808.10567.
[92] FASER collaboration, A. Ariga et al., *FASER: ForwArd Search ExpeRiment at the LHC*,

1901.04468.
[93] S. Alekhin et al., *A facility to Search for Hidden Particles at the CERN SPS: the SHiP physics case*, *Rept. Prog. Phys.* **79** (2016) 124201 [1504.04855].
[94] J. P. Chou, D. Curtin and H. J. Lubatti, *New Detectors to Explore the Lifetime Frontier*, *Phys. Lett.* **B767** (2017) 29 [1606.06298].
[95] LDMX collaboration, T. ÃĚkesson et al., *Light Dark Matter eXperiment (LDMX)*, 1808.05219.
[96] S. Sarkar, *Big bang nucleosynthesis and physics beyond the standard model*, *Rept. Prog. Phys.* **59** (1996) 1493 [hep-ph/9602260].
[97] F. Iocco, G. Mangano, G. Miele, O. Pisanti and P. D. Serpico, *Primordial Nucleosynthesis: from precision cosmology to fundamental physics*, *Phys. Rept.* **472** (2009) 1 [0809.0631].
[98] M. Pospelov and J. Pradler, *Big Bang Nucleosynthesis as a Probe of New Physics*, *Ann. Rev. Nucl. Part. Sci.* **60** (2010) 539 [1011.1054].
[99] ParticleDataGroup collaboration, M. Tanabashi et al., *Review of Particle Physics*, *Phys. Rev.* **D98** (2018) 030001.
[100] E. W. Kolb, M. S. Turner and T. P. Walker, *The Effect of Interacting Particles on Primordial Nucleosynthesis*, *Phys. Rev.* **D34** (1986) 2197.
[101] P. D. Serpico and G. G. Raffelt, *MeV-mass dark matter and primordial nucleosynthesis*, *Phys. Rev.* **D70** (2004) 043526 [astro-ph/0403417].
[102] C. Boehm, M. J. Dolan and C. McCabe, *A Lower Bound on the Mass of Cold Thermal Dark Matter from Planck*, *JCAP* **1308** (2013) 041 [1303.6270].
[103] K. M. Nollett and G. Steigman, *BBN And The CMB Constrain Light, Electromagnetically Coupled WIMPs*, *Phys. Rev.* **D89** (2014) 083508 [1312.5725].
[104] K. M. Nollett and G. Steigman, *BBN And The CMB Constrain Neutrino Coupled Light WIMPs*, *Phys. Rev.* **D91** (2015) 083505 [1411.6005].
[105] C. Boehm, M. J. Dolan and C. McCabe, *Increasing Neff with particles in thermal equilibrium with neutrinos*, *JCAP* **1212** (2012) 027 [1207.0497].
[106] C. M. Ho and R. J. Scherrer, *Limits on MeV Dark Matter from the Effective Number of Neutrinos*, *Phys. Rev.* **D87** (2013) 023505 [1208.4347].
[107] R. J. Wilkinson, A. C. Vincent, C. Boehm and C. McCabe, *Ruling out the light weakly interacting massive particle explanation of the Galactic 511 keV line*, *Phys. Rev.* **D94** (2016) 103525 [1602.01114].
[108] P. F. Depta, M. Hufnagel, K. Schmidt-Hoberg and S. Wild, *BBN constraints on the annihilation of MeV-scale dark matter*, *JCAP* **1904** (2019) 029 [1901.06944].
[109] M. Escudero, *Neutrino decoupling beyond the Standard Model: CMB constraints on the Dark Matter mass with a fast and precise $N_{\rm eff}$ evaluation*, *JCAP* **1902** (2019) 007 [1812.05605].
[110] M. Escudero, *Neutrino Decoupling Beyond the Standard Model II: Fast and Precise BSM observables in the Early Universe, to appear*, .
[111] C. Pitrou, A. Coc, J.-P. Uzan and E. Vangioni, *Precision big bang nucleosynthesis with improved Helium-4 predictions*, *Phys. Rept.* **754** (2018) 1 [1801.08023].
[112] M. W. Goodman and E. Witten, *Detectability of Certain Dark Matter Candidates*, *Phys. Rev.* **D31** (1985) 3059.
[113] T. Bringmann and M. Pospelov, *Novel direct detection constraints on light dark matter*, *Phys. Rev. Lett.* **122** (2019) 171801 [1810.10543].
[114] Y. Ema, F. Sala and R. Sato, *Light Dark Matter at Neutrino Experiments*, 1811.00520.
[115] C. Kouvaris and J. Pradler, *Probing sub-GeV Dark Matter with conventional detectors*, *Phys. Rev. Lett.* **118** (2017) 031803 [1607.01789].
[116] M. Ibe, W. Nakano, Y. Shoji and K. Suzuki, *Migdal Effect in Dark Matter Direct Detection Experiments*, *JHEP* **03** (2018) 194 [1707.07258].
[117] M. J. Dolan, F. Kahlhoefer and C. McCabe, *Directly detecting sub-GeV dark matter with*

electrons from nuclear scattering, *Phys. Rev. Lett.* **121** (2018) 101801 [1711.09906].

[118] C. Kouvaris, *Probing Light Dark Matter via Evaporation from the Sun*, *Phys. Rev.* **D92** (2015) 075001 [1506.04316].

[119] H. An, M. Pospelov, J. Pradler and A. Ritz, *Directly Detecting MeV-scale Dark Matter via Solar Reflection*, *Phys. Rev. Lett.* **120** (2018) 141801 [1708.03642].

[120] T. Emken, C. Kouvaris and N. G. Nielsen, *The Sun as a sub-GeV Dark Matter Accelerator*, *Phys. Rev.* **D97** (2018) 063007 [1709.06573].

[121] LUX-ZEPLIN collaboration, D. S. Akerib et al., *Projected WIMP Sensitivity of the LUX-ZEPLIN (LZ) Dark Matter Experiment*, 1802.06039.

[122] MiniBooNE DM collaboration, A. A. Aguilar-Arevalo et al., *Dark Matter Search in Nucleon, Pion, and Electron Channels from a Proton Beam Dump with MiniBooNE*, *Phys. Rev.* **D98** (2018) 112004 [1807.06137].

[123] B. Batell, A. Freitas, A. Ismail and D. Mckeen, *Probing Light Dark Matter with a Hadrophilic Scalar Mediator*, 1812.05103.

[124] F. Bonnet, M. Hirsch, T. Ota and W. Winter, *Systematic study of the d=5 Weinberg operator at one-loop order*, *JHEP* **07** (2012) 153 [1204.5862].

[125] Y. Farzan, *Strategies to link tiny neutrino masses with huge missing mass of the Universe*, *Int. J. Mod. Phys.* **A26** (2011) 2461 [1106.2948].

[126] V. A. Bednyakov, N. D. Giokaris and A. V. Bednyakov, *On Higgs mass generation mechanism in the Standard Model*, *Phys. Part. Nucl.* **39** (2008) 13 [hep-ph/0703280].

[127] J. Kubo, E. Ma and D. Suematsu, *Cold Dark Matter, Radiative Neutrino Mass, $\mu \to e\gamma$, and Neutrinoless Double Beta Decay*, *Phys. Lett.* **B642** (2006) 18 [hep-ph/0604114].

[128] S. Davidson and A. Ibarra, *A Lower bound on the right-handed neutrino mass from leptogenesis*, *Phys. Lett.* **B535** (2002) 25 [hep-ph/0202239].

[129] E. Ma, *Naturally small seesaw neutrino mass with no new physics beyond the TeV scale*, *Phys. Rev. Lett.* **86** (2001) 2502 [hep-ph/0011121].

[130] C.-Y. Yao and G.-J. Ding, *Systematic analysis of Dirac neutrino masses from a dimension five operator*, *Phys. Rev.* **D97** (2018) 095042 [1802.05231].

[131] Super-Kamiokande collaboration, Y. Fukuda et al., *Evidence for oscillation of atmospheric neutrinos*, *Phys. Rev. Lett.* **81** (1998) 1562 [hep-ex/9807003].

[132] E. Ma, *Pathways to naturally small neutrino masses*, *Phys. Rev. Lett.* **81** (1998) 1171 [hep-ph/9805219].

[133] E. Ma, *Verifiable radiative seesaw mechanism of neutrino mass and dark matter*, *Phys. Rev.* **D73** (2006) 077301 [hep-ph/0601225].

[134] C. Boehm, M. J. Dolan and C. McCabe, *A Lower Bound on the Mass of Cold Thermal Dark Matter from Planck*, *JCAP* **1308** (2013) 041 [1303.6270].

[135] Y. Farzan, *A Minimal model linking two great mysteries: neutrino mass and dark matter*, *Phys. Rev.* **D80** (2009) 073009 [0908.3729].

[136] E. Ma, *Common origin of neutrino mass, dark matter, and baryogenesis*, *Mod. Phys. Lett.* **A21** (2006) 1777 [hep-ph/0605180].

[137] T. Franarin, M. Fairbairn and J. H. Davis, *JUNO Sensitivity to Resonant Absorption of Galactic Supernova Neutrinos by Dark Matter*, 1806.05015.

[138] Y. Farzan, *A Framework to Simultaneously Explain Tiny Neutrino Mass and Huge Missing Mass Problem of the Universe*, *Mod. Phys. Lett.* **A25** (2010) 2111 [1009.1234].

[139] E949 collaboration, A. V. Artamonov et al., *Search for the rare decay $K^+ \to \mu^+ \nu\bar{\nu}\nu$*, *Phys. Rev.* **D94** (2016) 032012 [1606.09054].

[140] Y. Farzan, S. Pascoli and M. A. Schmidt, *AMEND: A model explaining neutrino masses and dark matter testable at the LHC and MEG*, *JHEP* **10** (2010) 111 [1005.5323].

[141] KLOE collaboration, F. Ambrosino et al., *Precise measurement of*

$\Gamma(K \to e\nu(\gamma))/\Gamma(K \to \mu\nu(\gamma))$ *and study of* $K \to e\nu\gamma$, *Eur. Phys. J.* **C64** (2009) 627 [0907.3594].

[142] Y. Farzan and S. Palomares-Ruiz, *Dips in the Diffuse Supernova Neutrino Background*, *JCAP* **1406** (2014) 014 [1401.7019].

[143] C. Boehm, Y. Farzan, T. Hambye, S. Palomares-Ruiz and S. Pascoli, *Is it possible to explain neutrino masses with scalar dark matter?*, *Phys. Rev.* **D77** (2008) 043516 [hep-ph/0612228].

[144] P. D. Serpico and G. G. Raffelt, *MeV-mass dark matter and primordial nucleosynthesis*, *Phys. Rev.* **D70** (2004) 043526 [astro-ph/0403417].

[145] C. Boehm and R. Schaeffer, *Constraints on dark matter interactions from structure formation: Damping lengths*, *Astron. Astrophys.* **438** (2005) 419 [astro-ph/0410591].

[146] C. Boehm, T. A. Ensslin and J. Silk, *Can Annihilating dark matter be lighter than a few GeVs?*, *J. Phys.* **G30** (2004) 279 [astro-ph/0208458].

[147] K. J. Kelly and P. A. N. Machado, *Multimessenger Astronomy and New Neutrino Physics*, *JCAP* **1810** (2018) 048 [1808.02889].

[148] P. Padovani, P. Giommi, E. Resconi, T. Glauch, B. Arsioli, N. Sahakyan et al., *Dissecting the region around IceCube-170922A: the blazar TXS 0506+056 as the first cosmic neutrino source*, *Mon. Not. Roy. Astron. Soc.* **480** (2018) 192 [1807.04461].

[149] IceCube, *Icecube: South pole neutrino observatory*, 2018.

[150] IceCube collaboration, M. G. Aartsen et al., *Neutrino emission from the direction of the blazar TXS 0506+056 prior to the IceCube-170922A alert*, *Science* **361** (2018) 147 [1807.08794].

[151] IceCube, Fermi-LAT, MAGIC, AGILE, ASAS-SN, HAWC, H.E.S.S., INTEGRAL, Kanata, Kiso, Kapteyn, Liverpool Telescope, Subaru, Swift NuSTAR, VERITAS, VLA/17B-403 collaboration, M. G. Aartsen et al., *Multimessenger observations of a flaring blazar coincident with high-energy neutrino IceCube-170922A*, *Science* **361** (2018) eaat1378 [1807.08816].

[152] A. DiFranzo and D. Hooper, *Searching for MeV-Scale Gauge Bosons with IceCube*, *Phys. Rev.* **D92** (2015) 095007 [1507.03015].

[153] D. Hooper, T. Linden and A. Vieregg, *Active Galactic Nuclei and the Origin of IceCube's Diffuse Neutrino Flux*, *JCAP* **1902** (2019) 012 [1810.02823].

[154] K. Ioka and K. Murase, *IceCube PeVâĂŞEeV neutrinos and secret interactions of neutrinos*, *PTEP* **2014** (2014) 061E01 [1404.2279].

[155] A. D. Dolgov, *Neutrinos in cosmology*, *Phys. Rept.* **370** (2002) 333 [hep-ph/0202122].

[156] E. W. Kolb and M. S. Turner, *The Early Universe*, *Front. Phys.* **69** (1990) 1.

[157] M. Peimbert, A. Peimbert and V. Luridiana, *A new determination of the primordial helium abundance*, in *Revista Mexicana de Astronomia y Astrofisica Conference Series*, vol. 49 of *Revista Mexicana de Astronomia y Astrofisica, vol. 27*, pp. 181–181, July, 2017.

[158] E. Aver, K. A. Olive and E. D. Skillman, *The effects of He I ?10830 on helium abundance determinations*, *JCAP* **1507** (2015) 011 [1503.08146].

[159] Y. I. Izotov, T. X. Thuan and N. G. Guseva, *A new determination of the primordial He abundance using the He i λ10830 ÃĚ emission line: cosmological implications*, *Mon. Not. Roy. Astron. Soc.* **445** (2014) 778 [1408.6953].

[160] R. J. Cooke, M. Pettini, K. M. Nollett and R. Jorgenson, *The primordial deuterium abundance of the most metal-poor damped Lyα system*, *Astrophys. J.* **830** (2016) 148 [1607.03900].

[161] S. A. Balashev, E. O. Zavarygin, A. V. Ivanchik, K. N. Telikova and D. A. Varshalovich, *The primordial deuterium abundance: subDLA system at* $z_{\rm abs} = 2.437$ *towards the QSO J 1444+2919*, *Mon. Not. Roy. Astron. Soc.* **458** (2016) 2188 [1511.01797].

[162] E. O. Zavarygin, J. K. Webb, V. Dumont and S. Riemer-Sørensen, *The primordial deuterium abundance at* $z_{abs} = 2.504$ *from a high signal-to-noise spectrum of Q1009+2956*, *Mon. Not. Roy. Astron. Soc.* **477** (2018) 5536 [1706.09512].

[163] S. Riemer-SÃÿrensen, S. KotuÅą, J. K. Webb, K. Ali, V. Dumont, M. T. Murphy et al., *A*

precise deuterium abundance: remeasurement of the z = 3.572 absorption system towards the quasar PKS1937âĂŞ101, *Mon. Not. Roy. Astron. Soc.* **468** (2017) 3239 [1703.06656].

[164] A. G. Riess, S. Casertano, W. Yuan, L. M. Macri and D. Scolnic, *Large Magellanic Cloud Cepheid Standards Provide a 1% Foundation for the Determination of the Hubble Constant and Stronger Evidence for Physics beyond ΛCDM*, *Astrophys. J.* **876** (2019) 85 [1903.07603].

[165] J. L. Bernal, L. Verde and A. G. Riess, *The trouble with H_0*, *JCAP* **1610** (2016) 019 [1607.05617].

[166] L. Verde, T. Treu and A. G. Riess, *Tensions between the Early and the Late Universe*, 2019, 1907.10625.

[167] F. Beutler, C. Blake, M. Colless, D. H. Jones, L. Staveley-Smith, L. Campbell et al., *The 6dF Galaxy Survey: Baryon Acoustic Oscillations and the Local Hubble Constant*, *Mon. Not. Roy. Astron. Soc.* **416** (2011) 3017 [1106.3366].

[168] A. J. Ross, L. Samushia, C. Howlett, W. J. Percival, A. Burden and M. Manera, *The clustering of the SDSS DR7 main Galaxy sample ? I. A 4 per cent distance measure at z = 0.15*, *Mon. Not. Roy. Astron. Soc.* **449** (2015) 835 [1409.3242].

[169] BOSS collaboration, S. Alam et al., *The clustering of galaxies in the completed SDSS-III Baryon Oscillation Spectroscopic Survey: cosmological analysis of the DR12 galaxy sample*, *Mon. Not. Roy. Astron. Soc.* **470** (2017) 2617 [1607.03155].

[170] Planck collaboration, N. Aghanim et al., *Planck 2018 results. V. CMB power spectra and likelihoods*, 1907.12875.

[171] D. Blas, J. Lesgourgues and T. Tram, *The Cosmic Linear Anisotropy Solving System (CLASS) II: Approximation schemes*, *JCAP* **1107** (2011) 034 [1104.2933].

[172] J. Lesgourgues, *The Cosmic Linear Anisotropy Solving System (CLASS) I: Overview*, 1104.2932.

[173] T. Brinckmann and J. Lesgourgues, *MontePython 3: boosted MCMC sampler and other features*, 1804.07261.

[174] B. Audren, J. Lesgourgues, K. Benabed and S. Prunet, *Conservative Constraints on Early Cosmology: an illustration of the Monte Python cosmological parameter inference code*, *JCAP* **1302** (2013) 001 [1210.7183].

[175] E. Di Valentino, A. Melchiorri and J. Silk, *Reconciling Planck with the local value of H_0 in extended parameter space*, *Phys. Lett.* **B761** (2016) 242 [1606.00634].

[176] E. Di Valentino, A. Melchiorri, E. V. Linder and J. Silk, *Constraining Dark Energy Dynamics in Extended Parameter Space*, *Phys. Rev.* **D96** (2017) 023523 [1704.00762].

[177] NASA PICO collaboration, S. Hanany et al., *PICO: Probe of Inflation and Cosmic Origins*, 1902.10541.

[178] CORE collaboration, E. Di Valentino et al., *Exploring cosmic origins with CORE: Cosmological parameters*, *JCAP* **1804** (2018) 017 [1612.00021].

[179] Simons Observatory collaboration, J. Aguirre et al., *The Simons Observatory: Science goals and forecasts*, *JCAP* **1902** (2019) 056 [1808.07445].

[180] CMB-S4 collaboration, K. N. Abazajian et al., *CMB-S4 Science Book, First Edition*, 1610.02743.

[181] K. Abazajian et al., *CMB-S4 Science Case, Reference Design, and Project Plan*, 1907.04473.

[182] N. Sehgal et al., *CMB-HD: An Ultra-Deep, High-Resolution Millimeter-Wave Survey Over Half the Sky*, 1906.10134.

[183] E. B. Grohs, J. R. Bond, R. J. Cooke, G. M. Fuller, J. Meyers and M. W. Paris, *Big Bang Nucleosynthesis and Neutrino Cosmology*, 1903.09187.

[184] LUNA collaboration, D. Trezzi and Trezzi, *Study of the 2H(p,Îş)3He reaction in the BBN energy range at LUNA*, *J. Phys. Conf. Ser.* **940** (2018) 012059.

[185] A. LaguÃń and J. Meyers, *Prospects and Limitations for Constraining Light Relics with Primordial Abundance Measurements*, 1908.05291.

[186] G. Krnjaic and S. D. McDermott, *Implications of BBN Bounds for Cosmic Ray Upscattered Dark Matter*, 1908.00007.

[187] G. Arcadi, T. Hugle and F. S. Queiroz, *The Dark $L_\mu - L_\tau$ Rises via Kinetic Mixing*, *Phys. Lett.* **B784** (2018) 151 [1803.05723].

[188] P. Foldenauer, *Light dark matter in a gauged $U(1)_{L_\mu - L_\tau}$ model*, *Phys. Rev.* **D99** (2019) 035007 [1808.03647].

[189] N. Okada and O. Seto, *Higgs portal dark matter in the minimal gauged $U(1)_{B-L}$ model*, *Phys. Rev.* **D82** (2010) 023507 [1002.2525].

[190] M. Escudero, S. J. Witte and N. Rius, *The dispirited case of gauged $U(1)_{B-L}$ dark matter*, *JHEP* **08** (2018) 190 [1806.02823].

[191] K. M. Zurek, *Asymmetric Dark Matter: Theories, Signatures, and Constraints*, *Phys. Rept.* **537** (2014) 91 [1308.0338].

[192] K. Petraki and R. R. Volkas, *Review of asymmetric dark matter*, *Int. J. Mod. Phys.* **A28** (2013) 1330028 [1305.4939].

[193] A. Berlin and N. Blinov, *Thermal Dark Matter Below an MeV*, *Phys. Rev. Lett.* **120** (2018) 021801 [1706.07046].

[194] A. Berlin, N. Blinov and S. W. Li, *Dark Sector Equilibration During Nucleosynthesis*, *Phys. Rev.* **D100** (2019) 015038 [1904.04256].

[195] N. Blinov, K. J. Kelly, G. Z. Krnjaic and S. D. McDermott, *Constraining the Self-Interacting Neutrino Interpretation of the Hubble Tension*, 1905.02727.

[196] P. Ilten, Y. Soreq, M. Williams and W. Xue, *Serendipity in dark photon searches*, *JHEP* **06** (2018) 004 [1801.04847].

[197] M. Bauer, P. Foldenauer and J. Jaeckel, *Hunting All the Hidden Photons*, *JHEP* **07** (2018) 094 [1803.05466].

[198] G. Steigman, *Equivalent Neutrinos, Light WIMPs, and the Chimera of Dark Radiation*, *Phys. Rev.* **D87** (2013) 103517 [1303.0049].

[199] Z. Berezhiani, A. Dolgov and I. Tkachev, *BBN with light dark matter*, *JCAP* **1302** (2013) 010 [1211.4937].

[200] P. F. de Salas, M. Lattanzi, G. Mangano, G. Miele, S. Pastor and O. Pisanti, *Bounds on very low reheating scenarios after Planck*, *Phys. Rev.* **D92** (2015) 123534 [1511.00672].

[201] T. Hasegawa, N. Hiroshima, K. Kohri, R. S. L. Hansen, T. Tram and S. Hannestad, *MeV-scale reheating temperature and thermalization of oscillating neutrinos by radiative and hadronic decays of massive particles*, 1908.10189.

[202] M. Kawasaki, K. Kohri, T. Moroi and Y. Takaesu, *Revisiting Big-Bang Nucleosynthesis Constraints on Long-Lived Decaying Particles*, *Phys. Rev.* **D97** (2018) 023502 [1709.01211].

[203] M. Hufnagel, K. Schmidt-Hoberg and S. Wild, *BBN constraints on MeV-scale dark sectors. Part II. Electromagnetic decays*, *JCAP* **1811** (2018) 032 [1808.09324].

[204] L. Forestell, D. E. Morrissey and G. White, *Limits from BBN on Light Electromagnetic Decays*, *JHEP* **01** (2019) 074 [1809.01179].

[205] W. Hu and J. Silk, *Thermalization and spectral distortions of the cosmic background radiation*, *Phys. Rev.* **D48** (1993) 485.

[206] W. Hu and J. Silk, *Thermalization constraints and spectral distortions for massive unstable relic particles*, *Phys. Rev. Lett.* **70** (1993) 2661.

[207] M. J. Boschini et al., *Solution of heliospheric propagation: unveiling the local interstellar spectra of cosmic ray species*, *Astrophys. J.* **840** (2017) 115 [1704.06337].

[208] AMS 02 collaboration, C. Consolandi, *Primary Cosmic Ray Proton Flux Measured by AMS-02*, in *Proceedings, 33rd International Cosmic Ray Conference (ICRC2013): Rio de Janeiro, Brazil, July 2-9, 2013*, p. 1265, 2014, 1402.0467, http://www.slac.stanford.edu/econf/C131112/papers/1402.0467.pdf.

[209] T. Pierog, I. Karpenko, J. M. Katzy, E. Yatsenko and K. Werner, *EPOS LHC: Test of collective*

hadronization with data measured at the CERN Large Hadron Collider, *Phys. Rev.* **C92** (2015) 034906 [1306.0121].

[210] C. Baus, T. Pierog and R. Ulrich, *Cosmic Ray Monte Carlo (CRMC)*.

[211] A. S. Jursa, *Handbook of geophysics and the space environment*. Hanscom Air Force Base, Mass. : Air Force Geophysics Laboratory, Air Force Systems Command, United States Air Force, 4 ed., 1985.

[212] S. Haino et al., *Measurements of primary and atmospheric cosmic - ray spectra with the BESS-TeV spectrometer*, *Phys. Lett.* **B594** (2004) 35 [astro-ph/0403704].

[213] Particle Data Group collaboration, M. Tanabashi et al., *Review of Particle Physics*, *Phys. Rev.* **D98** (2018) 030001.

[214] B. J. Kavanagh, R. Catena and C. Kouvaris, *Signatures of Earth-scattering in the direct detection of Dark Matter*, *JCAP* **1701** (2017) 012 [1611.05453].

[215] CRESST collaboration, G. Angloher et al., *Results on MeV-scale dark matter from a gram-scale cryogenic calorimeter operated above ground*, *Eur. Phys. J.* **C77** (2017) 637 [1707.06749].

[216] A. Bhoonah, J. Bramante, F. Elahi and S. Schon, *Calorimetric Dark Matter Detection With Galactic Center Gas Clouds*, *Phys. Rev. Lett.* **121** (2018) 131101 [1806.06857].

[217] E. O. Nadler, V. Gluscevic, K. K. Boddy and R. H. Wechsler, *Constraints on Dark Matter Microphysics from the Milky Way Satellite Population*, 1904.10000.

[218] G. Duda, A. Kemper and P. Gondolo, *Model Independent Form Factors for Spin Independent Neutralino-Nucleon Scattering from Elastic Electron Scattering Data*, *JCAP* **0704** (2007) 012 [hep-ph/0608035].

[219] G. Bellini, L. Ludhova, G. Ranucci and F. L. Villante, *Neutrino oscillations*, *Adv. High Energy Phys.* **2014** (2014) 191960 [1310.7858].

[220] G. Steigman, B. Dasgupta and J. F. Beacom, *Precise Relic WIMP Abundance and its Impact on Searches for Dark Matter Annihilation*, *Phys. Rev.* **D86** (2012) 023506 [1204.3622].

[221] K. M. Nollett and G. Steigman, *BBN And The CMB Constrain Neutrino Coupled Light WIMPs*, *Phys. Rev.* **D91** (2015) 083505 [1411.6005].

[222] M. Escudero, *Neutrino decoupling beyond the Standard Model: CMB constraints on the Dark Matter mass with a fast and precise $N_{\rm eff}$ evaluation*, *JCAP* **1902** (2019) 007 [1812.05605].

[223] C. D. Kreisch, F.-Y. Cyr-Racine and O. DorÃľ, *The Neutrino Puzzle: Anomalies, Interactions, and Cosmological Tensions*, 1902.00534.

[224] R. J. Wilkinson, A. C. Vincent, C. BÅŞhm and C. McCabe, *Ruling out the light weakly interacting massive particle explanation of the Galactic 511 keV line*, *Phys. Rev.* **D94** (2016) 103525 [1602.01114].

[225] C. Dermer and G. Menon, *High Energy Radiation from Black Holes: Gamma Rays, Cosmic Rays, and Neutrinos*, Princeton Series in Astrophysics. Princeton University Press, 2009.

[226] P. Padovani, F. Oikonomou, M. Petropoulou, P. Giommi and E. Resconi, *TXSâĂĽ0506+056, the first cosmic neutrino source, is not a BL Lac*, *Mon. Not. Roy. Astron. Soc.* **484** (2019) L104 [1901.06998].

[227] S. Gao, A. Fedynitch, W. Winter and M. Pohl, *Modelling the coincident observation of a high-energy neutrino and a bright blazar flare*, *Nat. Astron.* **3** (2019) 88 [1807.04275].

[228] X. Rodrigues, S. Gao, A. Fedynitch, A. Palladino and W. Winter, *Leptohadronic Blazar Models Applied to the 2014âĂŞ2015 Flare of TXS 0506+056*, *Astrophys. J.* **874** (2019) L29 [1812.05939].

[229] A. Keivani et al., *A Multimessenger Picture of the Flaring Blazar TXS 0506+056: implications for High-Energy Neutrino Emission and Cosmic Ray Acceleration*, *Astrophys. J.* **864** (2018) 84 [1807.04537].

[230] I. Taboada, *Hawc gamma ray data prior to icecube-170922a*, 2018.

[231] K. Murase, Y. Inoue and C. D. Dermer, *Diffuse Neutrino Intensity from the Inner Jets of Active Galactic Nuclei: Impacts of External Photon Fields and the Blazar Sequence*, *Phys. Rev.* **D90**

(2014) 023007 [1403.4089].
[232] A. Olivares-Del Campo, C. BÅŞhm, S. Palomares-Ruiz and S. Pascoli, *Dark matter-neutrino interactions through the lens of their cosmological implications*, *Phys. Rev.* **D97** (2018) 075039 [1711.05283].
[233] G. Mangano, G. Miele, S. Pastor, T. Pinto, O. Pisanti and P. D. Serpico, *Relic neutrino decoupling including flavor oscillations*, *Nucl. Phys.* **B729** (2005) 221 [hep-ph/0506164].
[234] P. F. de Salas and S. Pastor, *Relic neutrino decoupling with flavour oscillations revisited*, *JCAP* **1607** (2016) 051 [1606.06986].
[235] L. Kawano, *Let's Go: Early Universe. Guide to Primordial Nucleosynthesis Programming*, .
[236] L. Kawano, *Let's go: Early universe. 2. Primordial nucleosynthesis: The Computer way*, .
[237] O. Pisanti, A. Cirillo, S. Esposito, F. Iocco, G. Mangano, G. Miele et al., *PArthENoPE: Public Algorithm Evaluating the Nucleosynthesis of Primordial Elements*, *Comput. Phys. Commun.* **178** (2008) 956 [0705.0290].
[238] R. Consiglio, P. F. de Salas, G. Mangano, G. Miele, S. Pastor and O. Pisanti, *PArthENoPE reloaded*, *Comput. Phys. Commun.* **233** (2018) 237 [1712.04378].
[239] T. M. Bania, R. T. Rood and D. S. Balser, *The cosmological density of baryons from observations of 3He+ in the Milky Way*, *Nature* **415** (2002) 54.
[240] E. Vangioni-Flam, K. A. Olive, B. D. Fields and M. Casse, *On the baryometric status of He-3*, *Astrophys. J.* **585** (2003) 611 [astro-ph/0207583].
[241] L. Perotto, J. Lesgourgues, S. Hannestad, H. Tu and Y. Y. Y. Wong, *Probing cosmological parameters with the CMB: Forecasts from full Monte Carlo simulations*, *JCAP* **0610** (2006) 013 [astro-ph/0606227].
[242] Planck collaboration, N. Aghanim et al., *Planck 2018 results. VI. Cosmological parameters*, 1807.06209.
[243] S. F. King, *Models of Neutrino Mass, Mixing and CP Violation*, *J. Phys.* **G42** (2015) 123001 [1510.02091].
[244] F. Couchot, S. Henrot-VersillÃľ, O. Perdereau, S. Plaszczynski, B. RouillÃľ d'Orfeuil, M. Spinelli et al., *Cosmological constraints on the neutrino mass including systematic uncertainties*, *Astron. Astrophys.* **606** (2017) A104 [1703.10829].
[245] A. Ringwald and Y. Y. Y. Wong, *Gravitational clustering of relic neutrinos and implications for their detection*, *JCAP* **0412** (2004) 005 [hep-ph/0408241].
[246] A. De Lavallaz and M. Fairbairn, *Voids as Alternatives to Dark Energy and the Propagation of Gamma Rays through the Universe*, *Phys. Rev. Lett.* **108** (2012) 171301 [1111.4577].
[247] A. Mucke, J. P. Rachen, R. Engel, R. J. Protheroe and T. Stanev, *On photohadronic processes in astrophysical environments*, *Publ. Astron. Soc. Austral.* **16** (1999) 160 [astro-ph/9808279].
[248] A. P. Szabo and R. J. Protheroe, *Implications of particle acceleration in active galactic nuclei for cosmic rays and high-energy neutrino astronomy*, *Astropart. Phys.* **2** (1994) 375 [astro-ph/9405020].
[249] J. D. Finke, S. Razzaque and C. D. Dermer, *Modeling the Extragalactic Background Light from Stars and Dust*, *Astrophys. J.* **712** (2010) 238 [0905.1115].

Appendix

A Big Bang Nucleosynthesis

A.1 Temperature Evolution and Universe's Expansion

When a neutrinophilic BSM particle is present, the differential equations governing the evolution of T_ν and T_γ read:

$$\begin{cases} \dfrac{dT_\nu}{dt} = -\dfrac{12H\rho_\nu + 3H(\rho_\chi + p_\chi) - 3\frac{\delta\rho_\nu}{\delta t}}{3\,\frac{\partial\rho_\nu}{\partial T_\nu} + \frac{\partial\rho_\chi}{\partial T_\nu}}\,, & \text{(4.16a)} \\ \dfrac{dT_\gamma}{dt} = -\dfrac{4H\rho_\gamma + 3H\,(\rho_e + p_e) + 3H\,T_\gamma\frac{dP_{\rm int}}{dT_\gamma} + 3\frac{\delta\rho_\nu}{\delta t}}{\frac{\partial\rho_\gamma}{\partial T_\gamma} + \frac{\partial\rho_e}{\partial T_\gamma} + T_\gamma\frac{d^2P_{\rm int}}{dT_\gamma^2}}\,, & \text{(4.16b)} \end{cases}$$

whilst for an electrophilic particle, they are given by:

$$\begin{cases} \dfrac{dT_\nu}{dt} = -\dfrac{12H\rho_\nu - 3\frac{\delta\rho_\nu}{\delta t}}{3\,\frac{\partial\rho_\nu}{\partial T_\nu}}\,, & \text{(4.17a)} \\ \dfrac{dT_\gamma}{dt} = -\dfrac{4H\rho_\gamma + 3H\,(\rho_e + p_e) + 3H\,(\rho_\chi + p_\chi) + 3H\,T_\gamma\frac{dP_{\rm int}}{dT_\gamma} + 3\frac{\delta\rho_\nu}{\delta t}}{\frac{\partial\rho_\gamma}{\partial T_\gamma} + \frac{\partial\rho_e}{\partial T_\gamma} + \frac{\partial\rho_\chi}{\partial T_\gamma} + T_\gamma\frac{d^2P_{\rm int}}{dT_\gamma^2}}\,, & \text{(4.17b)} \end{cases}$$

where ρ_i and p_i correspond to the energy density and pressure of a given particle respectively, $H = \sqrt{(8\pi/3)\sum_i \rho_i/M_{\rm Pl}^2}$ is the Hubble parameter, $M_{\rm Pl} = 1.22\times10^{19}\,\text{GeV}$ the Planck mass, and $P_{\rm int}$ and its derivatives account for finite temperature corrections. The reader is referred to [109] for further details. Here, $\delta\rho_\nu/\delta t$ corresponds to the energy exchange rate between neutrinos and electrons. Accounting for Fermi-Dirac statistics in the rates and setting $m_e = 0$, it reads [110]:

$$\left.\frac{\delta\rho_\nu}{\delta t}\right|_{\rm SM} = \frac{G_F^2}{\pi^5}\left(1 - \frac{4}{3}s_W^2 + 8s_W^4\right)\times\left[32\,f_a^{\rm FD}\,\left(T_\gamma^9 - T_\nu^9\right) + 56\,f_s^{\rm FD}\,T_\gamma^4\,T_\nu^4\,\left(T_\gamma - T_\nu\right)\right]\,, \qquad (4.18)$$

where $s_{\rm W}^2 = 0.223$ [99], $G_{\rm F}$ is Fermi's constant, $f_a^{\rm FD} = 0.884$, $f_s^{\rm FD} = 0.829$, and we account for the electron mass as in [110].

We solve Equations (4.16a) – (4.17b) for $1\,\text{keV} < T_\gamma < 30\,\text{MeV}$. We start the integration at $t_0 = 1/(2H)|_{T=30\,\text{MeV}}$ for which we use as an initial condition $T_\gamma = T_\nu = 30\,\text{MeV}$, since for such high temperatures SM neutrino-electron interactions are highly efficient. By solving this set of differential

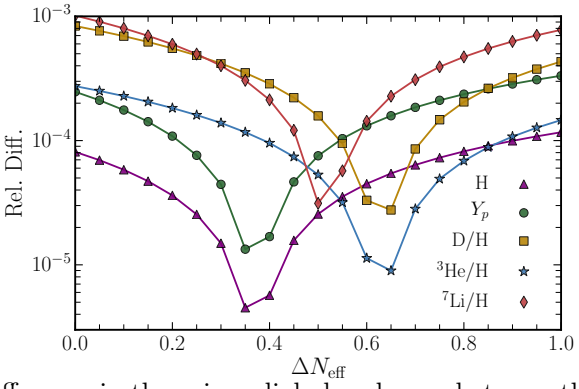

Figure A.1 Relative difference in the primordial abundances between the default version of PRIMAT and our modified version of it as a function of $\Delta N_{\rm eff}$. Predictions are done using $\Omega_{\rm b}h^2 = 0.02225$ and $\tau_n = 879.5$ s.

equations, we find all the key background evolution quantities as a function of time, scale factor and temperature. In addition, we evaluate the number of effective relativistic degrees of freedom $N_{\rm eff}$ as relevant for CMB observations,

$$N_{\rm eff} \equiv \frac{8}{7}\left(\frac{11}{4}\right)^{4/3}\left(\frac{\rho_{\rm rad}-\rho_\gamma}{\rho_\gamma}\right) = 3\left(\frac{11}{4}\right)^{4/3}\left(\frac{T_\nu}{T_\gamma}\right)^4 , \tag{4.19}$$

where in the last step we have assumed that $\rho_{\rm rad} = \rho_\nu + \rho_\gamma$. By solving this system of equations in the SM we find $N_{\rm eff}^{\rm SM} = 3.046$ [110], a result that is in perfect agreement with state-of-the-art calculations [233, 234].

A.2 Consistency Checks of Modified BBN Code

We checked whether our modifications do not significantly change the values of the primordial helium and deuterium abundances in Standard Model BBN compared to the base version of PRIMAT. Table IV.3 shows the relative difference in the output of the two codes and it is clear that the accuracy is better than 0.1%.

Abundances	PRIMAT	**Modified** PRIMAT	**Relative Difference (%)**
$Y_{\rm p}$	0.24709	0.24717	0.03
$10^5 \times {\rm D/H}\vert_{\rm P}$	2.4592	2.4613	0.08

Table IV.3: Primordial abundances as computed using PRIMAT and our modified version with $\Omega_{\rm b}h^2 = 0.02225$ and $\tau_n = 879.5$ s.

We also compared our modifications to PRIMAT when massless dark radiation is present, which we parametrize in terms of $\Delta N_{\rm eff}$. In PRIMAT this is done by increasing $N_{\rm eff}$ directly in the Friedmann equations while in our modified version of the code it is done by including the evolution of a non-interacting, relativistic component. The result is shown in Figure A.1. The test shows an accuracy better than 0.1% for all relevant nuclides in the range $0 \leq \Delta N_{\rm eff} \leq 1$.

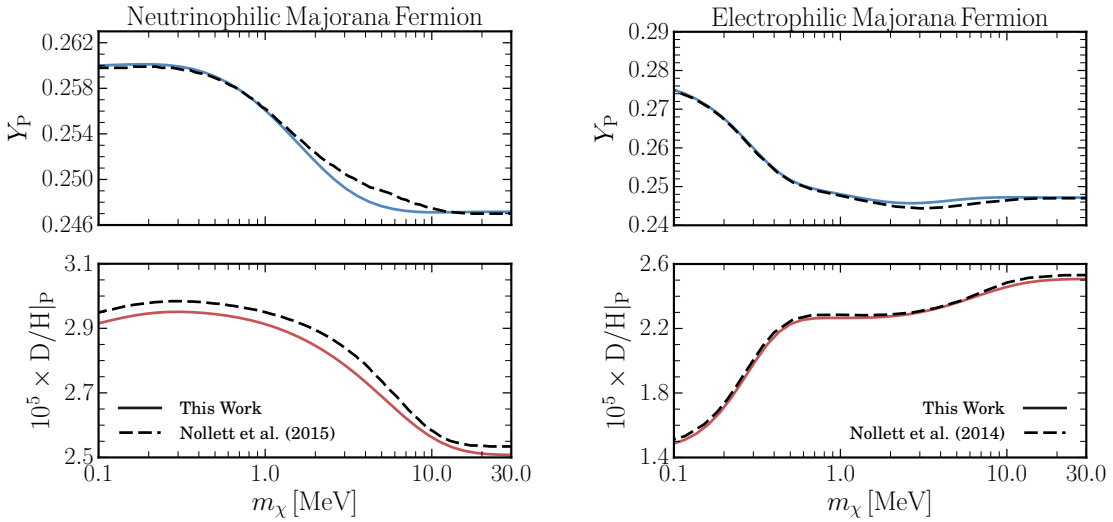

Figure A.2 Comparison with previous literature for the primordial abundances Y_P and $D/H|_P$ as a function of the mass of a Majorana BSM particle that couples exclusively to neutrinos (left panels) or electrons (right panels). The solid lines are from this work and the dashed lines from [103] and [104].

A.3 Comparison with Previous Literature

In this appendix we make a direct comparison between our results and those reported in [103] and [104]. Refs [103] and [104] used a modified version of the Kawano code [235, 236]. In Figure A.2, we consider two cases: a Majorana fermion that is purely neutrinophilic or electrophilic. We compute the predictions for helium and deuterium using $\tau_n = 880.1$ s and $\Omega_b h^2 = 0.022$ as in [103] and [104]. We observe a few small differences:

1. Our predicted values of $D/H|_P$ are smaller than those reported in [103, 104]. Since the difference is WIMP mass independent, we attribute it to updated nuclear reaction rates in `PRIMAT`.
2. The predicted values of Y_P are slightly different for $1\,\text{MeV} \lesssim m_\chi \lesssim 15\,\text{MeV}$. The reason is twofold:
   (a) [103, 104] considered that neutrinos decoupled instantaneously and tracked the temperature evolution by using entropy conservation, while we solve for the time evolution of neutrino decoupling. Imposing entropy conservation leads to a feature in the neutrino temperature evolution that affects both the Universe's expansion and the proton-to-neutron conversion rates, see Figure 2 of [109].
   (b) [103, 104] considered instantaneous neutrino decoupling at $T_\nu^{\rm dec} = 2.0\,\text{MeV}$, while an estimate based on the actual neutrino temperature time evolution yields $T_\nu^{\rm dec} = 1.91\,\text{MeV}$ [109]. Considering a smaller neutrino decoupling temperature leads to an impact on the proton-to-neutron rates and also reduces the impact of heavier BSM species in neutrino decoupling.

We have also compared our predictions of Y_P and $D/H|_P$ with those reported in [102] (which used `PArthENoPEv1` [237], see [238] for an updated version of the code). We find good overall agreement with [102] and small differences similar to those we find when comparing to [103, 104]. Note that [107] provided updated bounds to those presented in [102] although the predictions for Y_P and $D/H|_P$ are not displayed in that reference.

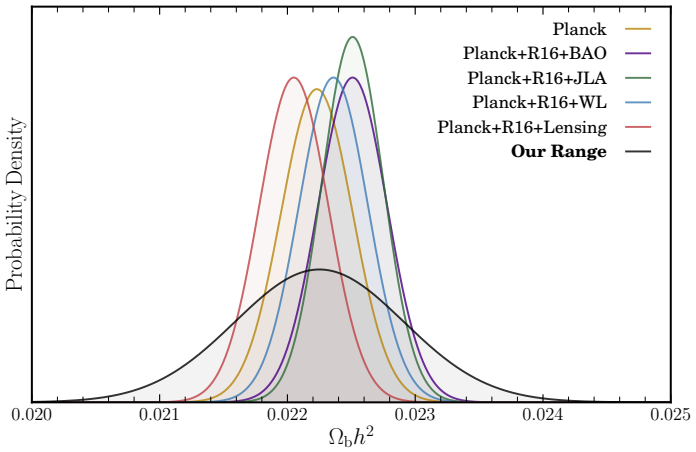

Figure A.3 Illustration of the parameter range for the baryon density we consider in the BBN+$\Omega_b h^2$ analysis as compared to the best-fit values and errors given in Table II of [176]. The authors of [176] infer $\Omega_b h^2$ in a well-motivated 12-parameter extension to ΛCDM using the different data sets shown in the legend. Note in particular that our conservative range for the baryon density encompasses all derived central values and errors.

A.4 Conservative Range for the Baryon Density from CMB observations

In the BBN+$\Omega_b h^2$ analysis we consider $\Omega_b h^2 = 0.02225 \pm 0.00066$ to be a conservative and cosmological model independent determination of the baryon energy density by current CMB observations. $\Omega_b h^2 = 0.02225 \pm 0.00066$ has a 4.4 times larger error bar than the one associated with ΛCDM using Planck 2018 observations [14], and furthermore, it covers well the inferred value of $\Omega_b h^2$ in a well-motivated 12-parameter extensions of ΛCDM using different data sets [175, 176]. In Figure A.3, one can appreciate that indeed the range with a central value of $\Omega_b h^2 = 0.02225 \pm 0.00066$ covers very well the posterior distributions of $\Omega_b h^2$ of such a 12-parameter extension of ΛCDM including various data sets in conjuntion to Planck CMB observations.

A.5 Implications for Lithium-7 and Helium-3

We show the evolution of the primordial $^7\mathrm{Li/H}|_\mathrm{P}$ and $^3\mathrm{He/H}|_\mathrm{P}$ abundances in Figure A.4 as a function of the mass of a thermal BSM particle. We note that the upper panels do not include any confidence intervals, since it is well known that current measurements of the primordial lithium-7 are in disagreement with SM predictions using the baryon-to-photon ratio inferred from CMB observations [99]. The excluded regions in the lower panels are based on observations of helium-3 in our galaxy [239]. Helium-3 can be both produced and destroyed in stars, which makes it difficult to precisely determine the time evolution of its primordial abundance [240]. Therefore, we have not included measurements of either lithium-7 or helium-3 in our analysis. Nevertheless, if the situation changes in the future, it will be straightforward to obtain bounds from Figure A.4 and see how it improves the current BBN constraints.

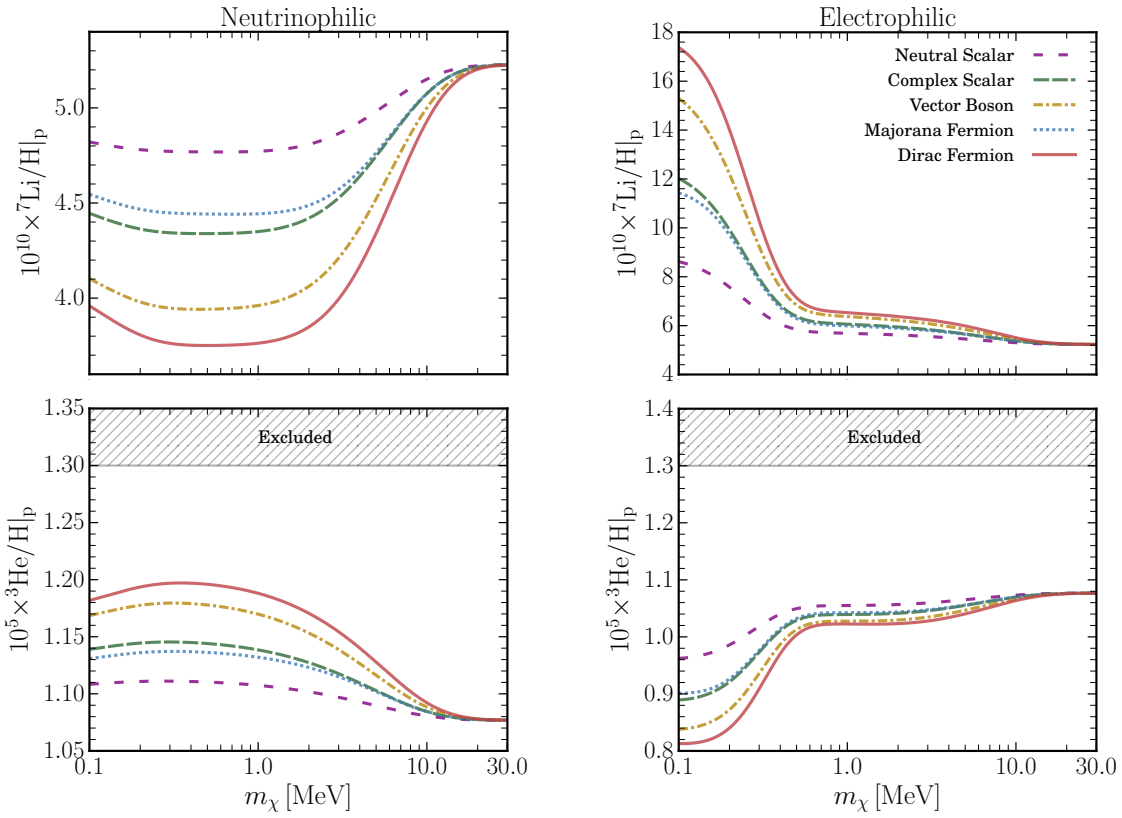

Figure A.4 Cosmological impact of light BSM particles in thermal equilibrium with the SM plasma as a function of their mass m_χ. The *left/right panels* correspond to neutrinophilic/electrophilic particles. *Upper panels:* The lithium-7 primordial abundance ${}^7\mathrm{Li/H}|_\mathrm{P}$. Measurements of ${}^7\mathrm{Li/H}|_\mathrm{P}$ are not shown for clarity, see e.g. [99] for current measurements. *Lower panels:* The helium-3 primordial abundance ${}^3\mathrm{He/H}|_\mathrm{P}$. The grey contours correspond to an upper limit as reported by [239]. The predictions are made with $\Omega_\mathrm{b}h^2 = 0.021875$ and $\tau_n = 879.5\,\mathrm{s}$.

A.6 CMB-S4 Forecast

In order to forecast the reach of CMB-S4 constraints, we first choose a fiducial cosmology with cosmological parameters equal to the Planck 2018 TTTEEE+lowE mean values as in Table 2 of [14], which are reproduced below in Table IV.4. The fiducial helium abundance is obtained by running `PRIMAT` within the Standard Model and fiducial cosmology.

To forecast the sensitivity of future CMB experiments, we employ the same procedure as used in the CMB-S4 Science Book [180]. Assuming Gaussian statistics, the Fisher matrix for CMB experiments is given by

$$F_{ij} = \sum_{X,Y} \sum_{\ell=\ell_\mathrm{min}}^{\ell_\mathrm{max}} \frac{\partial \mathcal{C}_\ell^X}{\partial \theta_i} \left[\mathbf{C}_\ell^{XY}\right]^{-1} \frac{\partial \mathcal{C}_\ell^Y}{\partial \theta_i} \tag{4.20}$$

with indices $X = ab$, $Y = cd$ and $a, b, c, d \in \{T, E, B\}$. The covariance matrix $\mathbf{C}_\ell^{XY}$ for each multipole ℓ is defined as

$$\mathbf{C}_\ell^{abcd} = \frac{1}{(2\ell+1) f_{\rm sky}} \left[\left(\mathcal{C}_\ell^{ac} + N_\ell^{ac}\right) \left(\mathcal{C}_\ell^{bd} + N_\ell^{bd}\right) + \left(\mathcal{C}_\ell^{ad} + N_\ell^{ad}\right) \left(\mathcal{C}_\ell^{bc} + N_\ell^{bc}\right) \right] \,, \tag{4.21}$$

with $f_{\rm sky}$ the effective fraction of sky covered by the experiment, $\mathcal{C}_\ell^X$ the simulated CMB power spectra and N_ℓ^X (Gaussian) noise power spectra. The noise is approximated as

$$N_\ell^{aa} = (\Delta X)^2 \exp\left(\frac{\ell(\ell+1)\theta^2_{\rm FWHM}}{8 \ln 2} \right) \,, \tag{4.22}$$

where $\Delta X \in \{\Delta T, \Delta P\}$ and $N_\ell^{TE} = 0$. We adopt a similar configuration as used in the CMB-S4 Science Book: lensed power spectra with $\ell_{\rm min} = 30$, $\{\ell^{TT}_{\rm max}, \ell^{TE}_{\rm max}\} = 3000$, $\{\ell^{EE}_{\rm max}, \ell^{BB}_{\rm max}\} = 5000$, $f_{\rm sky} = 0.4$, $\theta_{\rm FWHM} = 1'$, $\Delta T = 1$ μK-arcmin and $\Delta P = \sqrt{2}$ μK-arcmin.

The `CLASS` code [171] is used to obtain the power spectra. The numerical derivatives are computed using the symmetric derivative $\mathcal{C}'_\ell(\theta) = \left[\mathcal{C}_\ell(\theta + \Delta\theta) - \mathcal{C}_\ell(\theta - \Delta\theta)\right] / (2\Delta\theta)$, with fiducial parameter θ and stepsize $\Delta\theta$. The stepsizes used are of order $\Delta\theta_i \sim \sigma(\theta_i)$, as to output a more reliable estimate of the confidence level [241]. The CMB-S4 Fisher matrix is then added to the Planck 2018 low-ℓ TTTEEE+lowP+lowE Fisher matrix to obtain the combined constraints. The fiducial parameters and step sizes used in our computations, together with the forecasted sensitivities, are listed in Table IV.4. We find good overall agreement with the forecasts performed in [180] within ΛCDM.

Parameter	**Fiducial Value**	$\boldsymbol{\Delta\theta}$	**CMB-S4**	**CMB-S4+Planck**
$\Omega_{\rm b}h^2$	0.02236	3×10^{-5}	4.9×10^{-5}	4.7×10^{-5}
$\Omega_{\rm c}h^2$	0.1202	6×10^{-4}	1.8×10^{-3}	1.3×10^{-3}
$100\theta_{\rm s}$	1.04090	2×10^{-4}	2.3×10^{-4}	1.8×10^{-4}
$\ln(10^{10} A_{\rm s})$	3.045	9.5×10^{-3}	1.2×10^{-2}	8.1×10^{-3}
$n_{\rm s}$	0.9649	2×10^{-3}	3.7×10^{-3}	2.9×10^{-3}
τ	0.0544	6×10^{-3}	7.2×10^{-3}	4.8×10^{-3}
$N_{\rm eff}$	3.046	3×10^{-2}	1.1×10^{-1}	8.1×10^{-2}
$Y_{\rm P}$	0.2472	4×10^{-3}	6.1×10^{-3}	4.3×10^{-3}

Table IV.4: Forecasted sensitivities of CMB-S4 and CMB-S4+Planck 2018 for the parameters of $\Lambda\text{CDM} + N_{\rm eff} + Y_{\rm P}$. The column $\Delta\theta$ refers to the stepsizes used to compute the numerical derivatives.

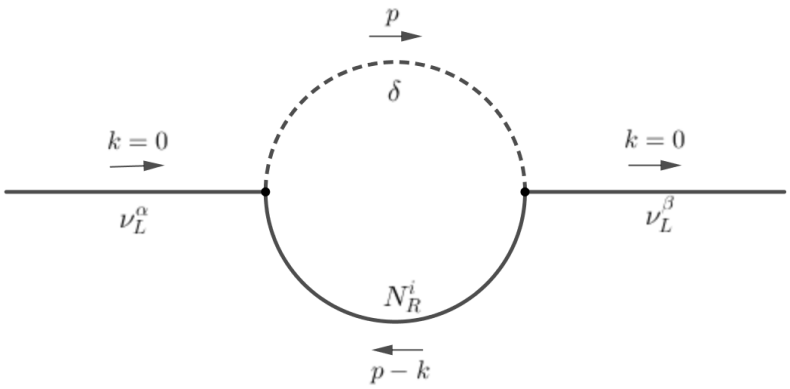

Figure B.1 The one loop diagram contributing to the neutrino mass in the case that δ is a real scalar. The external neutrinos are evaluated at zero incoming momenta so as to extract only the mass contribution as opposed to the quadratic derivative interactions.

B Neutrino Propagation

B.1 Neutrino Masses

In this section we will present the contribution to the neutrino mass matrix that arises due to interaction term in (4.5). The Majorana mass term for the neutrino is of the form;

$$\frac{1}{2}(m_\nu)_{\alpha\beta}\left(\bar{\nu}_L^\alpha \nu_L^\beta + \text{h.c.}\right) \tag{4.23}$$

We are interested in the mass matrix $(m_\nu)_{\alpha\beta}$. To do so, we will need to distinguish between the two cases where either (i) δ is a real scalar field, or, (ii) δ is a complex scalar field.

Case 1: Real Scalar Field In this case, there is only one diagram that contributes to the neutrino mass, as shown in Figure B.1. As in [125, 138, 143], the result in the real case is;

$$(m_\nu)_{\alpha\beta} = \sum_i \frac{g_{i\alpha}g_{i\beta}}{16\pi^2} m_{N^i}\left(\log\frac{\Lambda^2}{m_{N^i}^2} - \frac{m_\delta^2}{m_{N^i}^2 - m_\delta^2}\log\frac{m_{N^i}^2}{m_\delta^2}\right) \tag{4.24}$$

Case 2: Complex Scalar Field To repeat the calculation for the complex scalar field, we should first think about the scalar degrees of freedom. Since the field is in the trivial representation of the electroweak gauge group, the most general hermitian mass term for δ can be written as [138];

$$V_m = M^2\delta^\dagger\delta - \frac{1}{2}(m^2\delta\delta + \text{h.c.}) \tag{4.25}$$

Consider expanding the scalar field as $\delta = \frac{1}{\sqrt{2}}(\delta_1 + i\delta_2)$ where $\delta_{1,2}$ are both real fields. Expanding the terms above in terms of these real degrees of freedom;

$$V_m = \frac{1}{2}M^2(\delta_1 + i\delta_2)(\delta_1 - i\delta_2) - \frac{1}{4}m^2\left((\delta_1 + i\delta_2)(\delta_1 + i\delta_2) + (\delta_1 - i\delta_2)(\delta_1 - i\delta_2)\right) \tag{4.26}$$

Collecting the terms together for each field we find;

$$V_m = \frac{1}{2}(M^2 - m^2)\delta_1^2 + \frac{1}{2}(M^2 + m^2)\delta_2^2 \tag{4.27}$$

We can then immediately see that the mass eigenstates are simply δ_1 and δ_2 themselves, with masses $m_{\delta_1}^2 = M^2 - m^2$, $m_{\delta_2}^2 = M^2 + m^2$. The lighter of these will be our Dark Matter candidate. Also note that interaction term (4.5) is diagonal in this mass basis;

$$\mathcal{L}_{\text{int}} = g_{i\alpha}\bar{N}_R^i\nu_L^\alpha(\delta_1 + i\delta_2) \tag{4.28}$$

The contributions to the neutrino mass are then two diagrams of the form in Figure B.1. One will have δ_1 running round the loop, whilst the other will have δ_2. We note that the only difference between them is that the second diagram will have two couplings with an extra factor of i, $(ig_{i\alpha})(ig_{i\beta}) = -g_{i\alpha}g_{i\beta}$. As such the second will come with a negative sign. The total contribution is then a sum of two contributions of the form (4.24). Importantly, we see that the dependence on the cutoff drops out in the complex case and we find;

$$(m_\nu)_{\alpha\beta} = \sum_i \frac{g_{i\alpha}g_{i\beta}}{16\pi^2} m_{N^i}\left(\frac{m_{\delta_2}^2}{m_{N^i}^2 - m_{\delta_2}^2}\log\frac{m_{N^i}^2}{m_{\delta_2}^2} - \frac{m_{\delta_1}^2}{m_{N^i}^2 - m_{\delta_1}^2}\log\frac{m_{N^i}^2}{m_{\delta_1}^2}\right) \tag{4.29}$$

B.2 Why do we only have to worry about one process?

In Section 4.2.3 where we detailed how to do the calculation for $\nu\nu \to \delta\delta$, we neglected to calculate the cross section for other processes within the model that may also lead to a neutrino interaction. These additional processes are as follows;

1. $\nu\nu \to NN$: One can construct scenarios in parameter space where this dominates. However the centre of mass energy: $E_{\text{com}} = \sqrt{2E_\nu m_\nu}$ where m_ν is the mass of the cosmic neutrino background neutrino, is close to the mass of the lightest scalar δ. By construction if the scalar is the dark matter candidate, then the mass of N, m_N, must be larger. Thus, even in scenarios where the centre of mass energy is large enough to produce two N particles, the cross section is likely to lie at the front tail of the distribution and so be subdominant.

2. $\nu N \to \nu N$: There is an s-channel and a t-channel diagram for this process. Independent of this however, we have assumed that N is not the dark matter candidate. As such, we expect the relic density to be very low in comparison to all other particles. The vertex structure ensures that we expect the cross section to be of a similar order of magnitude to the $\nu\nu \to \delta\delta$ case. Hence, the contribution to the mean free path is negligible.

3. $\nu\delta \to \nu\delta$: It is not immediately clear as to whether this will be negligible. Firstly, there is a t-channel process that will have a similar algebraic cross section as previously calculated in

$\nu\nu \to \delta\delta$. There is also an s-channel process, whose cross-section we obtain from [137]. Secondly, we must check the contribution to the mean free path in two regimes;

- On a cosmological scale where n_δ is given by the relic density of dark matter,
- On a galactic scale, where the density is much higher within the dark matter halo.

Note that neglecting these processes is of course a simplifying assumption about the nature of the cross-sections, but they do not affect the interpretation of the results. This is because including any of the additional contributions above can only *improve* the bounds; for a given ℓ, introducing a new process increases the effective cross section, and reduces the mean free path leading to tighter constraints.

B.3 Contribution from $\nu\delta \to \nu\delta$

As mentioned above, we must check whether the $\nu\delta \to \nu\delta$ process contributes significantly to the mean free path of the blazar neutrino. In what follows, we will find that it does not contribute significantly. This is due to the fact that, even within the galactic halo, the cross-section is too small to generate a significant contribution.

t-Channel Cross Section

The relationship;

$$u = m_\delta^2 - \frac{1}{2}s - \sqrt{s\left(\frac{1}{4}s - m_\delta^2\right)}\cos\theta \tag{4.30}$$

along with the observation that for $\nu\delta \to \nu\delta$ with $m_\delta \sim \mathcal{O}(\text{MeV})$ and $E_\nu \sim \mathcal{O}(TeV)$, it follows that $s \sim \mathcal{O}(GeV) \gg m_\delta$. This then implies in this energy regime, $u \simeq s$. By crossing symmetry, we then deduce that the dependence of $\sigma_t(\nu\delta \to \nu\delta)$ on the centre of mass energy is just given by $\sigma(s)$ as in (4.11). To compare $\sigma(\nu\nu \to \delta\delta)$ and $\sigma_t(\nu\delta \to \nu\delta)$ we need only to evaluate $\sigma(s)$ at the different centre of mass energies, $s = 2E_\nu m_\nu$ and $s = 2E_\nu m_\delta$. For an explicit comparison, we put in the values $g_e = 3 \times 10^{-3}$, $g_\mu = 10^{-2}$, $g_\tau = 3 \times 10^{-1}$, $m_\delta = 0.5\,\text{MeV}$, $m_\nu = 0.15\,\text{eV}$, $m_N = 5\,\text{MeV}$. We find;

$$\sigma(\nu\nu \to \delta\delta) \simeq 4.7 \times 10^{-10}\,\text{MeV}^{-2}, \quad \sigma_t(\nu\delta \to \nu\delta) \simeq 6.2 \times 10^{-16}\,\text{MeV}^{-2} \tag{4.31}$$

So we find there is a difference of five to six orders of magnitude. After computing the number density of the dark matter in the galactic and cosmological cases, we will use this to deduce that the t-channel does not contribute.

s-Channel Cross Section

We obtain an analytic expression for the s-channel cross-section from [137];

$$\sigma_s(\nu_\mu\delta \to \nu_\ell\delta) = \frac{g_\mu^2 g_\ell^2}{16\pi}\frac{(m_N^2 - m_\delta^2)^2}{m_N^2 + m_\delta^2}\frac{1}{(s - m_N^2)^2 + \Gamma_N^2 m_N^2} \tag{4.32}$$

where Γ_N is the width of N, it is given by;

$$\Gamma_N = \sum_\ell \frac{g_\ell^2}{16\pi} \frac{(m_N^2 - m_\delta^2)^2}{m_N^3} \tag{4.33}$$

In this case, we simply do an order of magnitude estimate with;

$$m_N = \mathcal{O}(\text{MeV}), \quad m_\delta = \mathcal{O}(\text{MeV}), \quad s - m_N^2 = \mathcal{O}(\text{GeV}^2), \quad g = \mathcal{O}(10^{-2}) \tag{4.34}$$

We note that this implies that $(s - m_N^2)^2 \gg \Gamma_N^2 m_N^2$. Putting these into (4.33), we find;

$$\sigma_s(\nu\delta \to \nu\delta) \simeq \mathcal{O}(10^{-21}\,\text{MeV}^{-2}) \tag{4.35}$$

As such we deduce that the contribution is certainly negligible at this energy, since even if the number density of δ was high enough, the t-channel process will dominate by 4 or 5 orders of magnitude.

The interference term

To argue that the interference term between the s and the t channel amplitudes, which we denote $\mathcal{M}_s$ and $\mathcal{M}_t$ respectively, also leads to a negligible contribution to the cross section, we note that by the triangle inequality;

$$|\mathcal{M}_s + \mathcal{M}_t| \leq |\mathcal{M}_s| + |\mathcal{M}_t| \Rightarrow |\mathcal{M}_s + \mathcal{M}_t|^2 \leq |\mathcal{M}_s|^2 + |\mathcal{M}_t|^2 + 2\,|\mathcal{M}_s|\,|\mathcal{M}_t| \tag{4.36}$$

Furthermore, integrals of these quantities which ultimately lead to the total cross section will satisfy equivalent relations due to the positive definite nature of the integrands. Finally then, if we denote the amplitude for $\nu\nu \to \delta\delta$ as $\mathcal{M}$, the calculations in the previous two sections indicate that $|\mathcal{M}_s|^2 \sim \mathcal{O}(10^{-10})\,|\mathcal{M}|^2$ and $|\mathcal{M}_t|^2 \sim \mathcal{O}(10^{-6})\,|\mathcal{M}|^2$. Hence, by the triangle inequality, we deduce that $|\mathcal{M}_s|\,|\mathcal{M}_t| \sim \mathcal{O}(10^{-8})\,|\mathcal{M}|^2$ and therefore leads to a neglible contribution to the total squared amplitude, $|\mathcal{M}_s + \mathcal{M}_t|^2 \sim |\mathcal{M}_t|^2 \sim \mathcal{O}(10^{-6})\,|\mathcal{M}|^2$. Hence we deduce that the total cross section for $\nu\delta \to \nu\delta$, where ν in the initial state has energy $\mathcal{O}(\text{TeV})$ satisfies $\sigma(\nu\delta \to \nu\delta) \sim 10^{-6} \cdot \sigma(\nu\nu \to \delta\delta)$. It therefore remains to check the number density of dark matter in the cosmological and galactic cases and compute the mean free path using the t-channel cross-section.

Number Density on Cosmological Scales

The dark matter density on a cosmological scale, at a redshift z, is given by [142];

$$n(z) = \frac{\Omega_{\text{DM},0}\rho_c}{m_{\text{DM}}}(1+z)^3 \simeq 1.26 \times 10^{-3}(1+z)^3 \left(\frac{\text{MeV}}{m_{\text{DM}}}\right) \text{cm}^{-3} \tag{4.37}$$

where we have used $\Omega_{\text{DM},0} \simeq 0.265$ and $\rho_c = 3H_0^2/8G \simeq 4.77\,\text{keV}\,\text{cm}^{-3}$. This is 5 orders of magnitude below the cosmic neutrino background number density. So in order to be relevant, $\sigma(\nu\delta \to \nu\delta)$ would have to be approximately 10^5 times larger than $\sigma(\nu\nu \to \delta\delta)$, evaluated at the neutrino energy. From Sections B.3, B.3, and B.3, we see this is not the case, and indeed the cross-section is significantly

smaller than the $\nu\nu \to \delta\delta$ cross-section. We can therefore neglect this cross section as the neutrino travels to the Milky Way.

Number Density on Galactic Scales

After deducing that the contribution to the mean free path from interaction with dark matter is negligible on cosmological scales, we just have to check whether the galactic overdesnity could lead to a significant contribution. As in [137], we use the Einasto profile with $\alpha = 0.15$ and $R_0 = 20\,\text{kpc}$ to model the dark matter energy density;

$$\rho_{\text{DM}}(r) = 7.2 \times 10^{-2}\,\text{GeV}\,\text{cm}^{-3} \cdot \exp\left(-\frac{2}{\alpha}\left(\left(\frac{r}{R_0}\right)^{\alpha} - 1\right)\right) \tag{4.38}$$

We can obtain the number density by dividing by the mass of the dark matter particle, $m_\delta \simeq \mathcal{O}(10^{-3}\,\text{GeV})$. Now, note that this is maximal when $r = 0$. In order to put an upper bound on the contribution to the optical depth, we assume that the whole halo has this maximal number density. With $m_\delta = 1\,\text{MeV}$;

$$n_{\text{DM}}^{\text{max}} \simeq \frac{\rho_{\text{DM}}(r=0)}{m_\delta} \simeq 4.4 \times 10^7\,\text{cm}^{-3} \simeq 10^5 n_\nu^0 \tag{4.39}$$

Now we are in a position to see why this does not contribute to the suppression of the neutino flux from the blazar. Whilst the combination of $n_{\text{DM}}^{\text{max}}\sigma_t(\nu\delta \to \nu\delta)$ is now of the same order of magnitude as $n_\nu\sigma(\nu\nu \to \delta\delta)$, the relevant consideration is the probability that such an interaction $(\nu\delta \to \nu\delta)$ occurs. This is dependent on the ratio between the length scale at which such a high number density is observed (i.e. the galactic radius), and the mean free path. Here, the mean free path, ℓ, is $\mathcal{O}(\text{Gpc})$, so the probability of survival is $\sim \exp(-d_g/\ell)$ where $d_g \simeq 1\,\text{kpc}$ is the galactic radius. We see that this is approximately unity. Finally, note that in the case where the mean free path is $\mathcal{O}(\text{kpc})$, we would not expect the neutrino to reach anywhere close to the galaxy, so this would be inconsequential also. Hence we deduce that both in the cosmological and galactic settings, the contribution from $\nu\delta \to \nu\delta$ is negligible in comparison to the dominant t-channel process $\nu\nu \to \delta\delta$.

To end this section, we emphasise that whilst we have neglected the contribution from these other processes, including any/all of them can only improve the bounds as the mean free path will decrease with new interactions. As such, it is only for the sake of simplicity that we make the assumptions, *not* at the cost of the validity of the bounds.

B.4 Mass Splitting in the Complex Case

We assume that each of the mass eigenstates is equally abundant $\nu_1, \bar{\nu}_1, \nu_2, \ldots$, with a number density given by;

$$n_{\nu_i} = \frac{1}{6}n_\nu = \frac{1}{6} \cdot 340\,\text{cm}^{-3} \tag{4.40}$$

Now, the contribution from each mass eigenstate to the inverse mean free path ℓ^{-1} is given by $n_{\nu_i}\sigma(\nu_\mu X \to Y)$. Importantly we argued in the last section that we thus need only consider $\sigma(\nu_\mu\nu \to \delta\delta)$. Now, in the real case, there is nothing more to say as there is only one scalar mass eigenstate. In the complex case however, we must consider the following. The theory we are considering is effective up to

some scale Λ. It therefore does not have to explicitly respect any of the symmetries that might apply in the UV. Indeed all we assume is that the new dark sector particles are odd under a $\mathbb{Z}_2$ symmetry, to ensure there is a stable candidate. As such, writing $\delta = \frac{1}{\sqrt{2}}(\delta_1 + i\delta_2)$, the most general hermitian mass term can be written;

$$V_m = M^2\delta^\dagger\delta - \frac{1}{2}(m^2\delta\delta + \text{h.c.}) \tag{4.41}$$

This leads to a mass splitting between the mass eigenstates $\delta_{1,2}$ given by $\Delta m_{12}^2 = 2m^2$. Now, we consider the possible processes $\nu\nu \to$ scalars. We have;

$$\nu\nu \to \delta_1\delta_1, \quad \nu\nu \to \delta_1\delta_2, \quad \nu\nu \to \delta_2\delta_2$$

From this we see that there are a couple of scenarios that might occur kinematically. We assume that the lightest scalar is δ_1, and that the first process can happen. Then it may the case that either (i) only the first process can occur, (ii) only the first and second processes can occur, or, (iii) all the processes can occur. This is where we make our simplifying assumption, which unlike the first case, will not necessarily improve the bounds if put in at a later date. We assume that if the first occurs, then the next two may also occur. This is equivalent to saying that there is a small mass gap between the two eigenstates. To simplify the situation then we assume that m is small compared to M, and therefore that we can approximate;

$$\sigma(\nu\nu \to \delta_1\delta_1) + \sigma(\nu\nu \to \delta_1\delta_2) + \sigma(\nu\nu \to \delta_2\delta_2) \simeq 3\sigma(\nu\nu \to \delta_1\delta_1) \tag{4.42}$$

B.5 Redshift Considerations

During the cosmological propagation, both the number density of the cosmic neutrino background neutrinos, and the energy of the blazar neutrino will be affected by redshift. Let the values now be denoted n_ν^0 and E_ν^0 respectively, then at a redshift z;

$$n_\nu(z) = n_\nu^0(1+z)^3, \quad E_\nu(z) = (1+z)E_\nu^0 \tag{4.43}$$

We now make the observation that the source of the 290 TeV neutrino is at a redshift $z = 0.3365$. In the case of the energy this means that the maximum possible multiplicative factor is $(1 + 0.3365)$, but this is within the confidence bounds on the energy measured at IceCube, so can be neglected. The redshift of the number density is not negligible however, although it only improves the bounds. We take the result from [142] that the optical depth is given by;

$$\tau = c\int_{z=z_1}^{z=z_2} \mathrm{d}z\, \frac{\mathrm{d}t}{\mathrm{d}z} n(z)\sigma(z) \tag{4.44}$$

Now, the energy of the muon observed at IceCube had a 1σ confidence interval of 23.7 ± 2.8 TeV [150]. This can be translated into an error on the energy of the incoming neutrino of an order 100 TeV. With this observation, we note that the energy of the 290 TeV neutrino at its source, i.e. before it is redshifted during the propagation, will lie within these bounds. Therefore, to simplify the analysis, we assume that $\sigma(z) = \sigma(E_\nu(z))$ does not depend on the redshift, z. With this assumption in mind, the

expression above reduces to;

$$\tau = cn_\nu^0 \sigma(E_\nu^0) \int_{z=z_1}^{z=z_2} \mathrm{d}z\,(1+z)^3 \frac{\mathrm{d}t}{\mathrm{d}z} \tag{4.45}$$

We can relate $\mathrm{d}t/\mathrm{d}z$ to the Hubble rate via;

$$\frac{\mathrm{d}t}{\mathrm{d}z} = -\frac{1}{(1+z)H(z)} \tag{4.46}$$

where;

$$H(z) = H_0\sqrt{\Omega_\Lambda + \Omega_{m,0}(1+z)^3} \tag{4.47}$$

We will take the values $\Omega_\Lambda \simeq 0.65$, $\Omega_{m,0} \simeq 0.315$, $H_0 \simeq 6.73\times10^4\,\mathrm{km\,s^{-1}Gpc^{-1}}$ [242], $c = 3\times10^5\,\mathrm{km\ s^{-1}}$. Letting $\ell_0^{-1} := n_\nu^0\sigma(E_\nu^0)$ to find;

$$\tau = \left(\frac{\ell_0}{\mathrm{Gpc}}\right)^{-1}\left(\frac{c\,/\,\mathrm{km\ s^{-1}}}{H_0\,/\,\mathrm{km\ s^{-1}Gpc^{-1}}}\right)\cdot\int_{z=z_1}^{z=z_2}\mathrm{d}z\,\frac{(1+z)^2}{\sqrt{\Omega_\Lambda+\Omega_{m,0}(1+z)^3}} \simeq 1.90\left(\frac{\ell_0}{\mathrm{Gpc}}\right)^{-1} \tag{4.48}$$

B.6 Including Neutrino Mass Hierarchies

The last technicality to introduce into the computation of the bounds are the facts that;

1. The neutrino *mass* eigenstates and *flavour* eigenstates are not the same
2. The neutrino masses are unknown, and indeed have two possible orderings (for the mass eigenstates); the *normal hierarchy* and the *inverted hierarchy*.

Within our calculation we aim to present the situation for both of these cases.

Mass Eigenstates and the PMNS Matrix

Within the Standard Model, we expect neutrinos to be massless. Experiments illustrating phenomena such as neutrino oscillations contradict this fact and we now believe they do indeed have a small mass. This complicates matters however for the reason mentioned above. The flavour eigenstates and the mass eigenstates are no longer the same in this case. Instead they are related by the *PMNS* matrix[5]. This encodes a unitary transformation between the flavour basis and the mass basis:

$$\nu_\ell := \begin{pmatrix}\nu_e\\ \nu_\mu\\ \nu_\tau\end{pmatrix} = \begin{pmatrix}U_{e1} & U_{e2} & U_{e3}\\ U_{\mu1} & U_{\mu2} & U_{\mu3}\\ U_{\tau1} & U_{\tau2} & U_{\tau3}\end{pmatrix} := U\nu_i \tag{4.49}$$

The Mass Hierarchy

A key fact in this discussion is that ultimately we do not know the absolute values, nor the ordering of the mass eigenstates. There are two common alternatives, which are illustrated in Figure 2 in [243];

1. *Normal Ordering:* In the normal hierarchy, ν_3 is the most massive state, whilst ν_1 and ν_2 are lighter.

[5] Pontecorvo-Maki-Nakagawa-Sakata

2. *Inverted Ordering:* On the other hand, in the inverted case, ν_3 is the lightest, whilst ν_1 and ν_2 are heavier.

Constraints on the Masses

We can go slightly further, whilst we do not know the precise masses of the neutrinos we have (i) a bound on the total sum of the masses that comes from Cosmology, and, (ii) values for the mass difference between the eigenstates. To be more precise;

- Combining constraints from Cosmic Microwave Background (CMB) anisotropies, Baryon Acoustic Oscillations, Type 1A Supernovae, and, CMB lensing, we will use the constraint [244];

$$\sum m_{\nu_i} < 0.17\,\text{eV} \tag{4.50}$$

- We also know the squared mass differences between some of the mass eigenstates [244];

$$\Delta m^2_{12} = m_2^2 - m_1^2 = 7.37 \times 10^{-5}\,\text{eV}^2 \tag{4.51}$$

$$\Delta m^2 = m_3^2 - \frac{1}{2}(m_1^2 + m_2^2) = +2.50 \times 10^{-3}\,\text{eV}^2\,(\text{NH}) \tag{4.52}$$

$$= -2.46 \times 10^{-3}\,\text{eV}^2\,(\text{IH}) \tag{4.53}$$

From the last of these constraints we see that fixing one of the masses automatically fixes the others. In our analysis we intend to vary one of the masses of the mass eigenstates and use the squared mass differences to compute the other masses, remaining within the bound set by the cosmological considerations. We will present the analysis in both the normal and inverted cases.

B.7 The Coupling Constants

There is one final consequence of the non-coincidence of the mass and flavour eigenstates. We are considering a coupling in the Lagrangian of the form;

$$\mathcal{L}_{\text{new}} = \sum_\ell g_\ell \delta \bar{N}_R \nu_{\ell,L} + \text{h.c.} \tag{4.54}$$

where importantly, the ν_ℓ are the flavour eigenstates. Furthermore, we quoted constraints on the couplings g_ℓ in this flavour basis e.g. $g_\ell < 10^{-3}$ in the case of real dark matter. Now consider expanding in the mass basis;

$$\mathcal{L} = \delta \bar{N}_R \sum_\ell g_\ell \sum_i U_{\ell i} \nu_{i,L} + \text{h.c.} := \sum_i g_i \delta \bar{N}_R \nu_{i,L} \tag{4.55}$$

We have defined the couplings to the neutrino mass eigenstates;

$$g_i := \sum_\ell U_{\ell i} g_\ell \tag{4.56}$$

Now, importantly, these will inherit constraints from the constraints on the flavour basis couplings, and are just related by a linear transformation. This means that we can still parametrise our

constraints in terms of the flavour couplings. The context of these comments is that the cosmic neutrino background consists of decoherent mass eigenstates. Therefore instead of considering flavour processes $\nu_\mu\nu_\ell, \nu_\mu\bar{\nu}_\ell \to \delta\delta$, we should instead consider $\nu_\mu\nu_i \to \delta\delta$. To do so we should use the $\{g_i\}$ couplings at the $\nu_i\delta N$ vertex, which we can compute as above. We also make use of the mass eigenstate masses as discussed above to compute the centre of mass energy in each of the different cases $i = 1, 2, 3$. Finally, we will assume that each of the mass eigenstates is equally abundant in the cosmic neutrino background so that we can take the number density of each species to be $n_\nu/6$ as noted previously.

B.8 Neutrino Clustering

This is the phenomenon relating to the gravitational clustering of neutrinos at late times once they become non-relativistic. This can increase their density inside gravitational wells such as the Milky Way today. An important reference is [245] which discusses the clustering of cosmic neutrino background neutrinos onto cold dark matter. In the context of this work, this would affect the number density $n_\nu(z)$ as the astrophysical neutrino passed through different dark matter distributions. In regions where there is more cold dark matter, [245] suggests that we should also see more cosmic neutrino background neutrinos. A precision analysis of the propagation of the neutrinos from the blazar should take this into account.

This being said, [245] only extends the analysis to the local group[6], across distances of Mpc. This is ultimately small scale structure in the context of Gpc propagation. Figure 8 in [245] illustrates the density contrast of the neutrinos on this scale. We see that density constrasts of $\mathcal{O}(2)$ are realistic, so including this effect could strengthen the bounds. Even an increase of an order of magnitude within the local group would only change the optical depth at the percent level, so we neglect this effect in this work.

B.9 Discussion regarding the consistency of the neutrino and photon flux

In this subsection we would like to discuss the neutrino flux we use above and see how it compares to the observed photon flux. The discussion here is a simple sanity check, this subsection therefore on its own contains no results which have any impact on the bound we obtain later. In particular, we are not using the photon flux to derive a bound, we just aim to discuss the discrepancy between the two fluxes.

Let us recall how neutrinos and photons are thought to be generated in the relativistic jets of active galaxies. In the hadronic scenario, highly boosted protons interact with photons in the jet from e.g. electron synchotron radiation. This leads to the production of neutral and charged pions via resonances (for example $p\gamma \to \Delta^+ \to p\pi^0$) or direct production (for example $p\gamma \to n\pi^+$). These highly relativistic pions then decay via $\pi^0 \to \gamma\gamma$ and $\pi^+ \to \ell^+\nu_\ell$ where ℓ is a lepton [247, 248]. This leads to a production of neutrinos and photons with $F_\nu \sim F_\gamma$ within the jet [229]. We might expect that the detection of high energy neutrinos should thus be accompanied by the EM emission of pionic gamma-rays. If this were the case, we would indeed expect the luminosities of the neutrinos and the photons to be comparable, $F_\nu \sim F_\gamma$, as was assumed in [147]. Unlike the HAWC constraint, the

[6]The *Greisen-Zatsepin-Kuzmin* zone

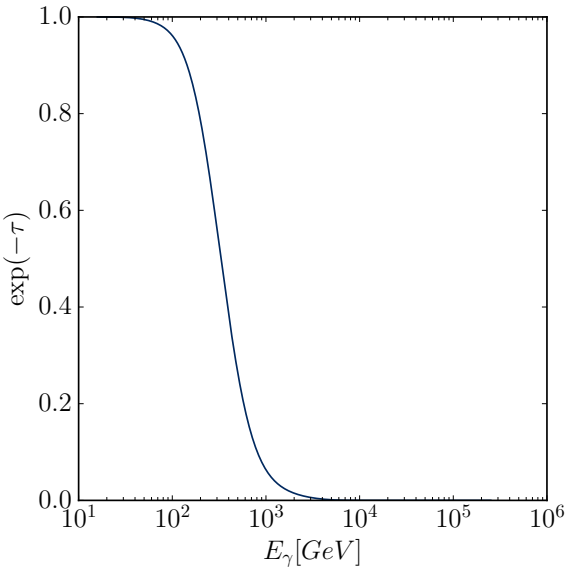

Figure B.2 The probability, $\exp(-\tau)$, where τ is the optical depth, of a photon produced in the blazar jet reaching the Earth due to interactions with the EBL. We see that at Fermi-LAT energies, $\mathcal{O}(290)$ GeV, this probability is close to 1, whilst at the higher, HAWC energies, $\mathcal{O}(1-100)$ TeV, there is significant attenuation of the flux due to scatterings $\gamma\gamma \to e^+e^-$. These calculations are based on [246].

Fermi-LAT data consisted of an actual measurement, and those authors used this assumption to make a direct prediction for the neutrino flux.

The assumption that $F_\nu \sim F_\gamma$ is however conservative — since the neutrinos are weakly interacting, they escape the jet without attenuation to the flux. On the other hand, the photons produced by neutral pion decays, may *not* be observed due to electromagnetic processes which may occur in the jet or attenuation during propagation across on the Universe. In the latter case this is due to $\gamma\gamma \to e^+e^-$ attentuation on the Extragalactic Background Light (EBL) [249]. In Figure B.2 we use code developed by one of the authors for a previous project [246] to show the attentuation due to pair production on the EBL for high energy photons from a blazar at redshift $z = 0.34$ is not very important at the Fermi-LAT energies considered in [147] (< 290 GeV) but really cuts off the photon flux at the HAWC energies relevant here (0.8 TeV — 74 TeV). Because of this, the HAWC data acting as an upper bound is in no conflict with the jet physics.

The HAWC data in Table IV.2 shows that the photon flux at this energy is less than the neutrino flux we have assumed. Given the fact it is much easier for photons to be attenuated and to lose energy than neutrinos, we assume this is in fact what has happened and note that we have assumed the lower of the two possible estimates of the neutrino flux based on the observed event.